# Imaging Spectroscopy of Aerosols using a Reference Spectrum Database

**Dissertation**

**zur**

**Erlangung der naturwissenschaftlichen Doktorwürde**
**(Dr. sc. nat.)**

**vorgelegt der**

**Mathematisch-naturwissenschaftlichen Fakultät**

**der**

**Universität Zürich**

**von**

**Stephan Bojinski**

**aus**

**Deutschland**

**Begutachtet von**

**Prof. Dr. Klaus I. Itten**
**Dr. ing. Rudolf Richter**
**Dr. phil. nat. Johannes Keller**

**Zürich 2003**

*Author:*
Stephan Bojinski
Remote Sensing Laboratories
Department of Geography
University of Zurich
Winterthurerstrasse 190
CH-8057 Zurich
Switzerland

stephan.bojinski@web.de
http://www.geo.unizh.ch

Printed on acid-free paper which falls within the ANSI guidelines to ensure permanence and durability.

Bojinski, Stephan:
Imaging Spectroscopy of Aerosols using a Reference Spectrum Database
Remote Sensing Series 40 – Zurich: Remote Sensing Laboratories, 2003
ISBN 3-03703-006-2



Printed by the Druckerei der Zentralstelle der Studentenschaft der Universität Zürich.

**Front cover:**
The background shows a TERRA/MODIS satellite image with high aerosol concentration over the Bay of Bengal (courtesy of NASA Visible Earth). The upper left sketch symbolises the entity-relationship diagram of the SPECCHIO reference spectrum database. Dust aerosol particles under the microscope are depicted in the lower left inset (courtesy of Tel Aviv University, Israel).

Die vorliegende Arbeit wurde von der Mathematisch-naturwissenschaftlichen Fakultät der Universität Zürich im Sommersemester 2003 aufgrund der Gutachten von Prof. Dr. Klaus I. Itten (Geographisches Institut, Universität Zürich), Dr. ing. Rudolf Richter (Deutsches Zentrum für Luft- und Raumfahrt (DLR), Oberpfaffenhofen) und Dr. phil. nat. Johannes Keller (Paul Scherrer Institut (PSI), Villigen) als Dissertation angenommen.

*Science is organized knowledge,*
*wisdom is organized life.*

Immanuel Kant

# Summary

The use of airborne or spaceborne imaging spectroscopy has in recent years become an invaluable means to determine the distribution of aerosols in the Earth's atmosphere on regional and global scales, e.g. in order to estimate the influence of aerosols on climate. Both spectral properties of the Earth's surface as well as composition and concentration of atmospheric aerosols influence the optical signal as measured by the imaging spectrometer. Over land, decomposition of these contributions is generally complex, and the potential of imaging spectroscopy in this regard is still largely untapped.

Representative and comprehensive information on the spectral properties of natural and man-made materials on the Earth's surface is hence required for the retrieval of aerosol properties from imaging spectroscopy. Surface spectral reference data is also indispensable in other spectroscopic applications, such as geological mapping, vegetation analysis, and water quality estimation. For the mentioned reasons, the reference spectrum database SPECCHIO (Spectral Input/Output) has been developed, offering ready access to currently about 4000 spectra from publicly available spectral collections, field campaigns, and modelling. Web-based and command line interfaces allow for the input of spectral data of heterogeneous formats and descriptions, as well as interactive queries, previews, and downloads. Data model and application software of SPECCHIO can be easily adapted to demands from the user community.

A new method for the retrieval of atmospheric aerosol parameters over land with imaging spectroscopy is proposed that uses spectral reflectance data from SPECCHIO. The Aerosol Retrieval by Interrelated Abundances (ARIA) method is based on unmixing of the short-wave infrared sensor signal by appropriate reference spectra from the database, and subsequent re-mixing of the visible wavelength range for approximating real surface reflectance. Contiguous and high-resolution spectral coverage of the sensor signal, a weak aerosol signal in the short-wave infrared, as well as the demonstrated spectral autocorrelation of natural surface spectra are preconditions for ARIA. Using year 2000 imagery from the Airborne Visible/Infrared Imaging Spectrometer, measured over rugged heterogeneous coastal terrain and an urban region in the Los Angeles (USA) area, retrieval results with ARIA for columnar aerosol optical depth at 0.55 $\mu$m wavelength are compared to existing single or double-band aerosol retrieval methods over land (dark target, Kaufman's band ratio). It is shown that ARIA leads to a more realistic representation of the spatial aerosol distribution, at comparable level of relative uncertainty. With ARIA, a novel contribution is made to spatial remote sensing of atmospheric aerosols in order to assess the distribution of aerosol types and concentrations in the Earth's atmosphere over land. More reliable quantification of the aerosol effect on regional and global climate, as well as of the atmospheric signal in spectral imagery is thus possible.

# Zusammenfassung

Die Verwendung von flugzeug- oder satellitengestützter Bildspektrometrie ist in den letzten Jahren für die Bestimmung der Aerosolverteilung in der Erdatmosphäre im regionalen und globalen Massstab unverzichtbar geworden und hat unter anderem zu einem verbesserten Verständnis der Rolle von Aerosolen im Klimasystem geführt. Sowohl spektrale Eigenschaften der Erdoberfläche, als auch die Zusammensetzung und Konzentration von atmosphärischen Aerosolen beeinflussen das vom Bildspektrometer gemessene optische Signal. Über Landflächen stellt die Trennung dieser Einflüsse ein im Allgemeinen schwieriges Unterfangen dar, wobei das Potential der Bildspektrometrie in dieser Hinsicht bisher weitgehend ungenutzt geblieben ist.
Umfassende Kenntnis der spektralen Eigenschaften von natürlichen oder vom Menschen erzeugten Materialien auf der Erdoberfläche ist für die bildspektrometrische Bestimmung von Aerosoleigenschaften daher von grosser Bedeutung. Spektrale Referenzdaten von Oberflächen sind in anderen spektroskopischen Anwendungen ebenfalls unverzichtbar, beispielsweise für geologische Kartierungen, Vegetationsanalysen oder die Bestimmung der Gewässerqualität. Vor diesem Hintergrund wurde die Spektrendatenbank SPECCHIO (*Spectral Input/Output*) entwickelt, welche über web- und zeilenbasierte Schnittstellen einen einfachen Zugriff auf zurzeit etwa 4000 Spektren ermöglicht. Diese stammen aus allgemein zugänglichen spektralen Sammlungen, Feldmessungen und Modellierungen. Die genannten Schnittstellen erlauben dem Benutzer das Einlesen von spektralen Daten, welche in heterogenem (Meta-)Format vorliegen können, sowie interaktives Anfragen, Visualisieren und Herunterladen der gewünschten Daten. Datenmodell und Applikationssoftware zu SPECCHIO können auf einfache Weise zukünftigen Erfordernissen der Benutzer angepasst werden.
Eine neue Methode zur Bestimmung von atmosphärischen Aerosolparametern über Landflächen mit Hilfe der Bildspektrometrie wird vorgestellt, welche spektrale Reflektanzdaten aus SPECCHIO benutzt. Die ARIA (*Aerosol Retrieval by Interrelated Abundances*)-Methode basiert auf der spektralen Entmischung des Bildspektrometer-Signals im kurzwelligen Infraroten (SWIR), unter Verwendung von Referenzspektren aus der Datenbank, und anschliessender Rekonstruktion der Bodenreflektanz im Sichtbaren. Voraussetzungen für diese Vorgehensweise sind ein hochaufgelöstes und kontinuierliches spektrales Signal am Sensor, ein schwacher Strahlungsantrieb der Aerosole im SWIR sowie die nachgewiesene spektrale Autokorrelation von natürlichen Oberflächenreflektanzen. Anhand von Bilddaten des flugzeuggestützten Bildspektrometers *Airborne Visible/Infrared Imaging Spectrometer* aus dem Jahre 2000, aufgenommen im Raum Los Angeles (USA) über einem hügeligen Küstengebiet mit variabler Oberflächenstruktur sowie einem Stadtgebiet, wird die aerosol-optische Dicke zwischen Sensor und Boden bei 0.55 $\mu$m Wellenlänge mit ARIA bestimmt. Der Vergleich mit herkömmlichen Einzelkanalmethoden ((*dark target, Kaufman's band ratio*)

zeigt die plausibleren Resultate für die ARIA-Methode. Ergebnisunsicherheiten dieser Resultate bewegen sich für alle Methoden in derselben Grössenordnung. Diese Arbeit zeigt mit ARIA eine neuartige Möglichkeit auf, die räumliche Verteilung von Aerosoltypen und -konzentrationen in der Erdatmosphäre mit Fernerkundung zu bestimmen. Die Genauigkeit der Quantifizierung des Aerosoleinflusses auf den atmosphärischen Strahlungstransport über Land kann mit der vorgeschlagenen Methode erhöht und dadurch die Rolle von Aerosolen im Klimasystem besser charakterisiert werden.

# Contents

# List of Symbols

| | | |
|---|---|---|
| $\rho_a$ | Aerosol optical effect at sensor | [-] |
| $\rho_r$ | Apparent reflectance due to molecular backscattering | [-] |
| $\rho_{app}$ | Apparent reflectance | [-] |
| $\rho_{app}^{sim}$ | Simulated apparent reflectance | [-] |
| $\rho^*$ | Apparent reflectance, corrected for molecular scattering contributions | [-] |
| $\rho_0$ | Apparent reflectance due to path radiance | [-] |
| $\rho_s$ | Surface reflectance | [-] |
| $t$ | Atmospheric transmittance | [-] |
| $L$ | Radiance | [W $m^{-2}$ $sr^{-1}$ $\mu m^{-1}$] |
| $L_0$ | Path radiance | [W $m^{-2}$ $sr^{-1}$ $\mu m^{-1}$] |
| $E_d$ | Downwelling irradiance at the surface level | [W $m^{-2}$ $\mu m^{-1}$] |
| $\lambda$ | Wavelength of electromagnetic radiation | [$\mu$m] |
| $E_0$ | Downwelling irradiance at the top of atmosphere | [W $m^{-2}$ $\mu m^{-1}$] |
| $s$ | Atmospheric albedo | [-] |
| $\tau_a$ | Aerosol optical depth at $\lambda = 0.55$ $\mu$m | [-] |
| $V$ | Horizontal visibility | [km] |
| $h$ | Terrain height above sea level | [m] |
| $\sigma_{e,a}$ | Aerosol extinction coefficient | [$m^{-1}$] |
| $\sigma_{s,a}$ | Aerosol scattering coefficient | [$m^{-1}$] |
| $\sigma_{e,r}$ | Molecular extinction coefficient | [$m^{-1}$] |
| $\theta_0$ | Sun zenith angle | [deg °] |
| $r_{xy}$ | Pearson's correlation coefficient | [-] |
| $\Delta X$ | Absolute error of quantity $X$ | [X] |
| $\delta X$ | Variation of quantity $X$ | [X] |
| $\omega_0$ | Single-scattering albedo | [-] |

| | | |
|---|---|---|
| $n(r)$ | Normalized size distribution | $[\mathrm{m}^{-3}\ \mu\mathrm{m}^{-1}]$ |
| $r$ | Particle radius | $[\mu\mathrm{m}]$ |
| $Q_e(r)$ | Extinction efficiency | [-] |
| $\alpha$ | Ångström turbidity coefficient | [-] |
| $P_a(\Theta)$ | Aerosol scattering phase function at scattering angle $\Theta$ | [-] |

# List of Abbreviations

| | |
|---|---|
| AATSR | Advanced Along-Track Scanning Radiometer |
| APEX | Airborne PRISM Experiment |
| ARIA | Aerosol Retrieval by Interrelated Abundances |
| ARVI | Atmospherically Resistant Vegetation Index |
| ASCII | American Standard Code for Information Interchange |
| ASD | Analytical Spectral Devices Inc. |
| ATSR | Along-Track Scanning Radiometer |
| AVHRR | Advanced Very High Resolution Radiometer |
| AVIRIS | Airborne Visible/Infrared Imaging Spectrometer |
| BRDF | Bi-directional Reflectance Distribution Function |
| CASI | Compact Airborne Spectrographic Imager |
| CGI | Common Gateway Interface |
| CHRIS | Compact High-Resolution Imaging Spectroscopy sensor |
| DAIS | Digital Airborne Imaging Spectrometer |
| DBMS | Database Management System |
| DLR | Deutsches Zentrum für Luft- und Raumfahrt |
| ENVI | Environment for Visualizing Images |
| ESA | European Space Agency |
| GER | Geophysical and Environmental Research Corp. |
| GOES | Geostationary Orbit Environmental Satellite |
| GOME | Global Ozone Monitoring Experiment |
| GSD | Ground Sampling Distance |
| HDF-EOS | Hierarchical Data Format of the Earth Observing System |
| HTML | Hypertext Markup Language |
| HTTP | Hypertext Transfer Protocol |
| HyMAP | Hyperspectral Mapper |
| IDL | Interactive Data Language |
| JCAMP | Joint Committee of Atomic and Molecular Physics |
| LAI | Leaf Area Index |

| | |
|---|---|
| MERIS | Medium Resolution Imaging Spectrometer |
| MISR | Multi-angular Imaging Spectroradiometer |
| MODIS | Moderate Resolution Imaging Spectrometer |
| NASA | National Aeronautics and Space Administration |
| NDVI | Normalized Differential Vegetation Index |
| NIR | Near-infrared range of the electromagnetic spectrum |
| NOAA | National Oceanic and Atmospheric Administration |
| PAF | Processing and Archiving Facility |
| POLDER | Polarization and Directionality of Earth Reflectances sensor |
| PROBA | Project for On-Board Autonomy |
| SAM | Spectral Angle Mapper |
| SeaWiFS | Sea Viewing Wide Field-of-view Sensor |
| SPECCHIO | Spectral Input/Output database |
| SQL | Structured Query Language |
| SWIR | Short-wave infrared range of the electromagnetic spectrum |
| TCL | Tool Command Language |
| TOMS | Total Ozone Mapping Spectrometer |
| USGS | United States Geological Survey |
| UV | Ultra-violet range of the electromagnetic spectrum |
| VIS | Visible range of the electromagnetic spectrum |

# 1

# Introduction

The subject of this dissertation is passive optical remote sensing of atmospheric particles – also referred to as aerosols – by a novel combination of two techniques: first, imaging spectroscopy, that is airborne or spaceborne imagery at spectral resolution around 10 nm, with contiguous spectral coverage from the visible to the infrared electromagnetic spectrum, and ground sampling distances of $10^1 - 10^2$ m. Secondly, a spectrum database that contains a large collection of surface reflectance measurements with reference character, a comprehensive description of these measurements, and appropriate interfaces. In the following, an introduction is given to the spectrum database concept as developed in this dissertation. A short treatise of the characteristics of aerosols and approaches to their remote sensing ensues. Finally, a new method of combining imaging spectroscopy and the spectrum database for the purpose of aerosol mapping is briefly presented in the rationale. The personal bibliography of the dissertation concludes this introduction.

## 1.1 SPECCHIO: Reference Spectrum Database of Surface Reflectances

A geoscientific information system that allows access to a large collection of spectral measurements of natural and artificial surfaces can in many remote sensing applications replace in-situ spectral measurements of the Earth's surface (Hunt, 1977; Roberts et al., 1998), and aid, e.g., in the geological mapping of minerals (Clark, 1990). If passive optical remote sensing in general, or downward-looking imaging spectroscopy in particular, is being used for characterization of the atmosphere including aerosols, information on the spectral characteristics of the Earth's surface are required. As ground-based measurements are rarely available, approximations for spectral surface reflectance $\rho_s(\lambda)$ are called for.

Publicly available spectral collections are mostly organized in a file-based way (e.g. Salisbury et al. (1991)), which is straightforward, but subject to a number of drawbacks (e.g., limited search capability and flexibility). In contrast to simply collecting files that contain spectral information, organization of the data and its entire description (meta data) in a database with appropriate interfaces greatly facilitates data access, and improves consistency, availability and documentation quality.

Based on these ideas, the spectrum database SPECCHIO (Spectral Input/Output)

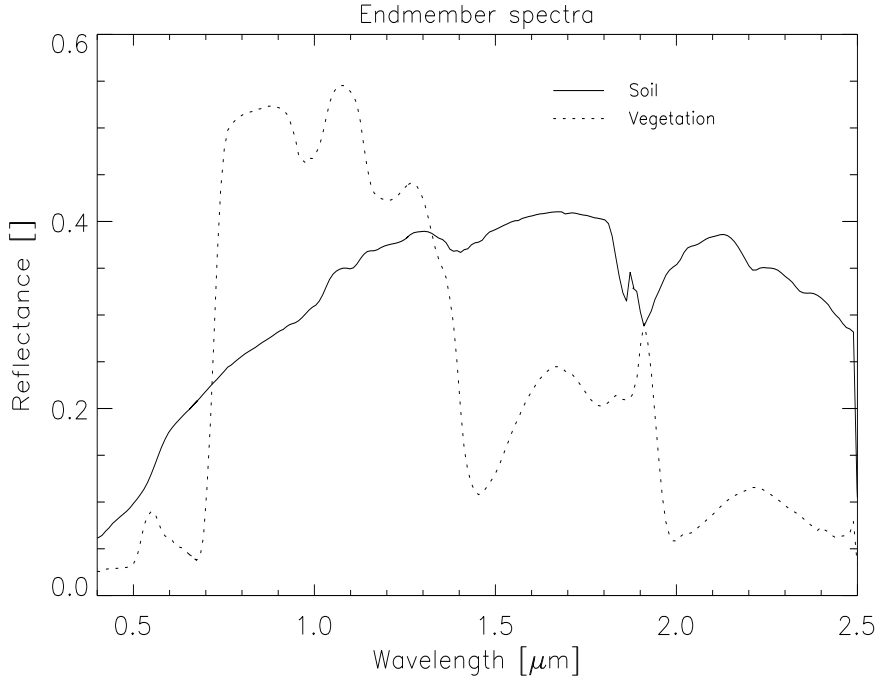


Figure 1.1: Typical reflectance spectra for vegetation and soil.

has been designed and implemented. It represents a large and easily accessible reference spectrum data source and is designed to overcome the limitations of file-based solutions. SPECCHIO consists of three major components, namely web and command line based user interfaces, an underlying relational database management system (DBMS), and a well-defined data model that describes the "surface reflectance spectrum" aspect of reality. Full online documentation of SPECCHIO is provided for maximum user friendliness. A more detailed description of SPECCHIO is given in chapters 2 and 3.

The database is designed for the management of heterogeneous data from different sources that depend on a high number of independent parameters. This considers the high diversity of spectral data in the field of imaging spectroscopy. Design principles were:

- Logical relations between data sets and consistency
- Intuitive interfaces (web browser and command line scripts)
- Flexibility to changes in science context (easy modification of meta data)
- Independence of file format
- Scalability

SPECCHIO currently contains data from the following sources: publicly accessible spectral collections, a limnological field campaign, a field campaign focussing on bi-directional reflectance behaviour of vegetation and soils, and a modelling study of vegetation and snow reflectances.

For illustration, Fig. 1.1 shows a typical reflectance spectrum of green vegetation and bright soil, taken from SPECCHIO. Green vegetation is relatively dark in the visible range, with a reflectance peak in the green around 0.55 $\mu$m due to chlorophyll absorption. Reflectance strongly increases across the red edge into the near-infrared because of the physical structure of plant cells. Soils exhibit a spectrally flatter behaviour than vegetation. Their spectral characteristics are mostly driven by grain size, water content, and mineral composition.

## 1.2 Aerosols and their Effects

In summer 2002, a scientific report commissioned by the United Nations Environment Programme revealed that air pollution in East and South East Asia had reached an unprecedented level of severeness (UNEP and C4, 2002). The report, based on data gathered by the Indian Ocean Experiment (Ramanathan et al., 2001b), said that the "Asian brown cloud" was reducing solar energy reaching the Earth's surface by 15 %, thus considerably affecting the growth of agricultural crops. At the same time, it caused heating of the lower atmosphere due to the absorption of sun irradiance, which is expected to alter the hydrological cycle in the area, that is, changing time, location, and intensity of seasonal monsoon rainfall. Increased air pollution also had an effect on human health by causing increased numbers of diseases of the respiratory tract, according to the study. The haze was the result of forest fires, the burning of agricultural wastes, wood, and other biomass in households, and dramatic increases in the burning of fossil fuels in vehicles, industries, and power stations.

This recent example sketches the importance of airborne particles, also referred to as aerosols, on climate, biosystems, and human health. Both naturally occurring processes and anthropogenic activity are origins of aerosols in the atmosphere. Globally speaking, total mass emissions of aerosols from natural sources outnumber anthropogenic aerosols by the ratio 9:1. On a regional scale though, mainly in industrialized areas of Europe, the United States, and Asia, anthropogenic aerosols can dominate (Baltensperger and Nyeki, 1998). In 1952, the city of London experienced a smog event from an atmospheric temperature inversion and high emissions of aerosols from coal burning, causing the death of about 4000 residents (Wilson and Spengler, 1996). Since then, in the older industrialized countries, considerable abatement of total mass emissions of anthropogenic aerosols has been achieved by the introduction of filters, clean fuels, and more efficient combustion cells. In emerging countries, however, increasing energy consumption due to high rates of economic growth, and the lack of modern abatement technology causes rapidly increasing emissions of aerosols.

Unlike long-lived greenhouse gases (e.g. carbon dioxide, methane), which distribute uniformly over the globe, aerosol lifetimes in the planetary boundary layer are only a week or less, resulting in substantial spatial and temporal variations with peak concentration near the source. An exception to this pattern are volcanic emissions, which are sporadically injected into higher altitudes of the atmosphere during eruptions (e.g. Mount Pinatubo 1991). With lifetimes in the order of months, these stratospheric aerosols have a longer-lasting global impact on radiative transfer and atmospheric chemistry (Seinfeld and Pandis, 1998).

Both direct (in-situ) and indirect (remote) measurement techniques are used to analyse atmospheric aerosol properties. Direct measurements, which take place on the

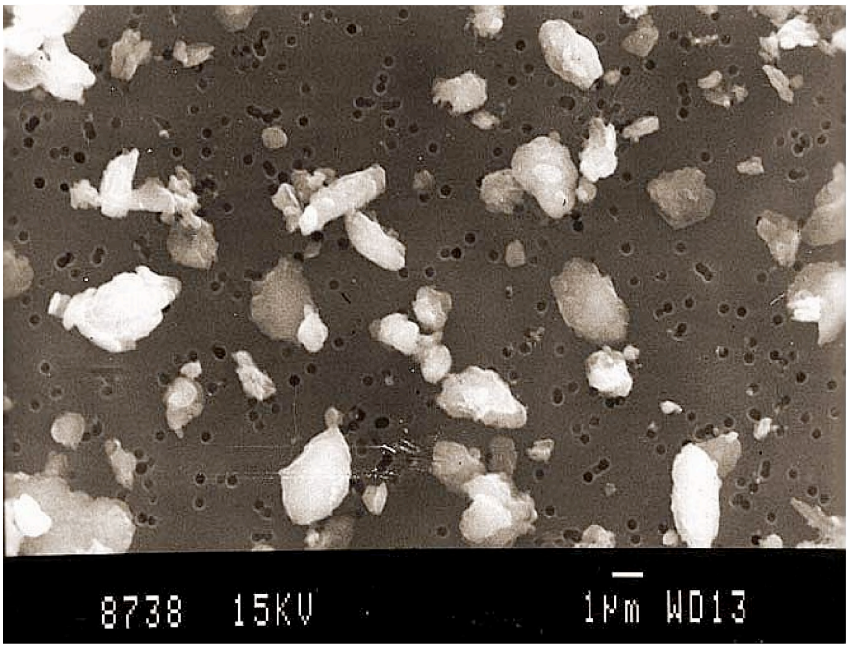


Figure 1.2: Enhanced picture of desert dust particles, mainly consisting of mineral compounds that are lifted off the surface or eroded from solid rocks by desert winds. Most particles are larger than 2 $\mu$m in diameter (courtesy of Tel Aviv University, Israel).

Earth's surface or on airplanes, allow accurate determination of physical and chemical aerosol characteristics on the spot (Baltensperger, 1997). For example, continuous monitoring of aerosols on the high-alpine research station Jungfraujoch (Switzerland) gave insight into seasonal and diurnal variations of aerosol number size distributions (Weingartner et al., 1999). On account of the high spatial and temporal variability of tropospheric aerosols, however, interpolation of direct measurements in the spatial dimensions is at best possible on a regional scale.

In order to obtain a broad picture of spatial aerosol distributions, on local and global scales, remotely sensed measurements from aircraft or satellites are needed (King et al., 1999). Preceded by an experimental phase, in which the potential of airborne or spaceborne measurements in view of aerosol retrieval has been explored, the operational quantitative determination of key aerosol parameters is now possible on a global scale (Kaufman et al., 2002).

### 1.2.1 Aerosol Models

Aerosols are solid or liquid particles with a range $0.001 - 100$ $\mu$m in diameter, freely floating in and surrounded by atmospheric gas. They are generally classified into a fine mode (less than 2 $\mu$m in diameter) and a coarse mode (larger than 2 $\mu$m), which together define the size distribution. Natural sources for aerosols are the ocean (sea-salt), deserts (wind-blown dust), vegetation (pollen, spores), and volcanic emissions (ash, sulphates). Fig. 1.2 shows desert dust particles, which have a particularly strong coarse mode, as seen under the microscope. Secondary natural aerosols may be formed

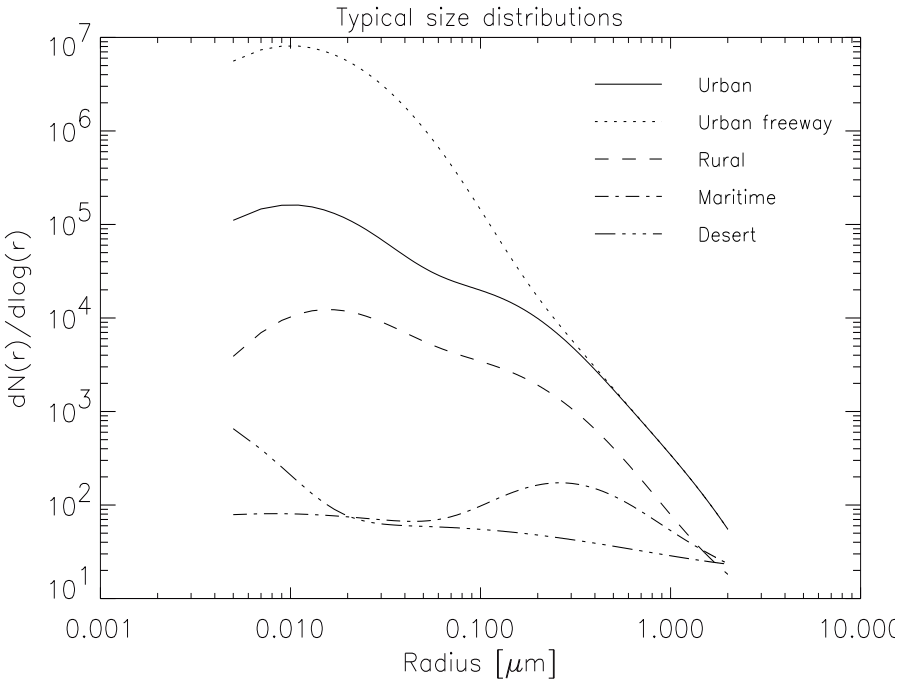


Figure 1.3: Number concentrations of typical aerosol size distributions (not normalized).

by gas-to-particle conversion, where release of the gas dimethyl sulphide from the oceans constitutes the main source. Anthropogenic sources include biomass burning (clearing of forests and savannah for agricultural purposes), industrial aerosols, and soot, the latter two mainly due to combustion processes. Secondary emissions here predominantly involve the oxidation of sulphate and nitrogen oxides (Baltensperger and Nyeki, 1998).

It is difficult to define a small number of aerosol models that would exhaustively describe the high variability of physical and chemical properties of aerosols in the planetary boundary layer. In general and simplified terms, a reduction to three major aerosol models seems appropriate in many situations (Shettle and Fenn, 1979): maritime, rural (continental), and urban aerosols, which are considered representative for different atmospheric conditions. Typical size distributions are given in Fig. 1.3. In an urban environment, total particle number concentrations can be higher than $10^6$ cm$^{-3}$ (Bukowiecki et al., 2002), whereas on a clean site such as Jungfraujoch, they typically float around 1000 cm$^{-3}$. It should be kept in mind that, given the natural variability of aerosols, almost any aerosol model is confirmed by some in-situ measurements, and no set of models will be consistent with all measurements (Shettle and Fenn, 1979). An exhaustive treatment on aerosol models is given by d'Almeida et al. (1991).

### 1.2.2 Aerosol Optical Properties

In contrast to atmospheric gases, aerosols in general do not exhibit uniquely defined scattering and absorption properties, mainly because they generally represent a mixture of particles of different origin. Strong spectral features in the electromagnetic

spectrum due to aerosols therefore do not exist. Scattering at aerosol particles is described by the Mie scattering approximation (Liou, 1980). Absorption of sunlight by aerosols mainly depends on the absorption capability of individual particles, which is above all determined by the amount of soot and black carbon. The ratio between scattering and and total extinction of radiation is the single scattering albedo

$$\omega_o = \sigma_{s,a}/\sigma_{e,a} \ . \tag{1.1}$$

$\sigma_{s,a}$ and $\sigma_{e,a}$ are aerosol scattering and extinction coefficients, respectively. $\sigma_{e,a}$ is related to the aerosol size distribution by

$$\sigma_{e,a}(\lambda) = \int_{r_1}^{r_2} \pi r^2 Q_e(r) n(r) dr \ , \tag{1.2}$$

where $n(r)$ denotes normalized size distribution, and $Q_e(r)$ extinction efficiency of the particles with radius $r$.

The optical aerosol effect most apparent to the human eye is the reduction of visibility due particle scattering and absorption. Horizontal visibility is defined by Koschmieder's formula (Twomey, 1977a)

$$V = \frac{3.192}{(\sigma_{e,a} + \sigma_{e,r})} \ , \tag{1.3}$$

where $\sigma_{e,a}$ and $\sigma_{e,r}$ are extinction coefficients due to aerosols and atmospheric gases, both evaluated at $\lambda = 0.55$ $\mu$m. It is mostly the $0.1 - 1$ $\mu$m particle fraction which is identified as visible in the air, because in this size range, the interaction between sun irradiance and particles is most efficient. In order to describe scattering and absorption of aerosols integrated over an atmospheric column, the aerosol optical depth $\tau_a$ is introduced, which is related to $\sigma_{e,a}$ and column height $h$ by

$$\tau_a(\lambda, h) = \int_0^h \sigma_{e,a}(\lambda, h') dh' \ . \tag{1.4}$$

$\tau_a$ is one of the most important parameters derived from airborne or satellite remote sensing. Its wavelength dependence is often approximated as $\tau_a(\lambda) \sim \lambda^{-\alpha}$ with the Ångström turbidity coefficient $\alpha$, ranging between 4 (Rayleigh scattering) and $\approx 0$ (Mie scattering at large particles), and being $0.5 - 1.5$ for dry aerosols (Twomey, 1977a).

Fig. 1.4 shows a global monthly mean of $\tau_a$ for the month of September 2001, as obtained from the aerosol product of the operational Moderate Resolution Imaging Spectrometer sensor on NASA's TERRA satellite (TERRA/MODIS). Low values $(0.0 - 0.2)$ cover most of the oceans and large parts of North Asia and the Americas. High values $(0.6 - 0.8)$ are concentrated over tropical rainforests zones (due to forest fires), over the ocean near deserts, in India, and in China.

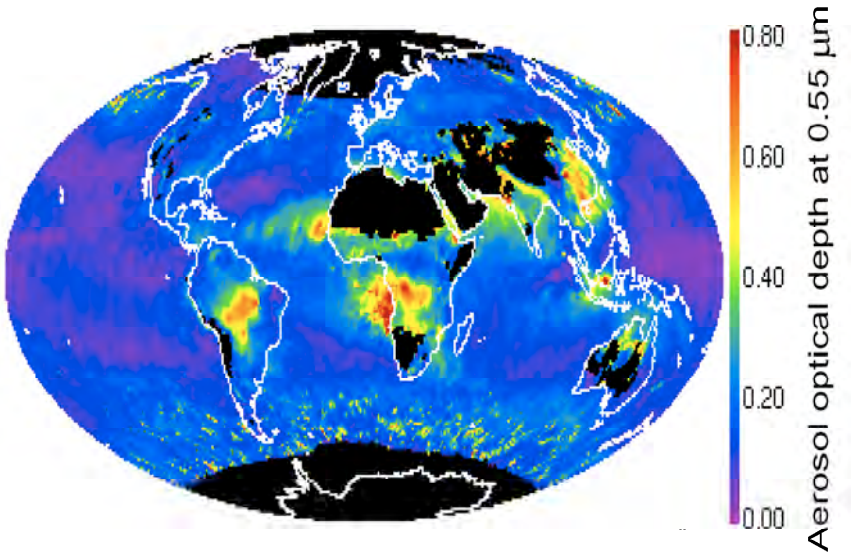


Figure 1.4: Global monthly mean of $\tau_a(0.55\mu\text{m})$ for September 2001 as obtained from the TERRA/MODIS aerosol product. In the black areas, no data is available (courtesy of MODIS science team).

### 1.2.3 Aerosol Radiative Forcing

As all-time record breaking rainfalls caused devastating floods in many parts of Central Europe in summer 2002, global warming and related higher probability of extreme weather events have again become top issues on political agendas. Aerosols in the atmosphere play an important role in the global radiation budget, although far more complex to quantify than greenhouse gases.

In contrast to greenhouse gases, which act only upon the outgoing thermal emission and thus have a warming effect on the atmosphere, aerosols interact with both incoming and outgoing radiation. They do so directly by particle scattering and absorption (direct effect), and indirectly by their contribution to the formation of clouds, which themselves scatter and absorb radiation (indirect effect). In the direct effect, the amounts of relative and total scattering and absorption, governed by $\omega_o$ and $\tau_a$, determine the net radiative effect, i.e. whether cooling or warming dominates. The indirect effect is mainly driven by cloud particle phases (liquid or ice), and difficult to quantify (Charlson et al., 1992).

It is subject of current research whether direct and indirect effects of aerosols have a net global warming or cooling effect on the Earth-atmosphere system (Lohmann and Feichter, 2001). Fig. 1.5 shows global annual-mean radiative forcing due to various atmospheric constituents, after Houghton et al. (2001). The height of the rectangular bar denotes a central or best estimate value, while its absence denotes no best estimate is possible. The vertical line about the rectangular bar with "X" delimiters indicates an estimate of the uncertainty range. A vertical line without a rectangular bar and with "O" delimiters denotes a forcing for which no central estimate can be given due

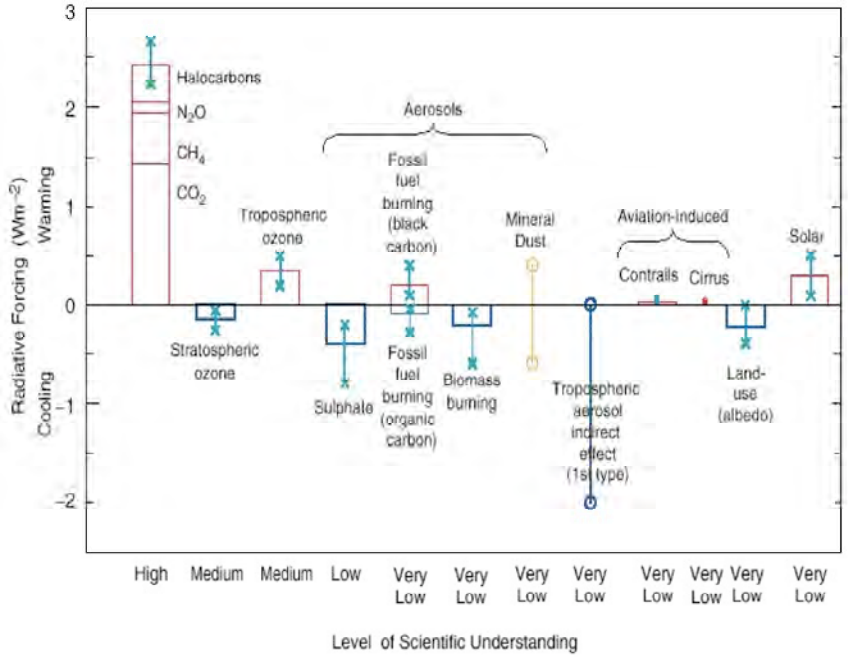


Figure 1.5: Global, annual-mean radiative forcings [W m$^{-2}$] due to atmospheric constituents for the period from pre-industrial (1750) to present (2000) (after Houghton et al., 2001).

to large uncertainties. A "level of scientific understanding" index is accorded to each forcing, with high, medium, low and very low levels, respectively. This represents the subjective judgment about the reliability of the forcing estimate. Reliability of scientific evidence is generally very low for the radiative effect of different aerosol types, and no clear cooling or warming trend can be discriminated. Radiative forcing of greenhouse gases (leftmost bar) is comparatively well understood.

## 1.3 Remote Sensing of Aerosols

Remote sensing instruments on aircraft or satellites can measure aerosol properties on both regional and global scales. Using passive optical satellite sensors that measure reflected sunlight from the Earth-atmosphere system, aerosol optical properties can be derived to assess the influence of aerosols on radiative forcing (Ramanathan et al., 2001a). Spatial mapping of aerosol optical properties can be used to infer on aerosol physical and chemical characteristics, e.g. for a global aerosol climatology, or locally for the investigation of exhaust plumes from major cities. Information on aerosols is also of major importance for the atmospheric correction of airborne or spaceborne imagery, which is a prerequisite to spectrally analyse the Earth's surface (Kaufman et al., 1997a; Richter, 1998).

Fig. 1.6 shows a satellite picture of the TERRA/MODIS sensor, where a situation of particularly high aerosol loading in the Indian Ganges valley, stretching far out into the Bay of Bengal, can be readily identified.

Figure 1.6: Satellite picture acquired 6 December 2000 by the TERRA/MODIS sensor over India, Bangladesh, the Bay of Bengal, and the Himalaya to the north. High aerosol concentration in the Ganges valley extends far out into the ocean, where it can be well discriminated by its brightening effect (courtesy of NASA Visible Earth).

### 1.3.1 Principles

Passive optical sensors collect sunlight that is backscattered from the Earth-atmosphere system into their field of view. Radiance $L$ at the satellite sensor level for a plane-parallel, cloud-free atmosphere and uniform Lambertian surface reflectance $\rho_s$ reads as (Liou, 1980)

$$L = L_o + \frac{\rho_s E_d t}{\pi(1 - s\rho_s)} \ , \tag{1.5}$$

with total downwelling irradiance at the surface $E_d$, total upward atmospheric transmittance (direct and diffuse) $t$, and the reflectance of the atmosphere from below $s$ ("atmospheric albedo") which is a measure for multiple scattering between atmosphere and surface. $L_o$ denotes at-sensor radiance for vanishing $\rho_s$, also known as path radiance or atmospheric radiance.

Normalizing radiance by the downwelling irradiance at the sensor level, apparent reflectance $\rho_s$ is obtained

$$\rho_{app} = \frac{\pi L}{E_0 cos\theta_0} \ , \tag{1.6}$$

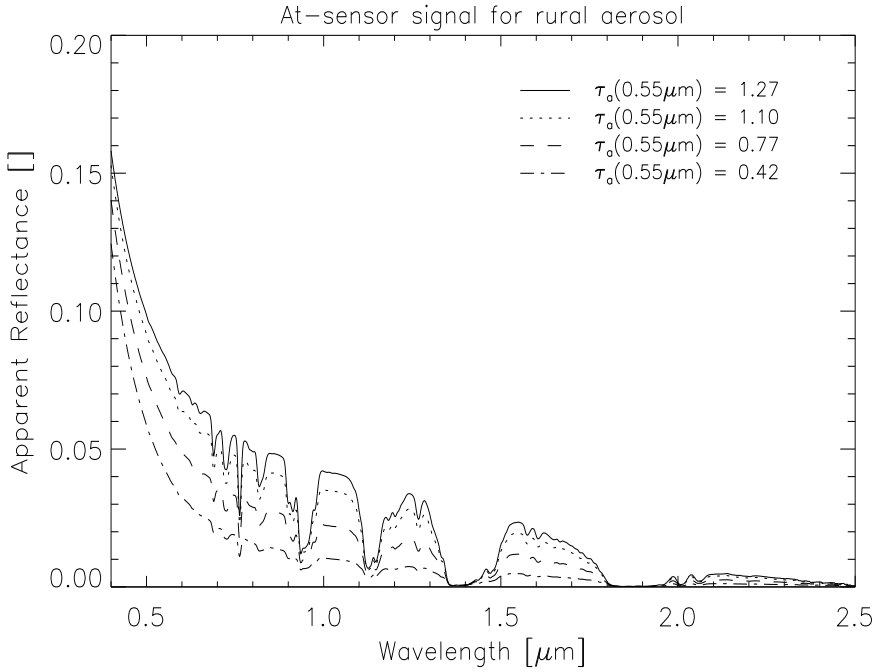


Figure 1.7: Total apparent modelled reflectance at sensor for a rural aerosol, zero surface reflectance, and four levels of aerosol optical depth $\tau_a(0.55\mu\text{m})$. Brightening of the signal is particularly apparent in the VIS.

where $E_0$ denotes the solar irradiance from the nadir direction (= extraterrestrial sun irradiance for spaceborne systems), and $\theta_0$ the sun zenith angle. Equation (1.5) then becomes

$$\rho_{app} = \rho_0 + \frac{\rho_s t E_d}{E_0 cos\theta_0 (1 - s\rho_s)} \ . \tag{1.7}$$

Normalized path radiance $\rho_0$ results from scattering and absorption processes at atmospheric gas molecules and aerosols. Molecular scattering of sunlight is described by the Rayleigh approximation, scattering at aerosols generally follows Mie theory. For small optical path lengths, the single-scattering approximation is valid, and both mechanisms can be decoupled (Tanré et al., 1992). In this case, $\rho_0 = \rho_r + \rho_a$ with Rayleigh and aerosol scattering contributions, respectively. The aerosol effect $\rho_a = \rho_{app} - \rho_{app}(\text{no aerosols})$ can then be expressed as

$$\rho_a = \omega_0 \tau_a P_a(\Theta)/(4\mu\mu_0) + O(\tau_a^2) \tag{1.8}$$

where $\omega_0$ denotes single scattering albedo, $\tau_a$ columnar aerosol optical depth, $P_a(\Theta)$ the scattering phase function with scattering angle $\Theta$, and $\mu_0, \mu$ the cosines of incident sun and viewing angles.

Fig. 1.7 illustrates the increase in $\rho_{app}$, i.e. the apparent brightening of the dark surface, with increased aerosol loading. This means that the aerosol effect $\rho_a$ is positive, which could already be observed in Fig. 1.6, especially over the ocean. The aerosol effect depends on $\rho_s$ and can become very small at the critical surface reflectance (Kaufman, 1987). Equation (1.8) holds for non-absorbing aerosols even in

| Sensor Type | Systems | GSD [km] | # of Bands UV | VIS/NIR | SWIR | Band width [nm] |
|---|---|---|---|---|---|---|
| | AVHRR (NOAA platforms) | 1.1 / 4.4 | 0 | 2 | 0 | 100-1000 |
| Multispectral | SeaWiFS (OrbView-2) | 1.1 / 4.5 | 0 | 8 | 0 | 20-40 |
| Near-Nadir | GOES 8 (GOES) | 0.57x1.0 / 2.3x4.0 | 4 | 1 | 0 | 220-900 |
| Sensors | TOMS (e.g. EarthProbe) | 50 | 6 | 0 | 0 | 0.2 |
| | GOME (ERS-2) | 320x40 | 4 | 0 | 0 | 0.2-0.4 |
| Narrowband | MODIS (TERRA, AQUA) | 0.25-1.0 | 0 | 16 | 4 | 10-300 |
| Radiometers | MERIS (ENVISAT) | 0.3 | 0 | 15 | 0 | 1.25-30 |
| Multiangle | MISR (TERRA) | 0.275-1.0 | 0 | 4 | 0 | 22-42 |
| Multispectral | ATSR-2 (ERS-2) | 1.0 | 0 | 3 | 2 | 20-300 |
| Sensors | AATSR (ENVISAT) | 1.0 | 0 | 3 | 2 | 20-300 |

Table 1.1: Sensors currently used for aerosol remote sensing.

case of large optical depths $\tau_a$ (Gordon and Wang, 1994). Only for strongly absorbing aerosols, the higher order dependence of $\rho_a$ on $\tau_a$ becomes non-negligible. Aerosol optical depth $\tau_a$ constitutes one of the most important physical quantitites aerosol remote sensing is aiming at. Optical properties of the atmosphere also govern parameters $t$, $E_d$, and $s$. For the inversion of aerosol parameters, the only observed quantity in equation (1.7) is $\rho_{app}$. Ancillary information from surface reflectance measurements for $\rho_s$ is scarcely available on a routine basis, and may be replaced by data from reference spectrum databases.

Only within the coordinated effort of a closure experiment, which usually includes a large number of co-located ground-, and airborne measurements of radiation and in-situ gas and aerosol properties (Quinn et al., 1998; Ansmann, 1999), the separation of surface and aerosol contributions in $\rho_{app}$ is feasible, and aerosol properties can be determined in detail according to equation (1.8).

In all other cases, i.e. for operational aerosol retrieval by airborne and spaceborne sensors without ground truth data, this inversion problem is ill-conditioned (Twomey, 1977b) and models to describe $\rho_a(\lambda)$ and $\rho_s(\lambda)$ are required. For the simulation of radiative transfer in the atmosphere, the MODTRAN 4.0 code (Berk et al., 1989) is used in this study, including aerosol models defined by Shettle and Fenn (1979).

### 1.3.2 Methods and Sensors

Methods for the retrieval of aerosol properties from airborne or spaceborne radiometers are closely linked to sensor design and measurement technique. Sensors differ, among other factors, in number, position and width of spectral bands, ground sampling distance, and repetition rate. A rough distinction between (1) multispectral, near nadir view looking radiometers, (2) near-nadir looking narrowband radiometers with moderate spectral and spatial resolution, and (3) multiwavelength, multiangle radiometers can be made. Imaging spectrometers with high spectral and spatial resolution are treated in detail in the next section. Table 1.1 gives an overview of all these sensors.

As for (1), the earliest studies on aerosol remote sensing from satellites focused on

mapping dust over the ocean using a single band in the visible spectral range (VIS) of the LANDSAT-1 sensor by Fraser (1976), making use of the general darkness of sea water in the VIS. In a modelling study, Gordon (1978) made first steps in the correction of ocean color measurements for aerosol influence using two spectral bands over the oceans. Two bands in VIS and near-infrared (NIR) of the ADVANCED VERY HIGH RESOLUTION RADIOMETER (AVHRR) sensor were employed by Mishchenko et al. (1999) on a global dataset to detect aerosol optical depths and aerosol types over the oceans, but accuracy was compromised mainly by calibration uncertainty of the sensor. Combined retrieval of water properties and aerosol optical depth over the ocean in eight VIS and NIR bands of the SEA-VIEWING-WIDE-FIELD-OF-VIEW-SENSOR (SeaWiFS) has been demonstrated by Gordon and Wang (1994). Unless models or in-situ measurements exist that account for the effects of wind speed and suspended matter, water is approximated to reflect $0-1$ % of the downwelling irradiance above its surface in the NIR, excluding specular reflection.

First studies on the retrieval of aerosol properties from satellite data over land, which is generally more complex due to variable surface reflectance, were aimed at atmospheric correction (Tanré et al., 1983), but soon focused equally on aerosol mapping (Kaufman and Sendra, 1988), making use of dark vegetation in the VIS. Dark vegetation is mostly approximated by $2-3$ % reflectance in this spectral range (Richter, 1996). In raw images, dark vegetation can be identified by thresholding of the atmospherically resistant vegetation index (ARVI) (Kaufman and Tanré, 1992).

For both dark water and dark vegetation areas, the presence of aerosols generally brightens these pixels at the sensor level, which is illustrated in Fig. 1.8(A,B). Given $\rho_s$, path radiance $\rho_0$ and thus $\rho_a$ can be better approximated, which contains all the information on aerosols in the spectrum for a particular wavelength band. Methods that use dark water or dark vegetation for that purpose are commonly referred to as dark target approaches.

The retrieval of aerosol parameters, mainly $\tau_a$, has also been demonstrated with multitemporal data from the GEOSTATIONARY ORBIT ENVIRONMENTAL SATELLITE (GOES) (Zhang et al., 2001), and in the ultraviolet spectral range, where surface reflectance is constantly low for most surfaces, with the TOTAL OZONE MAPPING SPECTROMETER (TOMS) (Torres et al., 1998) and the GLOBAL OZONE MONITORING EXPERIMENT (GOME) (Veefkind et al., 2000).

The dark target approach has been refined over land for sensors of type (2), in particular for the MODERATE RESOLUTION IMAGING SPECTROMETER (MODIS), which is the first operational sensor to specifically address aerosol retrieval over land and oceans. For surfaces which are relatively dark ($\rho_s < 0.1$) in the short-wave infrared (SWIR) wavelength range, an empirical relationship between SWIR reflectance at $\lambda = 2.1$ $\mu$m, and visible reflectances at $\lambda = 0.49$ $\mu$m and 0.66 $\mu$m has been shown for a variety of natural surface by Kaufman et al. (1997b). The thus called band ratio method makes use of the weak aerosol effect in the SWIR, except for very large dust-like or sea-salt particles. Application to dust detection has nevertheless been demonstrated by Kaufman et al. (2000). Fig. 1.8(C) shows the basic principle of the band ratio method, yielding $\rho_s$ for two bands in the VIS range. Over water, Tanré et al. (1997) used bands in the entire VIS, NIR, and SWIR spectral range between 0.55 and 2.13 $\mu$m of the MODIS airborne simulator and a forward modelling approach to derive aerosol properties over the ocean.

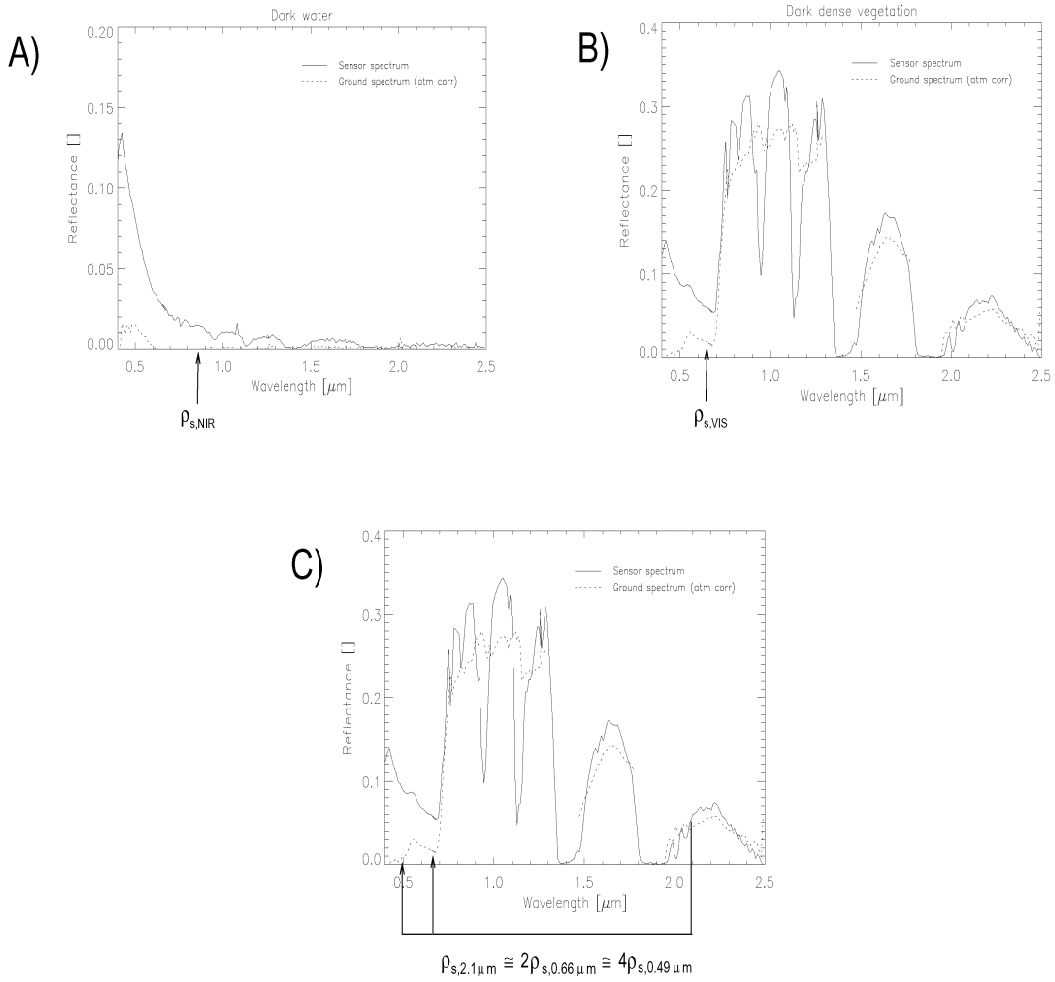


Figure 1.8: Single band-oriented principles for the approximation of surface reflectance $\rho_s$ in the VIS/NIR for aerosol retrieval: (A) example for approximation of water reflectance in NIR, where $\rho_s$ is mostly assumed zero; (B) $\rho_s = 0.02 - 0.03$ over dark dense vegetation; (C) the band ratio method empirically relates $\rho_s(2.1\mu\text{m})$ to $\rho_s(0.49\mu\text{m}, 0.66\mu\text{m})$.

For currently operational spaceborne imaging spectrometers, the dark target principle forms the basis of aerosol parameter retrieval algorithms, such as for the MEDIUM-RESOLUTION IMAGING SPECTROMETER (MERIS; see Santer et al. (1999)) and MODIS. In both algorithms, a dark pixel map is obtained by iterative application of reflectance thresholds. The MODIS sensor also provides SWIR coverage and thus allows application of the band ratio method also. Here too, the aerosol inversion process for the final aerosol product is preceded by iterative thresholding applied to reflectance values in the SWIR.

Finally, multiwavelength/multiangular sensors (type (3)) allow characterization of the aerosol scattering properties ($P_a(\Theta)$) and aerosol optical depth by looking into different directions with several autonomous cameras. The variation of optical path length with viewing direction gives rise to specific aerosol retrieval algorithms, using

the Multi-angular Imaging Spectroradiometer (MISR) with 9 cameras (Diner and Martonchik, 1985; Martonchik et al., 1998), and, both with dual-view capability, the Along-Track Scanning Radiometer (ATSR-2) (Veefkind and de Leeuw, 1998) and the Advanced Along-Track Scanning Radiometer (AATSR). Also, the bidirectional reflection distribution function (BRDF) of land surfaces can be better approximated by multiple viewing angle sensors than with mere nadir-looking sensors (Gobron et al., 2000). The Polarization and Directionality of Earth Reflectances (POLDER) sensor had the additional capability of measuring different polarization states of radiation in different directions relevant to aerosol retrieval, but is no longer in operation (Leroy et al., 1997).

## 1.4 Aerosol Retrieval with Imaging Spectroscopy

Imaging spectrometers with continuous spectral coverage in the VIS, NIR and SWIR in about 50 to 224 bands, band widths around 10 nm throughout the spectrum, and ground sampling distances of the order of 10 m, have opened new horizons in the determination of biophysical and geophysical variables that describe the Earth's surface (Goetz et al., 1985). Until the launch of Hyperion on EO-1 in 2000 (Ungar, 2002), and the Compact High-Resolution Imaging Spectrometer (CHRIS) instrument on PROBA (CHRIS, 2002), this sensor type was solely available airborne. Examples are the Compact Airborne Spectrographic Imager (CASI) (Anger et al., 1990), the Hyperspectral Mapper (HyMAP) (Cocks et al., 1998), the Digital Airborne Imaging Spectrometer (DAIS) (Strobl et al., 1997), and the Airborne Visible/Infrared Imaging Spectrometer (AVIRIS) (Green et al., 1998).

Airborne imaging spectrometers scan the Earth's surface and the atmosphere between surface and sensor on a regional scale. Accurate atmospheric correction of the imagery has been a focus of research (Roberts et al., 1997; Mustard et al., 2001), taking into account terrain effects (Richter and Schläpfer, 2002). Isakov et al. (1996) inferred aerosol optical depth from contrast reduction of uniform artificial land surface targets with high reflectance difference, due to atmospheric blurring. Over oceans, the assumption of zero water-leaving radiance greater than 1.0 $\mu$m has been combined with the forward calculation of at-sensor radiance look-up tables for a selection of aerosol models and aerosol optical depths (Gao et al., 2000).

None of the identified methods, however, makes specific use of the high spectral and spatial resolution of imaging spectrometers for the characterization of the atmosphere. A new approach for that matter will be briefly given in section 1.6, and treated in detail in chapter 4.

## 1.5 Modelling Aerosol Spectral Signatures

Primary sources of aerosols are mainly located on the Earth's surface. Therefore, atmospheric aerosol concentrations are largely confined to a region where atmosphere-surface interaction is highest, the planetary boundary layer, whose vertical extension is generally approximated as $2-4$ km above ground level (Seinfeld and Pandis, 1998). Maritime, rural (continental), and urban aerosol models, as defined previously, are

considered in this analysis. Dust is excluded because of too high expected aerosol effect in the SWIR. In addition, a tropospheric background model is used in all simulations. An exhaustive view on the variation of aerosol models depending on geography and climatology is given by d'Almeida et al. (1991). The proposed ARIA method for aerosol parameter retrieval from imaging spectroscopy relies on knowledge of the aerosol effect in the VIS and SWIR spectral regions. For this reason, the sensitivity of the aerosol effect was explored. The imaging spectrometer was considered nadir-looking at 20 km altitude above sea level. Columnar water vapour content (1.41 g/cm$^2$) and ozone content (7.36 g/cm$^2$) of the model atmosphere are held constant. A 15 cm$^{-1}$ band model was used in VIS, a 1 cm$^{-1}$ band model the SWIR range as input to the MODTRAN 4.0 radiative transfer code.

### 1.5.1 SWIR Aerosol Signature

To employ the short-wave infrared part of the electromagnetic spectrum for the retrieval of aerosol properties, as done in Kaufman's band ratio method, one must first investigate the aerosol effect for this spectral range. Under most natural conditions, it is considered small compared to the visible part of the spectrum, where most aerosol-light interaction takes place. A detailed investigation on the aerosol effect over natural surfaces for $\tau_a = 0.25$ shows a maximum aerosol effect of 0.01 for very bright surfaces in the SWIR (sand with $\rho_s = 0.3$), and 0.005 for $\rho_s < 0.15$ (Kaufman et al., 1997b). Particularly for the darkest surfaces ($\rho_s$(SWIR) $< 0.05$), the aerosol effect in VIS and SWIR can differ by a factor of 30. For the dust aerosol, this difference is much less pronounced, implying that the aerosol effect in the SWIR is relatively large due to the presence of large scattering particles.

In order to assess the aerosol effect with regard to high aerosol concentrations in the atmosphere ($\tau_a > 0.25$), modelling of these conditions over surfaces with spectrally uniform Lambertian reflectances was carried out. Results are depicted in Fig. 1.9. Upper two panels (a) show the aerosol effect for $\tau_a = 0.32$, corresponding to horizontal visibility $V = 23$ km, and different values for $\rho_s$. The lower panels (b) correspond to $\tau_a = 0.67$ ($V = 10$ km). It can be seen that the magnitude of the aerosol effect is only weakly dependent on wavelength ($\leq 0.03$ absolute variation), and generally increases with aerosol optical depth. Only for vanishing surface reflectance, a small ($\leq 0.01$) positive aerosol effect can be observed. In all other cases, negative effects, i.e. apparent darkening of the surface as seen from the sensor, prevail, and increasingly so for brighter surface reflectances. Rural and maritime model aerosol effects agree within 0.02 absolute deviation, whereas the urban model consistently causes larger negative aerosol effects, due to its high portion of absorbing particles. The effect can amount to more than 0.12 in absolute reflectance. The line at zero level indicates the presence of the background atmosphere only. Constraining the analysis to bands with high enough atmospheric transmission yields an effective SWIR1 range of 1.52 - 1.72 $\mu$m, and a SWIR2 between 2.09 and 2.31 $\mu$m.

Aerosol effects in the SWIR compromise the basic assumption of the ARIA method, that only the surface contribution is seen by the sensor in this spectral region. With the goal to obtain an averaged aerosol effect for each combination of $\tau_a$ and $\rho_s$, aerosol effects in Fig. 1.9 are averaged across the three aerosol models, and over the whole spectral range displayed. Results of this calculation are shown in Fig. 1.10, where the very hazy case $\tau_a = 1.00$ ($V = 6$ km) is also included.

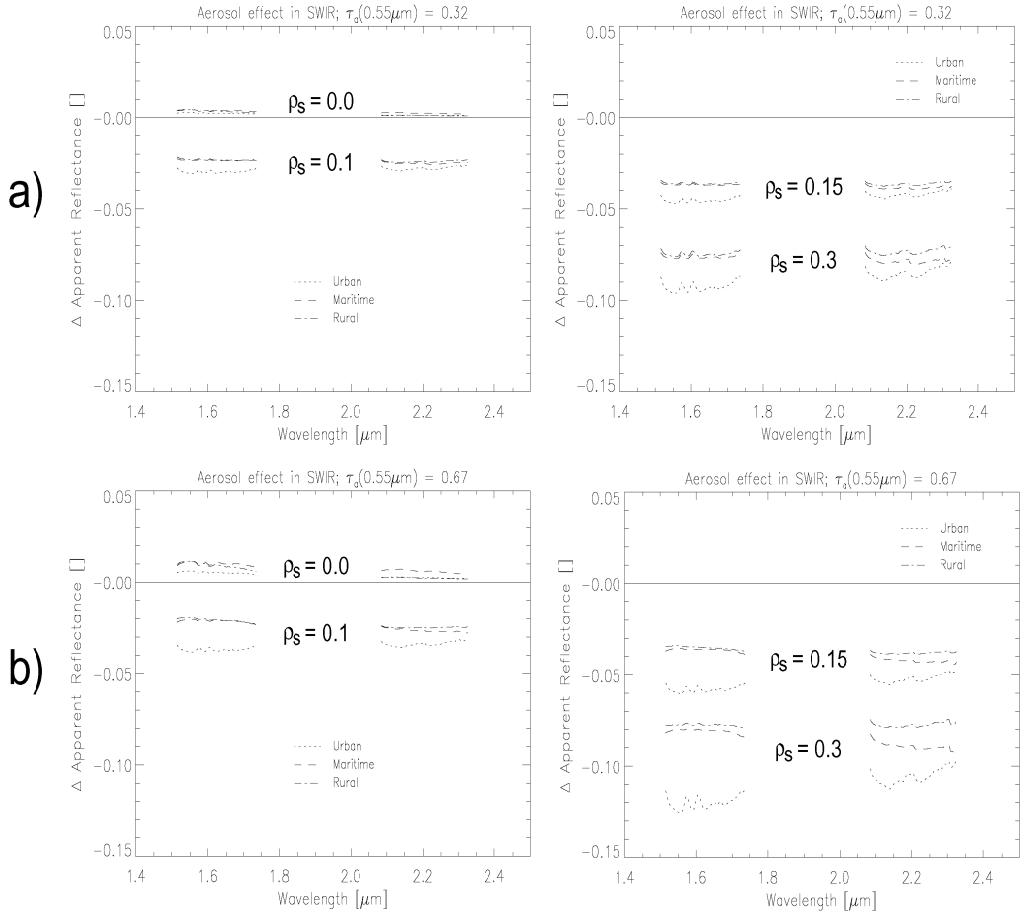


Figure 1.9: Aerosol spectral signature for varying background reflectances $\rho_s$ and nadir-looking sensor at 20 km height above ground. Panels (a) were obtained with $\tau_a = 0.32$, panels (b) with $\tau_a = 0.67$. The zero line indicates the presence of tropospheric background aerosol only.

Again it can be seen that over bright surfaces and for high aerosol loading, the aerosol effect in the SWIR can be up to 0.10 in absolute magnitude. Constraining the aerosol effect to 0.005, as postulated by Kaufman et al. (1997a) for $\rho_s < 0.15$ under clear conditions, would require an upper $\rho_s$ threshold of 0.04 approximately for the hazy cases considered here. With regard to the average reflectance of natural surface in the SWIR, this threshold is considered too strict. A maximum average $\overline{\rho_s(\lambda)}$ of 0.15 is therefore proposed (see Fig. 1.10), limiting the aerosol effect to 0.045 approximately for hazy and very hazy conditions.

### 1.5.2 VIS Aerosol Signature

Aiming at numerical inversion of aerosol parameters from the aerosol effect in the visible part of the spectrum, $\rho_s$(VIS) and forward modelling of radiative transfer in a model atmosphere is required. This is necessary as even for high-resolution spectral imaging data, parameters that describe the state of atmospheric aerosols are too

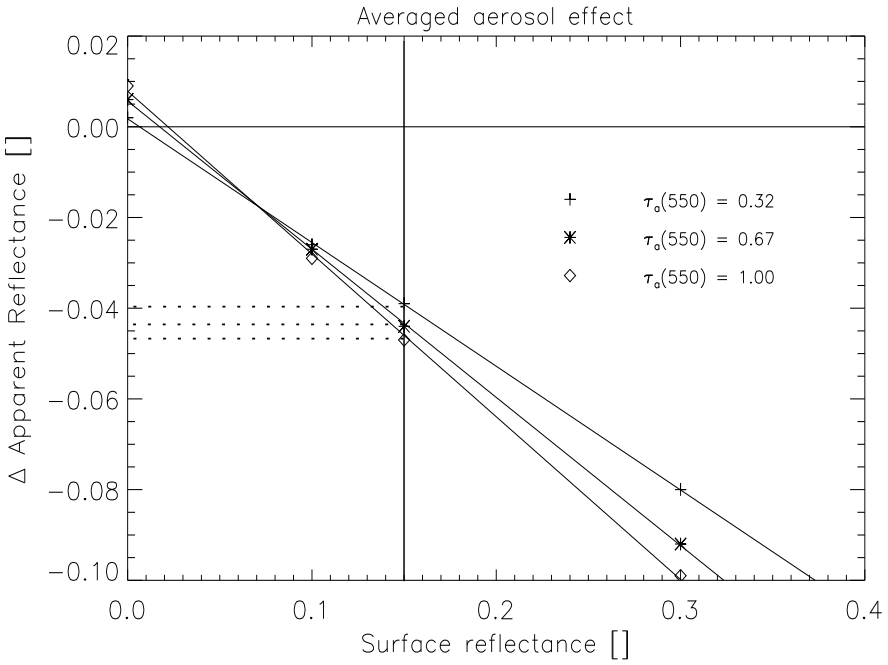


Figure 1.10: Averaged aerosol effect $\overline{\rho_a}$ for all aerosol models evaluated in the SWIR1 and SWIR2 ranges for uniform surface reflectances $\rho_s$, varying columnar optical depth at $\lambda = 0.55$ $\mu$m, and nadir-looking sensor at 20 km height above ground. With $\rho_s < 0.15$, $\rho_a$ is limited to $-0.045$ approximately.

manifold for a unique inversion (Veefkind et al., 2000). Due to the large number of influencing parameters, calculation of look-up tables must be preceded by a sensitivity analysis in which the most influential aerosol parameters are found, i.e. those causing the strongest change in aerosol effect $\delta\rho_a$.

Table 1.2 states the typical aerosol property variation range as given in tabulated works (d'Almeida et al., 1991; Seinfeld and Pandis, 1998). The resulting maximum change in aerosol effect $\delta\rho_a$ between 0.4 and 0.7 $\mu$m is stated in the rightmost column. In order to modify inherent properties, e.g. refractive index or number size distribution, of the standard urban, rural, and maritime aerosols, a simulation programme for Mie scattering on a microscale (Wiscombe, 1980) was employed prior to actual radiative transfer modelling. For comparison, a variation of the background atmosphere is also included in the analysis.

Aerosol optical depth $\tau_a(0.55\mu\text{m})$ was chosen as 0.67 unless otherwise specified, corresponding to fairly hazy conditions. Surface reflectance was modelled as spectrally uniform $\rho_s = 0.0$ generally providing a maximum positive aerosol effect according to the dark target principle. Size distributions were varied for the cases of strong fine modes compared to standard fine modes for the urban case (total number concentrations $10^5$ and $5 \cdot 10^5$ cm$^{-3}$, respectively), and relatively strong coarse modes compared to standard coarse modes for the maritime case (3 and 30 cm$^{-3}$). Average radii of the modes were not subject to variation.

The simulations gave the following results according to Table 1.2: surface reflectance $\rho_s$, columnar aerosol optical $\tau_a$ and the overall aerosol model cause the strongest fluctuations $\delta\rho_a$ of the aerosol effect. Changes in scattering properties due to changes

| Model parameter | Variation range | Maximum $\delta\rho_a$ |
|---|---|---|
| $\rho_s$ | 0.0 - 0.3 | 0.08 |
| $\tau_a$ | 0.08 - 1.08 | 0.11 |
| Aerosol model | rural, urban, maritime | 0.07 |
| Refractive particle index (real) | 1.52 - 3.1 | 0.05 |
| Size distribution | fine urban, coarse ocean | 0.04 |
| Aerosol layering | in 0-2, 3-5 km height layer | 0.04 |
| Background atmosphere | US Standard, Mid-latitude summer | 0.001 |

Table 1.2: Maximum variation of aerosol effect $\rho_a$ between 0.4 and 0.7 $\mu$m due to atmospheric model parameter fluctuations. Quantities are given for $\lambda = 0.55$ $\mu$m as applicable. Definitions of size distributions and atmosphere models are used according to d'Almeida et al. (1991).

in the real refractive particle index follow next, as enhanced multiple scattering gives rise to stronger effective aerosol backscattering. The latter is a generally small effect in the single scattering approximation, assuming that aerosols are predominantly forward scatterers. Variations in absorption properties (imaginary refractive index) are covered by the comparison of urban and rural aerosol models with all other parameters identical. They show a stronger impact on the aerosol effect (0.07) than the variation of the real refractive index (0.05). Altering the mode size does have a relatively small effect on $\rho_a$ but might need more extensive investigation. The aerosol effect is also sensitive to the vertical position of the aerosol layer, although the nadir-looking sensor cannot resolve any profile information from one vantage point. The effect of alternating the background atmosphere is negligible as expected.

As a conclusion, for the numerical inversion of the aerosol effect in terms of aerosol parameters, look-up table dimensions span in $\rho_s$, $\tau_a$ directions, for the urban, rural, and maritime aerosol models. These results are corroborated in an exhaustive analysis by Tanré et al. (1996).

## 1.6 Rationale of Dissertation

### 1.6.1 Motivation

The objectives in the development of the spectrum database SPECCHIO have been stated: in many remote sensing applications, such as geological mapping, vegetation analyses, water quality estimations, and characterization of the atmophere between sensor and Earth, spectral data from a reference spectrum database can replace in-situ measurements made by field operators. These data are frequently not available, especially on an operational basis, as cost and organizational effort become too high. In addition, storage, administration, and access to heterogeneous spectral data is greatly facilitated by the SPECCHIO database, as it is based on a comprehensive data model with a detailed description of each spectrum, as well as web and command line

user interfaces. This is in contrast to existing, file-based spectral collections. Spectral data from SPECCHIO comes into use in a novel method for the retrieval of aerosol parameters from imaging spectroscopy.

Above mentioned existing methods for the retrieval of aerosol parameters over land, such as Kaufman's band ratio method (Kaufman et al., 1997b), have been applied to imaging spectrometer data, but do not make specific use of the high spatial and spectral resolution of this imagery. In the spatial domain, aerosol distributions on regional scales could be determined in better detail using imaging spectroscopy. Over land, variations in aerosol parameters due to small-scale topography could be detected. For mapping and monitoring of urban area exhaust plumes, high spatial resolution aerosol mapping can be ideal complementary information to ground-based data. In turn, the accuracy of atmospheric correction of imaging spectroscopy can also be enhanced by closer knowledge of the aerosol variation within an image scene. More accurate spectral sampling of the sensor signal is expected to increase aerosol parameter accuracy, since bad bands as well as higher order $\lambda$-dependence of the aerosol signal $\rho_a$ are better considered.

To these ends, a new method is sought for aerosol retrieval over land using imaging spectroscopy, that relies on spectral unmixing of the SWIR spectral range as measured at sensor (details are given in chapter 4). The basic assumption is that the radiative influence of atmospheric gases and aerosols be low in these bands, which means that more or less the actual surface signature is "seen" in this range. From the SWIR unmixing with pre-defined spectral endmembers (typical spectra that characterize the surface reflectance, drawn from the SPECCHIO database), the surface spectrum in the VIS can be approximated by spectral re-mixing, assuming that endmember abundances are interrelated between VIS and SWIR. Based on this assumption, the method is named ARIA (Aerosol Retrieval by Interrelated Abundances). Spectral autocorrelation of surface reflectances is demonstrated, inspired by Kaufman et al. (1997b), who empirically found a significant proportionality between spectral reflectances of natural surfaces in one SWIR and two VIS bands. Surface reflectance is then approximated in a multitude of VIS bands by re-mixing the endmembers. Forward modelling of these reflectances to the sensor level allows best-fit inversion of aerosol parameters, using a look-up table approach. Gaps in the aerosol map are interpolated considering terrain height variations. ARIA is subsequently tested on airborne imaging spectrometer data from AVIRIS, with high calibration accuracy in both VIS and SWIR spectral ranges. However, with the first spaceborne imaging spectrometer now in operation (Ungar, 2002) and the prospect of upcoming instruments (e.g., CHRIS (2002)), ARIA is a contribution to improved retrieval of aerosol parameters on a global scale, provided sensor quality is sufficient (i.e., AVIRIS-like) in the VIS and SWIR.

### 1.6.2 Approach

A basic concept of the reference spectrum database SPECCHIO, including first versions of the data model and interfaces, has been presented as a contribution to the Second EARSeL Workshop on Imaging Spectroscopy in Enschede in July 2000 (Bojinski et al., 2002b), and was subsequently recommended for publication as a reviewed journal paper (Bojinski et al., 2002a). This paper is given in chapter 2 of this dissertation. As a consequence of two more prototype iterations in the SPECCHIO software

development process, a comprehensive data model for the description of remotely sensed spectra could be finalized, the programming code streamlined, interfaces to the database refined and adapted to specific data format requirements, and documentation for users provided. Alongside with an overview of possible applications, this latest version of SPECCHIO has been published (Bojinski et al., 2003) and is presented in chapter 3.

In the data description of SPECCHIO, data quality is a key factor, strongly influenced by the calibration state of the measuring spectroradiometer. Well-known calibration factors of an instrument are a prerequisite for the reliability of spectral measurements, which are supposedly among the least reliable of all physical measurements (Kostkowski, 1997). A laboratory campaign that involved five different spectroradiometers was carried out, aiming at absolute instrument gain calibration with an integrating sphere secondary calibration standard, and spectral feature calibration by means of rare earth reflectance standards. A good appreciation of the potential and limitations of this calibration effort was achieved; the detailed in-house report led to co-authorship in a paper by Schaepman et al. (2002a). Consequently, imagery from the airborne AVIRIS sensor was used in this work for remote sensing of the aerosol signal, as calibration state and signal-to-noise — especially in the visible range of the spectrum — were considered good enough.

The calibration and validation of the future airborne imaging spectrometer APEX (Airborne PRISM Experiment) required the definition of a processing and archiving facility (PAF) concept. In this context, a PAF relational database for the organization of data storage and flow has been developed and published with co-authorship in Schläpfer et al. (2000b). Calibration and signal-to-noise sensor requirements as defined by Earth remote sensing applications have been determined with respect to the atmosphere by means of radiative transfer modelling, and were published in Schläpfer et al. (2002). A more recent paper on the APEX PAF considered requirements from a high diversity of applications (e.g., vegetation, limnology, snow) for a detailed sensor specification, and presented strategy and components for the PAF software development (Schaepman et al., 2002b).

Development of the new Aerosol Retrieval by Interrelated Abundances (ARIA) regarding aerosol inversion over land surfaces using imaging spectroscopy was eventually possible, based on the knowledge gained from the afore mentioned work: availability of a reference spectrum database, awareness and quantification of data quality, familiarity with processing of imaging spectroscopy data, and radiative transfer modelling with regard to atmospheric parameters. In a first development phase, the ARIA method was set up to include combined geometric and atmospheric correction of AVIRIS imagery. This was based on a digital terrain model and a best guess on the atmospheric state. A treatment of these processing steps with low and high-altitude AVIRIS 1998 data has been presented in Schläpfer et al. (2000a). In a second iteration of ARIA, the need for an a priori assumption on the atmospheric state could be eliminated; endmember spectra required for the unmixing/re-mixing procedure were selected from ground reflectance measurements in the test imagery area. Bojinski et al. (2002c) describe this ARIA state of affairs. Adding an accuracy assessment, a quantitative comparison to existing aerosol retrieval methods, and the concept of generalized endmembers, a final description of the ARIA method, including processing scheme and proof-of-concept, was finally achieved (Bojinski et al., 2002d), and is

included in chapter 4.

### 1.6.3 Personal Bibliography

**Bojinski, S.**, Schaepman, M., Schläpfer, D., and Itten, K. (2002a). SPECCHIO: a web-accessible spectral database for the administration of heterogeneous campaign data. In *Proceedings of the 2nd EARSeL Workshop on Imaging Spectroscopy, Enschede, 11-13 July 2000.* EARSeL, Paris, France. 8 pp., CD-ROM.

**Bojinski, S.**, Schaepman, M., Schläpfer, D., and Itten, K. (2002b). SPECCHIO: a web-accessible database for the administration and storage of heterogeneous spectral data. *ISPRS Journal of Photogrammetry & Remote Sensing*, 57(3):204-211.

**Bojinski, S.**, Schläpfer, D., Schaepman, M., and Keller, J. (2002c). Aerosol mapping over rugged heterogeneous terrain with imaging spectrometer data. In *SPIE Imaging Spectrometry VIII*, volume 4816, pages 108-119, Bellingham, Washington, USA.

**Bojinski, S.**, Schläpfer, D., Schaepman, M., Keller, J., and Itten, K. (2002d). Aerosol mapping over land with imaging spectroscopy using spectral autocorrelation. *Remote Sensing of Environment.* Submitted.

**Bojinski, S.**, Schaepman, M., Schläpfer, D., and Itten, K. (2003). SPECCHIO: a spectrum database for remote sensing applications. *Computers & Geosciences*, 29(1):27-38.

Schläpfer, D., **Bojinski, S.**, Schaepman, M., and Richter, R. (2000a). Combination of geometric and atmospheric correction for AVIRIS data in rugged terrain. In Green, R.O., editor, *Proceedings of the Ninth JPL Airborne Earth Science Workshop*, volume 1, pages 429-436, Pasadena, California, USA.

Schläpfer, D., Schaepman, M., **Bojinski, S.**, and Börner, A. (2000b). Calibration and Validation Concept for the Airborne PRISM Experiment (APEX). *Canadian Journal of Remote Sensing/Journal canadien de télédétection*, 26(5):455-465.

Schläpfer, D., **Bojinski, S.**, and Schaepman, M. (2002). Radiometric Performance Requirements for Optimal Atmospheric Processing of Hyperspectral Imagery. In *Proceedings of the 2nd EARSeL Workshop on Imaging Spectroscopy, Enschede, 11-13 July 2000.* EARSeL, Paris, France. 9 pp., CD-ROM.

Schaepman, M., Dangel, S., Kneubühler, M., Schläpfer, D., **Bojinski, S.**, Brazile, J., Kötz, B., Strub, G., Kohler, R., Popp, Ch., Schopfer, J., and Itten, K. (2002a). Quantitative Field Spectroscopic Measurement Instrumentation and Techniques. In *Proceedings 1st EPFS Workshop on Field Spectrometry.* NERC, Southampton, UK. 13 pp., CD-ROM.

Schaepman, M., Schläpfer, D., Brazile, J., and **Bojinski, S.** (2002b). Processing of large-volume airborne imaging spectrometer data: the APEX approach. In *SPIE Imaging Spectrometry VIII*, volume 4816, pages 72-76, Bellingham, Washington, USA.

## References

Anger, C., Babey, S., and Adamson, R. (1990). A new approach to imaging spectroscopy. In *SPIE Imaging Spectroscopy of the Terrestrial Environment*, volume 1298, pages 72–86, Bellingham, Washington, USA.

Ansmann, A. (1999). Lindenberg aerosol characterization experiment LACE 98. In *Proceedings European Aerosol Conference 1999*, volume 30, pages 219–220. Elsevier, Amsterdam, The Netherlands.

Baltensperger, U. (1997). Analysis of aerosols. *Chimia*, 51(10):686–689.

Baltensperger, U. and Nyeki, S. (1998). *Atmospheric aerosols*, chapter 7, pages 280–330. Blackie Academic & Professional, London, UK.

Berk, A., Bernstein, L., and Robertson, D. (1989). MODTRAN: a moderate resolution model for LOWTRAN7. Technical report, Spectral Sciences Inc., Burlington, Massachusetts, USA. 38 pp.

Bojinski, S., Schaepman, M., Schläpfer, D., and Itten, K. (2002a). SPECCHIO: A web-accessible database for the administration and storage of heterogeneous spectral data. *ISPRS Journal of Photogrammetry and Remote Sensing*, 57(3):204–211.

Bojinski, S., Schaepman, M., Schläpfer, D., and Itten, K. (2002b). SPECCHIO: A web-accessible spectral database for the administration of heterogeneous campaign data. In *Proceedings of the 2nd EARSeL Workshop on Imaging Spectroscopy, Enschede, 11-13 July 2000*. EARSeL, Paris, France. 8 pp., CD-ROM.

Bojinski, S., Schaepman, M., Schläpfer, D., and Itten, K. (2003). SPECCHIO: a spectrum database for remote sensing applications. *Computers and Geosciences*, 29(1):27–38.

Bojinski, S., Schläpfer, D., Schaepman, M., and Keller, J. (2002c). Aerosol mapping over rugged heterogeneous terrain with imaging spectrometer data. In *SPIE Imaging Spectrometry VIII*, volume 4816, pages 108–119, Bellingham, Washington, USA.

Bojinski, S., Schläpfer, D., Schaepman, M., Keller, J., and Itten, K. (2002d). Aerosol mapping over land with imaging spectroscopy using spectral autocorrelation. *Remote Sensing of Environment*. Submitted.

Bukowiecki, N., Dommen, J., Prévôt, A., Richter, R., Weingartner, E., and Baltensperger, U. (2002). A mobile pollutant measurement laboratory — measuring gas phase and aerosol ambient concentrations with high spatial and temporal resolution. *Atmospheric Environment*, 36:5569–5579.

Charlson, R., Schwartz, S., Hales, J., Cess, R., Coakley, J., Hansen, J., and Hofmann, D. (1992). Climate forcing by anthropogenic aerosols. *Science*, 255:423–430.

CHRIS (2002). *CHRIS-on-PROBA Mission web page*. [http://www.chris-proba.org.uk].

Clark, R. (1990). High spectral resolution reflectance spectroscopy of minerals. *Journal of Geophysical Research*, 95(B8):12653–12680.

Cocks, T., Jenssen, R., Stewart, A., Wilson, I., and Shields, T. (1998). The HyMap airborne hyperspectral sensor: System, calibration, and performance. In *Proceedings of the 1st EARSeL Workshop on Imaging Spectrometry, Zürich, 6-8 October 1998*, pages 37–42. EARSeL, Paris, France.

d'Almeida, G., Koepke, P., and Shettle, E. (1991). *Atmospheric Aerosols: Global Climatology and Radiative Characteristics*. Deepak, Hampton, Virginia, USA. 561 pp.

Diner, D. and Martonchik, J. (1985). Atmospheric transmittance from spacecraft using multiple view angle imagery. *Applied Optics*, 24(21):3503–3511.

Fraser, R. (1976). Satellite measurements of mass of Saharan dust in the atmosphere. *Applied Optics*, 15:2471–2479.

Gao, B., Montes, M., Ahmad, Z., and Davis, C. (2000). Atmospheric correction algorithm for hyperspectral remote sensing of ocean color from space. *Applied Optics*, 39(6):887–896.

Gobron, N., Pinty, B., Verstraete, M., Martonchik, J., Knyazikhin, Y., and Diner, D. (2000). Potential of multiangular spectral measurements to characterize land surfaces: conceptual approach and exploratory application. *Journal of Geophysical Research*, 105(D13):17539–17549.

Goetz, A., Vane, G., Solomon, J., and Rock, B. (1985). Imaging spectrometry for Earth remote sensing. *Science*, 228(4704):1147–1153.

Gordon, H. (1978). Removal of atmospheric effects from satellite imagery of the oceans. *Applied Optics*, 17(10):1631–1636.

Gordon, H. and Wang, M. (1994). Retrieval of water-leaving radiance and aerosol optical thickness over the oceans with SeaWiFS: a preliminary algorithm. *Applied Optics*, 33(3):443–452.

Green, R., Eastwood, M., Sarture, C., Chrien, T., Aronsson, M., Chippendale, B., Faust, J., Pavri, B., Chovit, C., Solis, M., Olah, M., and Williams, O. (1998). Imaging spectroscopy and the airborne visible/infrared imaging spectrometer (AVIRIS). *Remote Sensing of Environment*, 65:227–248.

Houghton, J., Ding, Y., Griggs, D., Noguer, M., van der Linden, P., Dai, X., Maskell, K., and Johnson, C., editors (2001). *Climate Change 2001: The Scientific Basis. Contribution of Working Group I to the Third Assessment Report of the Intergovernmental Panel on Climate Change*. Cambridge University Press, Cambridge, UK and New York, New York, USA. 881 pp.

Hunt, G. (1977). Spectral signatures of particulate minerals in the visible and near infrared. *Geophysics*, 42(3):501–513.

Isakov, V., Feind, R., Vasilyev, O., and Welch, R. (1996). Retrieval of aerosol spectral optical thickness from AVIRIS data. *International Journal of Remote Sensing*, 17(11):2165–2184.

Kaufman, Y., Karnieli, A., and Tanré, D. (2000). Detection of dust over deserts using satellite data in the solar wavelengths. *IEEE Transactions on Geoscience and Remote Sensing*, 38(1):525–531.

Kaufman, Y. and Sendra, C. (1988). Algorithm for automatic atmospheric corrections to visible and near-IR satellite imagery. *International Journal of Remote Sensing*, 9(8):1357–1381.

Kaufman, Y. and Tanré, D. (1992). Atmospherically resistant vegetation index (ARVI) for EOS-MODIS. *IEEE Transactions on Geoscience and Remote Sensing*, 30(2):261–270.

Kaufman, Y., Tanré, D., and Boucher, O. (2002). A satellite view of aerosols in the climate system. *Nature*, 419:215–223.

Kaufman, Y., Tanré, D., Gordon, H., Nakajima, T., Lenoble, J., Frouin, R., Grassl, H., Herman, B., King, M., and Teillet, P. (1997a). Passive remote sensing of tropospheric aerosol and atmospheric correction for the aerosol effect. *Journal of Geophysical Research*, 102(D14):16815–16830.

Kaufman, Y., Wald, A., Remer, L., Gao, B., Li, R., and Flynn, L. (1997b). The MODIS 2.1-$\mu$m channel-correlation with visible reflectance for use in remote sensing of aerosol. *IEEE Transactions on Geoscience and Remote Sensing*, 35(5):1286–1297.

Kaufman, Y. J. (1987). Satellite sensing of aerosol absorption. *Journal of Geophysical Research*, 92(D4):4307–4317.

King, M., Kaufman, Y., Tanré, D., and Nakajima, T. (1999). Remote sensing of tropospheric aerosols from space: Past, present, and future. *Bulletin of the American Meteorological Society*, 80(11):2229–2259.

Kostkowski, H. (1997). *Reliable Spectroradiometry*. Spectrometry Consulting, La Plata, Massachusetts, USA. 609 pp.

Leroy, M., Deuzé, J. L., Bréon, F. M., Hautecoeur, O., Herman, M., Buriez, J. C., Tanré, D., Bouffiès, S., Chazette, P., and Roujean, J. L. (1997). Retrieval of atmospheric properties and surface bidirectional reflectances over land from POLDER/ADEOS. *Journal of Geophysical Research*, 102(D14):17023–17037.

Liou, K.-N. (1980). *An Introduction to Atmospheric Radiation*. Academic Press, New York, New York, USA. 392 pp.

Lohmann, U. and Feichter, J. (2001). Can the direct and semi-direct aerosol effect compete with the indirect effect on a global scale? *Geophysical Research Letters*, 28(1):159–161.

Martonchik, J., Diner, D., Kahn, R., Ackerman, T., Verstraete, M., Pinty, B., and Gordon, H. (1998). Techniques for the retrieval of aerosol properties over land and ocean using multiangle imagery. *IEEE Transactions on Geoscience and Remote Sensing*, 36(4):1212–1227.

Mishchenko, M., Geogdzhayev, I., Cairns, B., Rossow, W., and Lacis, A. (1999). Aerosol retrievals over the ocean by use of channels 1 and 2 AVHRR data: sensitivity analysis and preliminary results. *Applied Optics*, 38(36):7325–7341.

Mustard, J., Staid, M., and Fripp, W. (2001). A semianalytical approach to the calibration of AVIRIS data to reflectance over water, application in a temperate estuary. *Remote Sensing of Environment*, 75:335–349.

Quinn, P., Coffman, D., Kapustin, V., Bates, T., and Covert, D. (1998). Aerosol optical properties in the marine boundary layer during the first aerosol characterization experiment (ACE1) and the underlying chemical and physical aerosol properties. *Journal of Geophysical Research*, 103(D13):16547–16563.

Ramanathan, V., Crutzen, P., Kiehl, J., and Rosenfeld, D. (2001a). Aerosols, climate, and the hydrological cycle. *Science*, 294:2119–2124.

Ramanathan, V., Crutzen, P., Lelieveld, J., Mitra, A., Althausen, D., Anderson, J., Andreae, M., Cantrell, W., Cass, G., Chung, C., Clarke, A., Coakley, J., Collins, W., Conant, W., Dulac, F., Heintzenberg, J., Heymsfield, A., Holben, B., Howell, S., Hudson, J., Jayaraman, A., Kiehl, J., Krishnamurti, T., Lubin, D., McFarquhar, G., Novakov, T., Ogren, J., Podgorny, I., Prather, K., Priestley, K., Prospero, J., Quinn, P., Rajeev, K., Rasch, P., Rupert, S., Sadourny, R., Satheesh, S., Shaw, G., Sheridan, P., and Valero, F. (2001b). The Indian Ocean Experiment: An integrated assessment of the climate forcing and effects of the great Indo-Asian haze. *Journal of Geophysical Research*, 106(D22):28371–28399.

Richter, R. (1996). A spatially adaptive fast atmospheric correction algorithm. *International Journal of Remote Sensing*, 17(6):1201–1214.

Richter, R. (1998). Correction of satellite imagery over mountaineous terrain. *Applied Optics*, 37(18):4004–4014.

Richter, R. and Schläpfer, D. (2002). Geo-atmospheric processing of airborne imaging spectrometry data. Part 2: atmospheric/topographic correction. *International Journal of Remote Sensing*, 23(13):2631–2649.

Roberts, D., Gardner, M., Church, R., Ustin, S., Scheer, S., and Green, R. (1998). Mapping chaparral in the Santa Monica Mountains using multiple endmember spectral mixture models. *Remote Sensing of Environment*, 65(3):267–279.

Roberts, D., Green, R., and Adams, J. (1997). Temporal and spatial patterns in vegetation and atmospheric properties from AVIRIS. *Remote Sensing of Environment*, 62:223–240.

Salisbury, J., Walter, L., Vergo, N., and D'Aria, D. (1991). *Infrared (2.1-25 micrometers) Spectra of Minerals*. Johns Hopkins University Press, Baltimore, Maryland, USA. 294 pp.

Santer, R., Carrere, V., Dubuisson, P., and Roger, J. (1999). Atmospheric correction over land for MERIS. *International Journal of Remote Sensing*, 20(9):1819–1840.

Schaepman, M., Dangel, S., Kneubühler, M., Schläpfer, D., Bojinski, S., Brazile, J., Kötz, B., Strub, G., Kohler, R., Popp, C., Schopfer, J., and Itten, K. (2002a). Quantitative field spectroscopic measurement instrumentation and techniques. In *Proceedings 1st EPFS Workshop on Field Spectrometry*. NERC, Southampton, UK. 13 pp., CD-ROM.

Schaepman, M., Schläpfer, D., Brazile, J., and Bojinski, S. (2002b). Processing of large-volume airborne imaging spectrometer data: the APEX approach. In *SPIE Imaging Spectrometry VIII*, volume 4816, pages 72–79, Bellingham, Washington, USA.

Schläpfer, D., Bojinski, S., and Schaepman, M. (2002). Radiometric performance requirements for optimal atmospheric processing of hyperspectral imagery. In *Proceedings of the 2nd EARSeL Workshop on Imaging Spectroscopy, Enschede, 11-13 July 2000*. EARSeL, Paris, France. 9 pp., CD-ROM.

Schläpfer, D., Bojinski, S., Schaepman, M., and Richter, R. (2000a). Combination of geometric and atmospheric correction for AVIRIS data in rugged terrain. In Green, R. O., editor, *Proceedings of the Ninth JPL Airborne Earth Science Workshop*, volume 1, pages 429–436, Pasadena, California, USA.

Schläpfer, D., Schaepman, M., Bojinski, S., and Börner, A. (2000b). Calibration and validation concept for the Airborne PRISM Experiment (APEX). *Canadian Journal of Remote Sensing/Journal canadien de télédétection*, 26(5):455–465.

Seinfeld, J. and Pandis, S. (1998). *Atmospheric Chemistry and Physics*. Wiley, New York, New York, USA. 1326 pp.

Shettle, E. and Fenn, R. (1979). Models for the aerosols of the lower atmosphere and the effects of humidity variations on their optical properties. Technical Report AFGL-TR-79-0214, Air Force Geophysics Laboratory, Hanscom AFB, Massachusetts, USA. 94 pp.

Strobl, P., Müller, A., Schläpfer, D., and Schaepman, M. (1997). Laboratory calibration and in-flight validation of DAIS 7915 data. In *SPIE Algorithms for Multispectral and Hyperspectral Imagery III*, volume 3071, pages 225–236, Bellingham, Washington, USA.

Tanré, D., Herman, M., and Deschamps, P. (1983). Influence of the atmosphere on space measurements of directional properties. *Applied Optics*, 22(5):733–741.

Tanré, D., Herman, M., and Kaufman, Y. (1996). Information on aerosol size distribution contained in solar reflected spectral radiances. *Journal of Geophysical Research*, 101(D14):19043–19060.

Tanré, D., Herman, M., and Mattoo, S. (1997). Remote sensing of aerosol properties over oceans using the MODIS/EOS spectral radiances. *Journal of Geophysical Research*, 102(D14):16971–16988.

Tanré, D., Holben, B. N., and Kaufman, Y. J. (1992). Atmospheric correction algorithm for NOAA-AVHRR products: Theory and application. *IEEE Transactions on Geoscience and Remote Sensing*, 30(2):231–248.

Torres, O., Bhartia, P., Herman, J., Ahmad, Z., and Gleason, J. (1998). Derivation of aerosol properties from satellite measurements of backscattered ultraviolet radiation: theoretical basis. *Journal of Geophysical Research*, 103(D14):17099–17110.

Twomey, S. (1977a). *Atmospheric Aerosols*. Elsevier, Amsterdam, The Netherlands. 302 pp.

Twomey, S. (1977b). *Introduction to the mathematics of inversion in remote sensing and indirect measurements*. Dover, Mineola, New York, USA. 243 pp.

UNEP and C4 (2002). The Asian brown cloud: Climate and other environmental impacts. Technical report, UNEP Nairobi, Kenya. 7 pp.

Ungar, S. (2002). Overview of the Earth Observing One (EO-1) mission. In *Proceedings of the IEEE International Geoscience and Remote Sensing Symposium,*

*Toronto, Canada, 24-28 June 2002*. IEEE, New York, New York. 4 pp., CD-ROM.

Veefkind, J. and de Leeuw, G. (1998). A new algorithm to determine the spectral aerosol optical depth from satellite radiometer measurements. *Journal of Aerosol Science*, 29:1237–1248.

Veefkind, J., de Leeuw, G., Stammes, P., and Koelemeijer, R. (2000). Regional distribution of aerosol over land derived from ATSR-2 and GOME. *Remote Sensing of Environment*, 74:377–386.

Weingartner, E., Nyeki, S., and Baltensperger, U. (1999). Seasonal and diurnal variation of aerosol size distributions ($10 < d < 750$ mm) at a high-alpine site (Jungfraujoch 3580 m asl). *Journal of Geophysical Research*, 104(D21):26809–26820.

Wilson, R. and Spengler, J. (1996). *Particles in our air: concentrations and health effects*. Harvard University Press, Cambridge, Massachusetts, USA. 300 pp.

Wiscombe, W. (1980). Improved Mie scattering algorithms. *Applied Optics*, 19(9):1505–1509.

Zhang, J., Christopher, S., and Holben, B. (2001). Intercomparison of smoke aerosol optical thickness derived from GOES 8 imager and ground-based sun photometers. *Journal of Geophysical Research*, 106(D7):7387–7397.

# 2

# SPECCHIO: a Web-accessible Database for the Administration and Storage of Heterogeneous Spectral Data

*This chapter has been published as: S. Bojinski, M. Schaepman, D. Schläpfer, and K. Itten, 2002. SPECCHIO: a web-accessible database for the administration and storage of heterogeneous spectral data. ISPRS Journal of Photogrammetry & Remote Sensing, 57(3):204-211.*

## Abstract

The administration of spectral remote sensing data is a key factor for thorough, comparative analyses which take into account the entire information available to the investigator. Today, a great variety of spectrometers operate in the field, giving rise to a strong heterogeneity in data and meta data formats. For a holistic view on these data, a spectrum database must adhere to certain principles: independence of file format, flexibility to attribute changes, establishment of relations between data, content-based search capability, common interfaces, and scalability. SPECCHIO as a web-accessible spectrum database represents a new approach that incorporates the mentioned principles and overcomes the drawbacks of file-based solutions. It is based on a relational data model and provides a prototype that accounts for the complexity of heterogeneous spectral data. SPECCHIO can be used for administration and storage purposes, as well as for online data inspection. It may also serve as a reference database for the characterization of Earth surface targets.

## 2.1 Introduction

The high diversity of spectral measurements in remote sensing gives rise to a great variety of spectral data as well as meta data formats, where the latter describe the former by a set of attributes. Meta data, e.g. date and location of a measurement, are

frequently being stored in a file header, which is defined by some standard. There are several examples of format standards for spectral data other than columnar ASCII, such as HDF-EOS (NCSA, 2002), JCAMP (McDonald and Wilks, 1988), or ENVI spectral library (Research Systems Inc., 2000a).

Along with a file-based organization of the data comes a file system tree that provides a logical organizational structure. However, experience shows many limitations of this approach, especially for large amounts of data, as it poorly represents the whole complexity of information prevailing in remote sensing applications. As an example, given spectral measurements from many field campaigns, users can easily lose sight of the entirety of information available to them. For a comprehensive analysis of spectra, an intercomparison of data from different sensors is desired, but hard to achieve in practice. Even if spectra and meta data are available online, effective queries and compact downloads remain a challenge in file-based solutions. Most of the references given in section 2.2 of this work, however, use the file-based method of data administration.

Six principles can be identified that are to be fulfilled by a spectrum database that account for the heterogeneity of spectral remote sensing data: independence of file format, flexibility to attribute changes, establishment of relations between data, content-based search capability, common interfaces, and scalability.

In this paper, we present the spectrum database SPECCHIO (SPECtral Input Output) as a new prototype that matches the above mentioned criteria. It consists of a relational database system and appropriate user interfaces, script template-based and web-based. Section 2.3 presents the technology, section 2.4 the conceptual side of the system. Section 2.5 provides an insight to the interfaces to the database, followed by an outlook that outlines applications for SPECCHIO in remote sensing.

## 2.2 Overview of Spectral Remote Sensing Data Resources

There exists a large number of online remote sensing data archives that can be accessed by the scientific or commercial user to query and order the data needed. For the most part, these sites are set up by the data distibutor for a particular sensor or mission (e.g. USGS (2002a), DLR (2002)), and provide very large collections of airborne or spaceborne spectral scenes. The granularity of data is usually at scene level and does not break down spectral information to the single spectrum.

Only two publicly accessible sites, that contain single spectra retrievable in ASCII format, could be identified: the USGS Denver Spectroscopy Lab (Clark et al., 1993), (USGS, 2002b), which focuses on mineral spectra, and the ASTER Spectral Library (JPL, 2002), which includes about 2000 spectral entries from natural and man-made materials. Price (1995) created an offline collection of over 3400 spectra with reference character from various sources in ASCII format. These spectral collections are all file system-based. MedSpec (Preissler et al., 1998) is a standalone spectrum database solution that features a large number of meta data attributes for campaign data. It allows input and query of spectral data in ASCII format only, as well as of ancillary data.

## 2.3 SPECCHIO: Technology

Web access to databases is generally being established by (1) an application programming interface that enables communication between a programming language and a database, and (2) a method to call executable programs on a web server. As for (1), the scripting language TCL (Ousterhout, 1994) with a database interface extension is used to process structured query language (SQL) database queries. (2) has been implemented using the Common Gateway Interface (CGI) (Gundavaram, 1996) for web servers as provided by the Webshell (WEBSH, 2002) web application interface. All of these programming tools except the database software, are developed and distributed as Open Source software (OSI, 2002).

We use this approach for reasons of implementation speed and ease of maintenance. It uses the standard HTTP protocol for all communication between client and server. Users supply query or update parameters by means of HTML forms, and these parameters are sent in HTTP to the web server, which calls a CGI program to interpret the request and establish a connection to the SPECCHIO database. The query results provided by the database are encoded in HTML documents and returned to the client. Afterwards, it is possible to select individual datasets for run-time generated graphics display in the browser window, technically realized by a background process that generates GIF files, and for download to the local file system.

In many scientific applications, automated processing tasks are called for, performed by executable scripts. This gives rise to a script-based feed and query option to access the database. These scripts directly connect to the database and execute the requested transactions. Output is written into files on the local file system.

The relational database system Oracle 8i (Oracle, 2002), accessed by transactions coded in embedded SQL, is particularly suited for the consistent and reliable storage and backup of large amounts of data. Processing and display of spectral data has been implemented with IDL (Research Systems Inc., 2000b). Currently, SPECCHIO runs on a UNIX/Sun Solaris system with an Apache web server.

## 2.4 SPECCHIO: Data Model

The major goal of SPECCHIO in terms of data description is breaking down the 'spectral remote sensing data' aspect of reality to a data model in order to manage all spectral remote sensing data and meta data within one single relational database instance. In doing so, data security issues can be delegated to the database management system, such as the integrity of data, access control, consistency, and the recovery of data in case of hardware failure. Furthermore, the stored information can be efficiently retrieved by SQL statements.

In every relational database, all information is stored in two-dimensional tables that consist of columns and rows. Tables represent semantic entities, columns semantic attributes of an entity, and rows the actual datasets. Data cells that are defined by column name and row number contain atomic values. The data model consists of entities, that are specified by attributes and logically related by primary and foreign keys, all of which can be displayed in an entity-relationship diagram (Fig. 2.1). The relations are in the 3rd normal form to preclude update anomalies (Date, 1995).

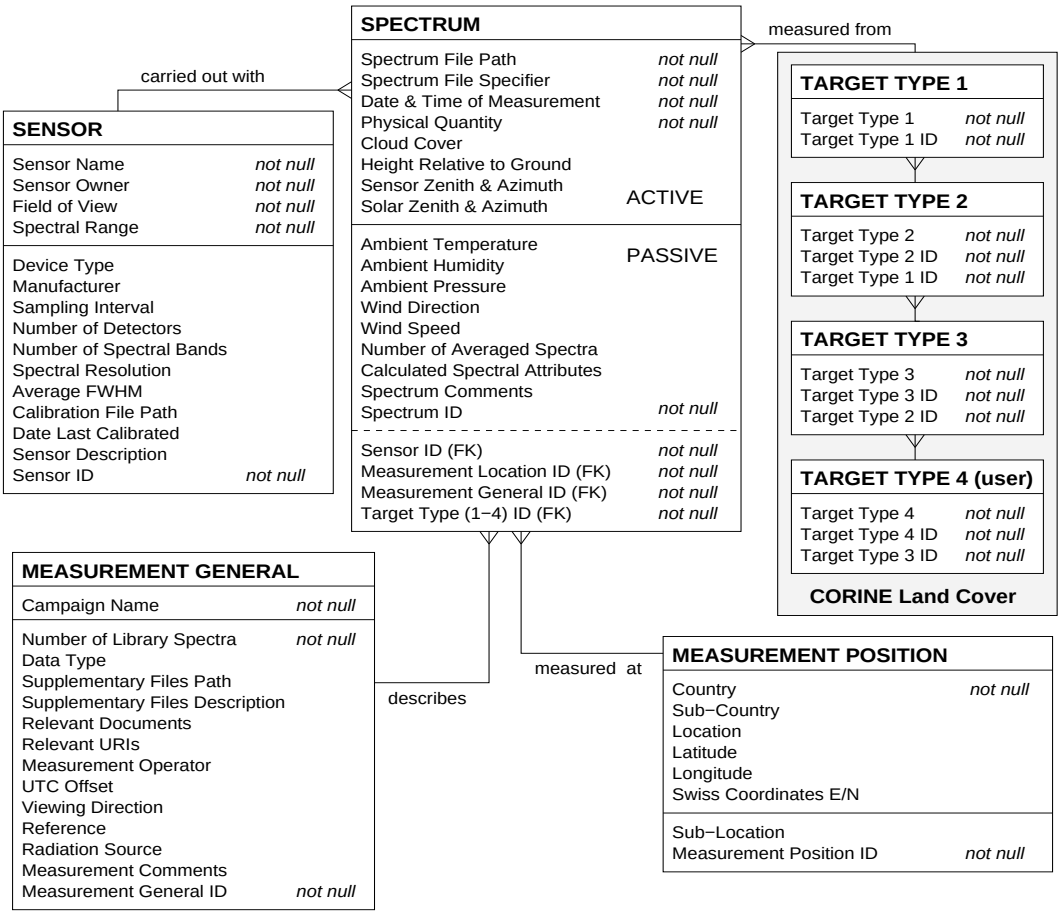


Figure 2.1: Entity-relationship diagram reflecting the data model, which describes the "spectral remote sensing data" aspect of reality. The principal "Spectrum" table is related to the surrounding tables by foreign keys (FK) defined on the respective IDs. "Active" attributes can be queried as opposed to "Passive" attributes. not null tags denote compulsory attributes. The hierarchical target type structure (Target Type 1-3) represents the CORINE Land Cover Schema (European Commission DG XI, 1993).

Grouped around the main entity "Spectrum" are four other entities that contain meta data, "Sensor", "Measurement General", "Measurement Position", and "Target Type", that are related to "Spectrum" by $1 : n$-relations. This means that each "Spectrum" dataset is uniquely related to exactly one entry in the "Sensor" table, "Measurement General" table, etc. Vice versa, an entry in the "Sensor" table can be related to one or many entries in the "Spectrum" table, and accordingly. As a result, a new entry into SPECCHIO is equivalent to $m \geq 1$ entries or updates in the "Spectrum" table, associated with $m \leq n$ entries or updates in each meta data table. Within each entity, a distinction is made between active and passive attributes. Active attributes can be queried in the query interfaces, passive ones come along as the result of a query transaction, but cannot be queried in their own right. As a quality control measure for the database, a number of attributes has been defined as not null, i.e., they must be stated at all times.

SPECCHIO stores data independent of sensor types and file formats. The actual

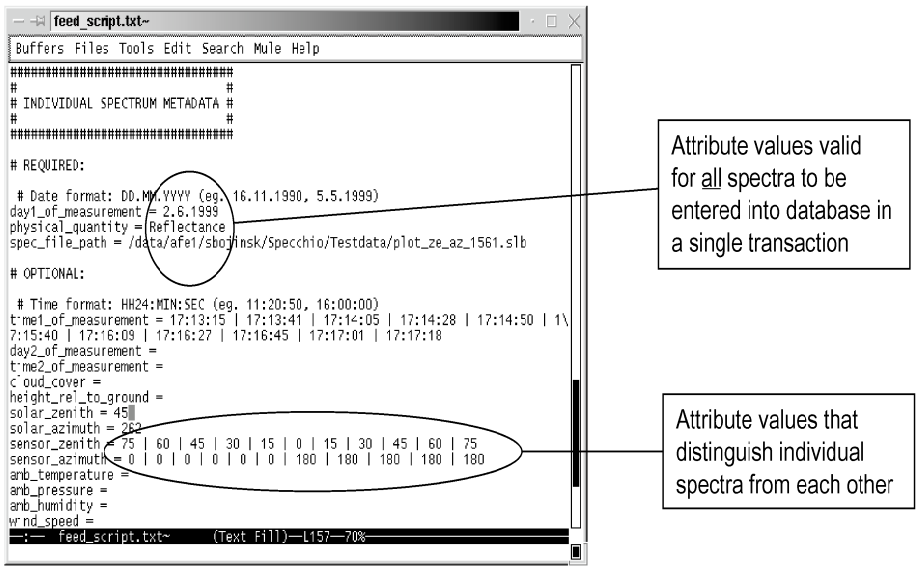


Figure 2.2: Feed input file syntax.

data defining the physical quantity of the spectrum physically remain outside the database, addressed online by a file location pointer, or offline by an external medium identifier. This concept makes the database server a "thin" server. Access to the database is provided by scripts as well as by standard web browsers, which are shown in section 2.5.

## 2.5 Interfaces to SPECCHIO

Interaction with the SPECCHIO database instance is intended to be easy to implement and widely usable. For remote and interactive access, dynamically created web forms provide a universal way to communicate with the database via a standard browser. Alternatively, for automated tasks, predefined script templates can be employed.

### 2.5.1 Feed Data

The web-based feed site grants a user-friendly possibility to enter information into the database. Returned dynamically by the server, the feed site shows the current range of values already present in the database for attributes with relatively small semantic variation. This feature reduces semantic redundancies, i.e. different concepts with the same meaning are prevented from being entered and conceived as different by the database. For data quality reasons, it is advisable to give as many attributes as possible, though some are compulsory and denoted as such. Currently, the implementation is mainly intended for small numbers of spectra to be entered. The issue

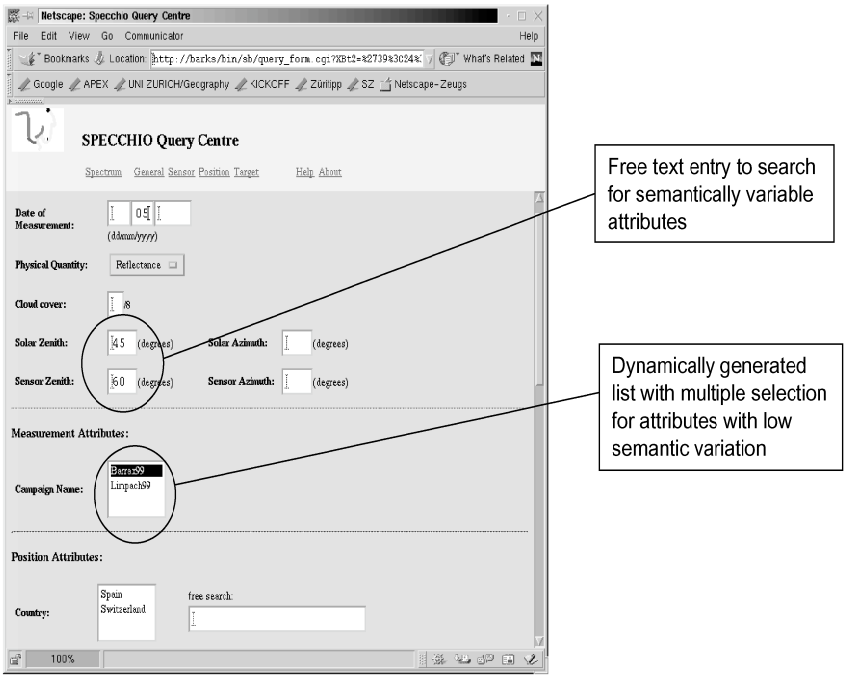


Figure 2.3: Query web site with different attribute input modes.

of large spectral sets in which individual spectra differ only in one or two attributes (e.g. sensor angles) is still to be considered closely.

The script-based feed is mainly intended for automated or large-scale input to the database (Fig. 2.2). It is currently optimized for spectra in the ENVI spectral library format. In principle though, any set of spectra stored in a number-distinguishable way can be entered, as they are automatically allocated a spectral specifier.

The feed web site may also serve as a database view to support the script-based alternative in terms of semantic redundancy. This means that users can look at existing attribute values in the database (e.g. "Switzerland" as value for the attribute "Country" in the "Measurement Position" entity) and align their feed script terminology accordingly.

### 2.5.2 Query Data

The majority of SPECCHIO users may have questions directed to the database, that are translated into a combination of selected attributes. For example,

- Who measured GER 3700 barley spectra in 1997, and how exactly were they measured?
- Show me all the grass spectra measured at sensor angle 45 degrees!
- Compare all bare soil spectra measured with the ASD device during the Barrax campaign!

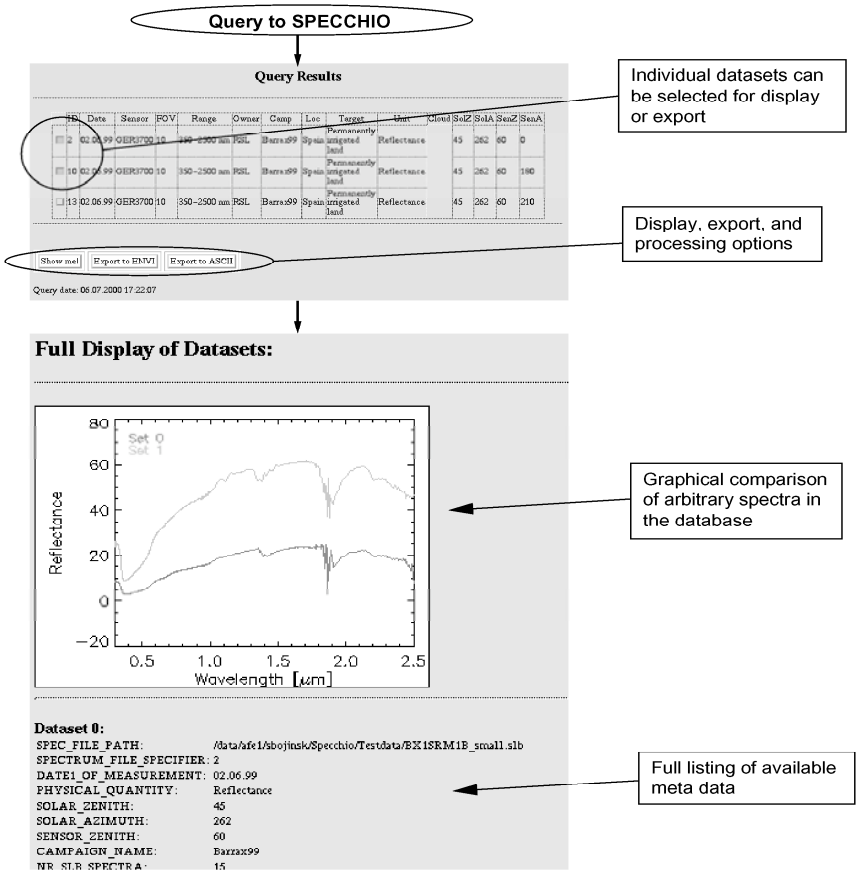


Figure 2.4: Query and display of spectral data.

For fast and possibly automated query of the database, a script solution exists, which is syntactically similar to the feed script. The output consists of a text file containing a list of datasets that match the search criteria, including all the associated meta data.

The web site allows an interactive one-step query set-up for a selection of attributes which are considered to be most important (see Fig. 2.3). Due to procedural modular internal programming, the appearance of the query site can be altered easily. Some multiple attribute lists are dynamically generated and form an up-to-date and distinct selection of attribute values, enabling more precise searching, as opposed to free text entries.

For both query interfaces, a specification of different attributes is logically equivalent to a Boolean AND operator; a multiple statement within a single attribute corresponds to an OR operator. If the web site query yields datasets that match the search criteria, a clickable table shows up with columns corresponding to the searchable attributes (cf. Fig. 2.4). It is then possible to select datasets for graphical display and full statement of all associated meta data, as well as download to the local system. Spectral plots can be chosen as single curves or overplots of all the selected spectra. The display feature as well as the export of spectral files to a file

system is currently enabled for ENVI spectral library and two-column ASCII data formats.

### 2.5.3 Advanced Features

For the moment, query and feed interfaces to the database are implemented on a prototype level. In many applications of imagin spectrometer data, a demand for information on spectral features or the statistics of spectral ensembles arises. Therefore, a low level of processing functionality is going to be added to SPECCHIO, aimed at the retrieval of spectral values for predefined spectral channels, or the calculation of statistical key values. The latter can as well be stored in the database to save processing time in subsequent applications. Accordingly, biophysical parameters, such as leaf area index (LAI), can be calculated for a selection of spectra and subsequently stored.

SPECCHIO truly serves as a reference database, once the full range of statistical functions exists. Another planned feature is the extension of display options after the selection of a query result, which include scaling and resampling of spectra. Lastly, the semi-automated input and output of selected data formats is realized. The routines called by the database to perform calculations are written in IDL or, if time-critical, in C/C++.

## 2.6 Outlook

We have presented a prototype for a web-accessible database for the storage and administration of spectral remote sensing data. After conceptual and technological considerations, a data model has been developed which, to our knowledge, comprehensively represents the field of spectral remote sensing. Large amounts of data with a great variety of meta data can be stored independently of the data format. User interfaces to the database are shown to demonstrate the state-of-the-art functionality of SPECCHIO. Full implementation, documentation, and a users' test phase of the software are the next steps to be taken. The demand for processing features that directly address the physical spectral data gives rise to the development of external routines.

The practical use of SPECCHIO is going to be manifold and beyond mere systematic storage of data: the problem of endmember selection and interpretation in the process of image classification requires reference spectra taken from exemplary targets, which can be automatically drawn from the spectrum database. More specifically, segmentation of imaging spectrometry data and subsequent spectral unmixing of segments can be greatly facilitated. This supports the analysis of bi-directional reflectance properties of the Earth's surface, as well as the characterization of atmospheric variability within imaging spectrometry data.

## Acknowledgements

This work was kindly made possible by a Swiss Science Foundation research grant, contract number 2000-050727.97. We would like to thank two anonymous reviewers

for their valuable comments.

## References

Clark, R., Swayze, G., Gallagher, A., King, T., and Calvin, W. (1993). The U.S. Geological Survey Digital Spectral Library: version 1: 0.2 to 3.0 $\mu$m. Open File Report 93-592, United States Geological Survey, Denver, Colorado, USA. 1340 pp.

Date, C. (1995). *Introduction to Database Systems*. Addison-Wesley, Reading, Massachusetts, USA. 839 pp.

DLR (2002). *Earth Observing System Data Gateway*. German Remote Sensing Data Center (DFD), [http://ims.dfd.dlr.de].

Gundavaram, S. (1996). *CGI Programming on the World Wide Web*. O'Reilly & Associates, Inc., Sebastopol, California, USA. 433 pp.

JPL (2002). *ASTER Spectral Library*. Jet Propulsion Laboratory, Pasadena, California, USA, [http://speclib.jpl.nasa.gov].

McDonald, R. and Wilks, P. (1988). JCAMP-DX: a standard form for exchange of infrared spectra in computer readable form. *Applied Spectroscopy*, 42(1):151–162.

NCSA (2002). *EOSDIS Hierarchical Data Format*. The National Center for Supercomputing Applications, University of Illinois at Urbana-Champaign, Illinois, USA, [http://hdfeos.gsfc.nasa.gov/hdfeos/index.cfm].

Oracle (2002). *Oracle Corporation*. [http://www.oracle.com].

OSI (2002). *Open Source Initiative*. [http://www.opensource.org].

Ousterhout, J. (1994). *Tcl and the Tk Toolkit*. Addison-Wesley, Reading, Massachusetts, USA. 458 pp.

Preissler, H., Bohbot, H., Mehl, W., and Sommer, S. (1998). MedSpec, a spectral database as a tool to support the use of imaging spectrometry data for environmental monitoring. In *Proceedings of the 1st EARSeL Workshop on Imaging Spectrometry, Zürich, 6-8 October 1998*, pages 455–462. EARSeL, Paris, France.

Price, J. (1995). Examples of high resolution visible to near-infrared reflectance spectra and a standardized collection for remote sensing studies. *International Journal of Remote Sensing*, 16(6):993–1000.

Research Systems Inc. (2000a). *ENVI User's Guide, Version 3.4*. Boulder, Colorado, USA. 930 pp.

Research Systems Inc. (2000b). *IDL User's Guide, Version 5.4*. Boulder, Colorado, USA. 320 pp.

USGS (2002a). *EROS Data Center Products*. United States Geological Survey, Sioux Falls, South Dakota, USA, [http://edc.usgs.gov/products/satellite.html].

USGS (2002b). *USGS Denver Digital Spectral Library*. United States Geological Survey, Denver, Colorado, USA, [http://speclab.cr.usgs.gov].

WEBSH (2002). *Webshell Documentation*. [http://tcl.apache.org/websh].

# 3

# SPECCHIO: a Spectrum Database for Remote Sensing Applications

*This chapter has been published as: S. Bojinski, M. Schaepman, D. Schläpfer, and K. Itten, 2003. SPECCHIO: a spectrum database for remote sensing applications. Computers & Geosciences, 29(1):27-38.*

## Abstract

Representative and comprehensive information on the spectral properties of natural and artificial materials on the Earth's surface is highly relevant in aircraft or satellite remote sensing, such as geological mapping, vegetation analysis, or water quality estimation. For this reason, the spectrum database SPECCHIO (Spectral Input/Output) has been developed, offering ready access to spectral campaign data, modelled data, and existing spectral libraries. Web-based and command line interfaces allow for the input of spectral data of heterogeneous formats and descriptions, as well as interactive queries, previews, and downloads. ASCII and ENVI spectral library data formats are currently supported. SPECCHIO is used as a reference database for the retrieval of geophysical and biophysical parameters from remotely sensed data, accounting for the frequent lack of surface spectra. The database is also used for the general management of spectral data, including detailed ancillary data.

## 3.1 Introduction

Spectral measurements from natural and artificial surfaces are a prerequisite for Earth surface and atmospheric remote sensing from nadir-looking airborne or spaceborne optical sensors. Thus, collecting and distributing these data forms the basis for many remote sensing applications, such as geological mapping (Clark, 1990), vegetation analysis (Li et al., 2001), and oceanography (Barnard et al., 1999). Particularly in imaging spectroscopy, a reference spectral collection can improve the characterization and classification of the image by providing endmember spectra (Roberts et al., 1998).

As an example, the classification of mineral samples by direct measurements of the spectral properties is facilitated by external reference data (Hunt, 1977).

In the majority of existing spectral data collections, information is distributed across physical files (Joint Committee on Atomic and Molecular Physics Data Exchange (JCAMP-DX) (McDonald and Wilks, 1988), United States Geological Survey (USGS) ASCII (Clark et al., 1993)). Except for the simplicity of storage, this approach has serious drawbacks, such as limited scalability and low-performance query of data, low flexibility of the descriptive data (meta data) structure, and direct dependence on file formats. In connection with the USGS spectral collection (Clark et al., 1993), these deficiencies have been partially removed by the SPECPR analysis tool (Clark, 1993) which allows spectral feature analyses as well as meta data queries based on regular expressions.

In this work, the spectrum database SPECCHIO (Spectral Input/Output) has been designed and implemented. It represents a large and easily accessible spectrum data source and is designed to overcome the limitations of file-based solutions. SPECCHIO consists of three major components, namely web and command line based user interfaces, an underlying relational database management system (DBMS), and a well-defined data model. The design of these components was guided by expected application requirements from scientists with a focus on imaging spectroscopy. Typical queries to a spectrum database may read:

- Give me all the spectra of calcite!
- Are there any hemispherical spectra available from summer wheat?
- Who measured barley reflectance spectra in 1997, and what was the overall set-up?
- Find all the grass reflectance spectra measured at sensor viewing angle 45 degrees!
- Show me all the bare soil radiance spectra measured during the 'Barrax' campaign!

SPECCHIO is designed to manage heterogeneous data from different sources, taking into account the high diversity of applications for spectral data in imaging spectroscopy. User-generated queries for common properties of spectral data yield result sets with detailed information on each matching spectrum, that can be downloaded to the user's local system. Input interfaces allow users to feed single as well as multiple spectra and associated meta data into the database within a single transaction. The consistency of all input data and requirements on the completeness of data documentation are enforced by conditional rules.

SPECCHIO serves as a spectrum reference database for geophysical and biophysical retrieval algorithms based on remotely sensed data. It can replace the direct measurement of spectra on the spot of interest, data which are seldom available outside a full-scale measurement campaign. For example, for atmospheric correction of airborne or spaceborne spectral images, spectra from the database can substitute in-situ ground target measurements, required as radiative transfer input. In addition,

SPECCHIO is currently employed to manage large bi-directional reflectance spectrum datasets from field campaigns with a multitude of independent measurement parameters.

We consider SPECCHIO a first step towards a complete spectral data collection providing all kinds of interactions that may be required in imaging spectroscopy research. Spectral data from different sources, such as field campaigns, modelling algorithms, and existing spectral libraries, have been entered into the database and are now available online to the user.

## 3.2 Concept

The scientific requirements for SPECCHIO in the field of imaging spectroscopy defined a set of design principles, which are as follows in order of priority:

1. Logical relations and consistency
   Relations are established between spectral attributes, allowing the query for common attributes of spectra. Each spectrum dataset is fully described, complying with prescribed consistency standards. In doing so, semantic redundancy in the database is reduced and data quality preserved.

2. Intuitive interfaces
   Easy data access and handling are a primary goal. Web and command line interfaces shall be best-suited to allow for users database interaction without a priori knowledge. Entering new data may require user instruction, which is entirely given online.

3. Flexibility to changes in science context
   Meta data describe the aspect of reality in which a spectrum is measured. Attributes are labels for meta data. The set of attributes in the database has to provide a sound basis for unambiguous spectrum description. New attributes can be added easily, if required.

4. Independence of file format
   High variety and frequent change of spectral data formats call for maximum flexibility of data input and output. Accordingly, the given I/O interfaces have to be extensible with respect to new spectrum data formats.

5. Scalability
   The amount of spectral data in SPECCHIO shall be limited only by disk size and access to the database. A separation of file and database server guarantees maximum upscaling flexibility.

The development process of the SPECCHIO database followed the rapid prototyping approach using an iterative software life cycle (Leach, 2000). A sequence of requirement, design, implementation, validation, and release phases accompanied by frequent changes in specifications of the individual parts resulted in the current version of the code.

The basic structure of SPECCHIO, defined by the abovementioned principles, is shown in Fig. 3.1. Typical forms of data sources, and examples of application areas for

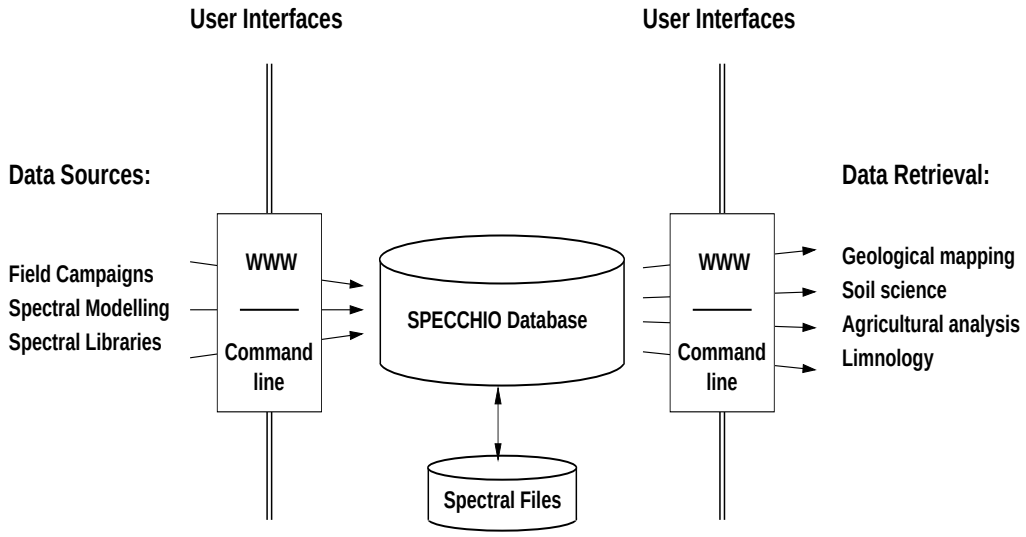


Figure 3.1: Basic layout of SPECCHIO.

retrieved data are given. Web and command line interfaces provide maximum access and input/output flexibility. Due to physical separation of database and spectral files, only meta data are stored in the database itself, uniquely linked to the actual spectral data on a file server.

## 3.3 Implementation

Design principles as given in the previous section gave rise to a concept that prescribed the software implementation process. Data model, data formats, and technology as used in the SPECCHIO application are described in the following sections.

### 3.3.1 Data Model

Data models formally describe the way in which information in databases is organized. A common representation for a data model is an entity-relationship diagram (Date, 1995). In this work, entity properties are referred to as attributes with associated meta data content. A complete set of attributes of one entity is called an instance of that entity.

Fig. 3.2 shows the data model of SPECCHIO. Spectral information is systematically divided up into seven thematic entities, each of which covers a different aspect of the spectrum description. The entity Spectrum contains attributes expected to be most variable between individual spectra, the other entities encompass attributes that are usually common to spectral ensembles. Each instance in the Spectrum entity is related to exactly one spectrum, and uniquely related to exactly one instance in each other entity. Vice versa, the relation between Spectrum and other instances is non-unique. In other words, Spectrum is linked to the entities General, Position, Model, Sensor, Target Type, and Landuse Type by $n$:1 relationships, enforced by referential integrity constraints (foreign keys). Relations are in the third normal

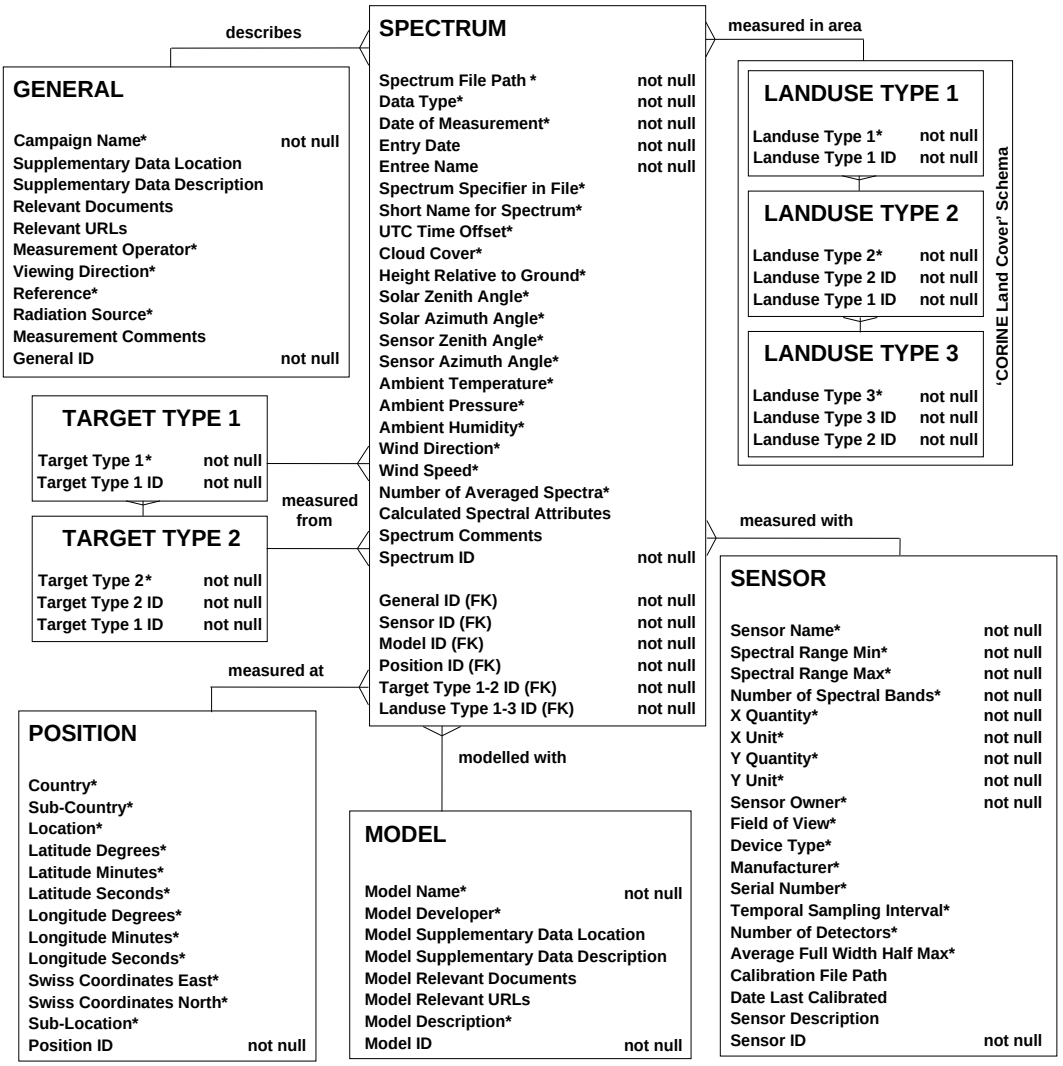


Figure 3.2: Data model of SPECCHIO expressed by an entity-relationship diagram, which describes the spectroradiometric aspect of reality. Identifiers (ID) uniquely define instances in all entities. SPECTRUM is related to other entities by referential constraints (foreign keys, FK) on respective IDs. Forks denote $n$:1 relationships, `not null` tags compulsory attributes, and (*) indicates attribute sets subject to uniqueness in each entity.

form to guarantee consistency and minimize redundancy of the data. This normal form requires for each entity compulsory key attributes (`not null`), specifically defined foreign keys (FK), and uniqueness constraints that apply to the most relevant attributes, as denoted by (*) in Fig. 3.2.

Spectral attributes as given in Fig. 3.2 were defined based on the scientific requirements, particularly in imaging spectroscopy applications, and the review of spectral data descriptions in existing spectral data collections (section 3.4).

Users can freely define instances in all entities, except for the specification of the TARGET TYPE captured by the spectrum, and the LANDUSE TYPE. The target type describes the physical type of object or part of the Earth's surface, and is often

referred to as land cover. Land use represents a subjective, anthropocentric view of a type of target, reflecting its value as natural resource in a spatial context. The two concepts "land use" and "land cover" are often used interchangeably, but shall hereafter be treated as defined above.

The target type can be specified on the lower hierarchy, subordered to a coarse classification of (bio-)physical surfaces on the Earth: artificial, vegetation, rocks/minerals, soil, and water. The pre-defined three-level hierarchy from the "CORINE Land Cover" scheme (European Commission DG XI, 1993) was employed for the land use type and remains unmodified in the database.

Files that contain the actual spectral information physically reside on a disk, accessible by SPECCHIO on a local network, rather than as objects in the database itself. SPECCHIO locates files uniquely via the `spec_file_path` attribute. The separation of DBMS and file storage maintains the integrity of the files, keeps the implementation process simple, and enables swift upscaling of the database.

### 3.3.2 Data Formats

Information about the format of spectrum data is used by SPECCHIO for data display and output. Therefore, this information needs to be provided for input of new data. In principle, this functionality is independent of the data format itself. The interface design is flexible enough to incorporate user-defined display and output routines for any kind of spectrum data format.

A number of file formats for spectrum-type data exists, each of which adapted to certain fields of application. This implies specific ways of organizing data and descriptive meta data in the file structure. Examples are JCAMP-DX (McDonald and Wilks, 1988) in applied spectroscopy, HDF-EOS (Ullman, 1999) for airborne or spaceborne data, ENVI spectral library (Research Systems Inc., 2000a) for spectroscopy data, and certainly all flavours of instrument-specific ASCII file formats.

The implementation of SPECCHIO supports the ENVI spectral library (SLB) and columnar ASCII formats in the current version. SPECCHIO offers programs written in the Interactive Data Language IDL (Research Systems Inc., 2000b) that allow for the conversion of spectral data from spectral collections, field spectrometers, and modelling codes into formats supported by SPECCHIO, considering all pertinent meta data (cf. section 3.4). Once entered into the database, the spectral data can subsequently be queried, displayed, and exported. If a query results in a large number of hits, it is desirable for users to obtain the data in a compact form. The ENVI-SLB file matches that purpose, as it consists of two components: descriptive ASCII header, which contains all meta data, and binary body. It is therefore chosen as the standard output format. If the ASCII export option is selected, export files appear as columnar ASCII, bundled in a tar "tape archive" file (section 3.3.4).

### 3.3.3 Technology

Main technical features of the SPECCHIO database application are depicted in Fig. 3.3. Web access to the Database Management System (DBMS) is generally being established by (1) an application programming interface that enables communication between a programming language and a database, and (2) a method to call executable

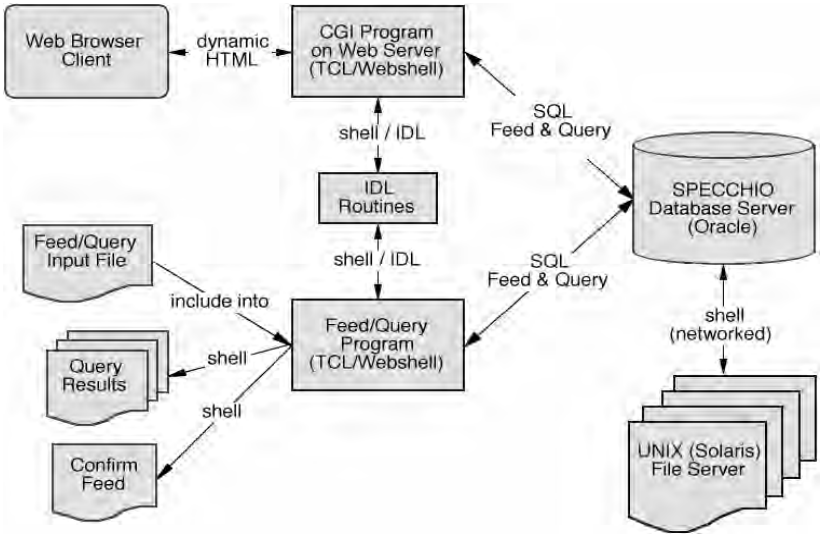


Figure 3.3: Technical layout of SPECCHIO. Two access interfaces are available: web browser-based (A), or script-based (B). The UNIX file server hosts the spectral source files.

programs on a web server. As for (1), the scripting language TCL (Ousterhout, 1994) with the Oratcl (ORATCL, 2002) database interface extension is used to process database queries that comply with the SQL-2 standard. (2) has been implemented using the Common Gateway Interface (CGI) (Gundavaram, 1996) for web servers as provided by the Webshell (WEBSH, 2002) web application interface extension for TCL. All of these programming tools except the Oracle 8i DBMS, are developed and distributed as Open Source software (OSI, 2002). We chose the CGI for reasons of implementation speed and ease of maintenance. It uses the standard HTTP protocol for communication between client (user) and SPECCHIO server. No disk volume requirements are imposed on the client side, and the lack of precise session management is compensated by expected low transaction rates. Dynamically created web pages are coded in HTML4.0 and Javascript. Command line-based user interaction is carried out via pre-defined scripts directly over the local area network. These scripts can be incorporated into other scientific application programs, allowing the interaction with SPECCHIO at run time.

The DBMS capabilities in terms of backup, recovery, and constraint support are crucial for SPECCHIO. In principle though, any equivalent relational database software with an interface to TCL could be used here. Spectral files are stored on a UNIX file server integrated in the local environment of the database server.

Scripts written in IDL are executed at run time for dynamic plotting and exporting of spectrum data. Flexible adaptation of other data formats is possible by adding IDL programs with full display and output capability.

The software at large is server-based and runs on all platforms that support Webshell (e.g., UNIX Solaris, Windows NT).

### 3.3.4 Interfaces

Interfaces to a spectrum reference database have to be intuitive and widely accessible, i.e. suitable for laboratory work as well as in the field. Accordingly, access to the database is twofold: (1) by a standard web browser, and (2) by command line scripts. Users can input and query data via either alternative.
(1) The web interface offers

- online query and visualization of spectra,
- remote download of spectrum data and meta data,
- online views of database content, and
- input of single spectrum datasets and meta data.

(2) Command line scripts allow

- local network based input and query of spectra,
- input of large amounts of spectrum datasets and meta data, and
- embedding of SPECCHIO functionality into other spectral analysis applications.

Operational, frequent users prefer way (2) on the local network of the SPECCHIO installation. Remote interaction on a more infrequent basis, as well as visualization of the current database content is provided by option (1). The following two subsections explain both interfaces in detail.

#### Input Data

Input of new data into SPECCHIO currently requires user authorization for both interfaces, as control over data quality has to be maintained. Access to the database server's local network is necessary as well. The most important attributes to be given on input are

- the file name including full local network path information of the spectrum data file to be read,
- the data format (ASCII or ENVI-SLB), and
- the sensor specification that belongs to the spectrum.

New spectrum meta data can be stated on the web site (Fig. 3.4) in text boxes or clickable menus. Text boxes are used for attributes where high semantic variability is expected. Menus are given for cases with low variation in meta data, or pre-defined selections. A dynamic view of instances of a selected entity (e.g., Sensor) is shown in the lower part of the main frame. Here, entries can be associated with the new spectrum, instead of defining a new instance (e.g., for the Sensor part) in the upper frame. This saves time and reduces semantic redundancy in SPECCHIO. The web

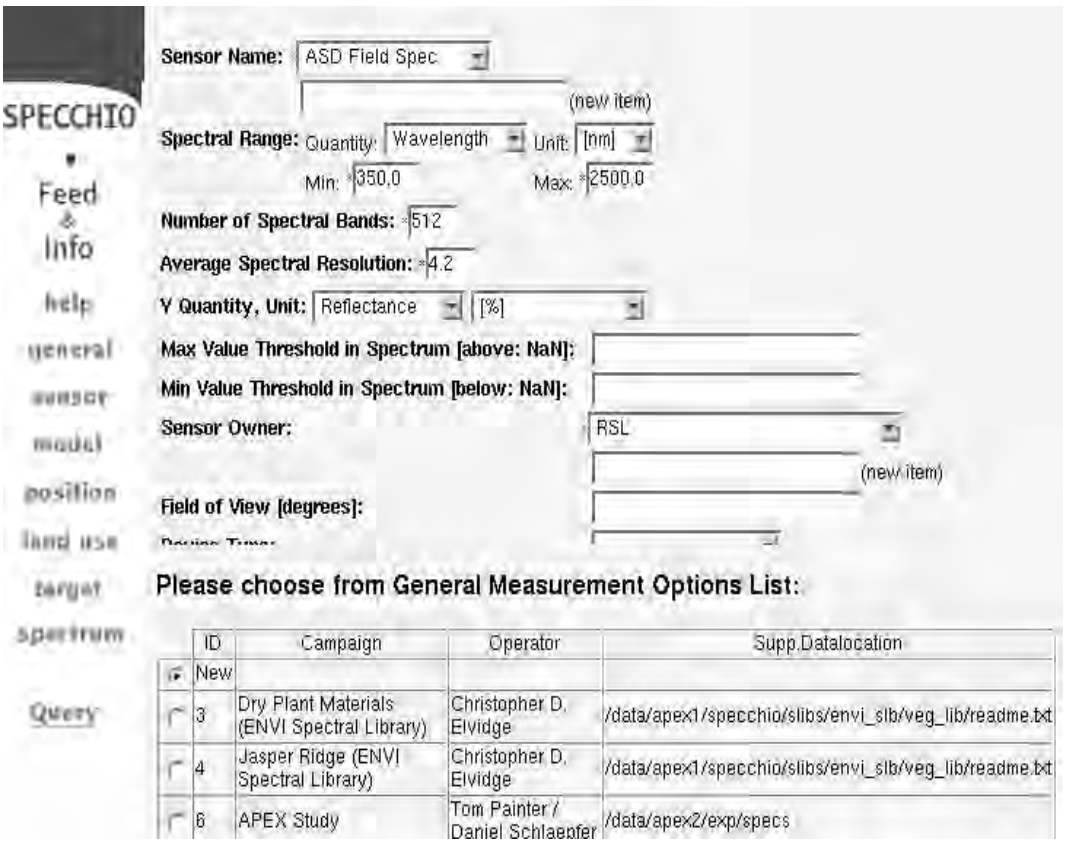


Figure 3.4: Web interface to feed data into SPECCHIO. The lower main frame of the web site also serves as a view on parts of the current database content.

site is updated on every reload so that it always represents the current database content.

Through the command line-based interface, large amounts of spectra can be read with only one input text file, following a prescribed syntax which is exemplary given as follows:

day of measurement = 03.06.1999
time of measurement = 12 : 42|12 : 43|12 : 44|12 : 45
spectral file path = /data/rsl/barrax/spectrum.slb
ambient temperature =
sensor angle = 45|45|45|60

In this example, the spectral file contains four spectra which are assigned different time and sensor angle, identical day, and no temperature information. Generally, multiple attributes as stated in the example have to be consistent in number and are attributed to single spectra. Attributes stated exactly once or not at all apply to the entire set of spectra to be read in. Spectral attributes are divided into compulsory and optional parts. Completeness and consistency of attributes are checked by appropriate statements in the database application, and again verified by key constraints in the

data model (Fig. 3.2). Concerning the target types in SPECCHIO, new entries can only be defined on the lower level of the target type hierarchical structure, and have to be associated with a pre-defined target type of the upper level. New definitions can be made online as well as script-based.

#### Query Data

Querying spectral data using SPECCHIO is free of authentication and feasible for everybody on the web with ordinary browser software. A command line option for local use also exists using a query text file. After submitting the web query, a list of matching spectra is loaded into the browser window, offering previews of spectral plots, as well as the export of spectra in a tar 'tape archive' file (Fig. 3.5). The export dataset is created at run time. To save loading time, a maximum of 10 plots is shown at once. Meta data from each spectrum appear at the bottom of the preview list and are exported as well.

Via the command line interface, the application reads a text file in which a query is made using a particular syntax. This is illustrated by the following example:

country = Spain
day of measurement = ∗06.1999
operator = Beisl | Strub

This text file fragment results in a query that looks for spectra measured in Spain AND measured sometime in June 1999 AND collected by operators Beisl OR Strub. Generally, Boolean logic is coded by stating the appropriate attribute and using the operator syntax as given by the example. As a result of the query, users can load the matching datasets into their current working directory.

The granularity of SPECCHIO data output in ENVI-SLB format, i.e., the effective number of files that make up the result of a query, is determined by the Sensor definition of the matching spectra. This definition contains spectral resolution, physical units, and spectral range of the data, i.e. no resampling or rescaling is performed in the current version.

In case of ASCII output, the tape archive file contains each spectrum represented as a single file.

## 3.4 Examples for Input Data

In this section, the storage and access capabilities of SPECCHIO with regard to heterogeneous spectrum data is demonstrated. The flexibility of our data model is shown by translating the characteristics of existing spectral library data, field campaign data, and modelled data into appropriate sets of meta data that are subsequently entered into SPECCHIO. The database is perfectly able to accommodate laboratory campaign data as well.

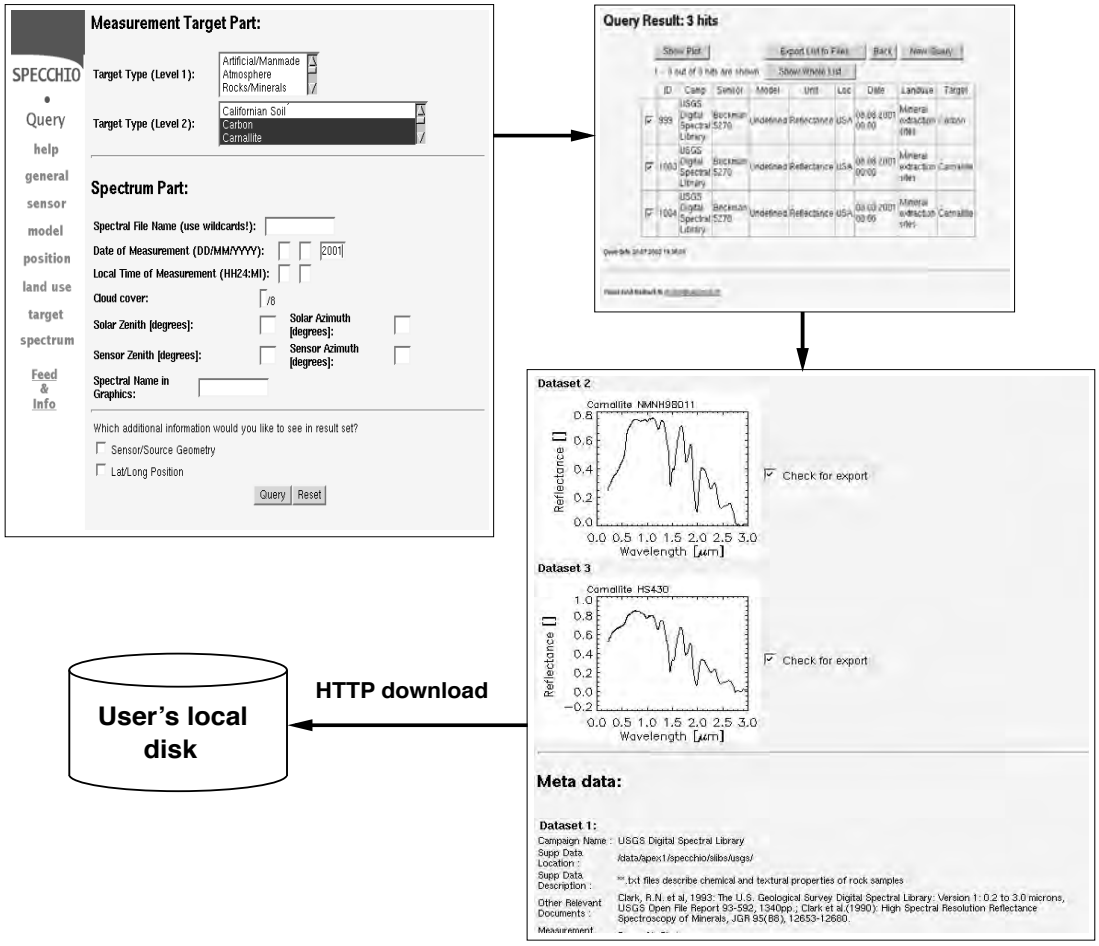


Figure 3.5: Web interfaces to query data from SPECCHIO. A suite of interactions leads to display and user download of spectral data. All associated meta data are included in the export datasets.

| Institution | Reference | Number of spectra | Target types |
|---|---|---|---|
| Johns Hopkins University | Salisbury et al. (1991) | 617 | Terrestrial, lunar, artificial |
| Jet Propulsion Laboratory | Grove et al. (1992) | 430 | Minerals |
| US Geological Survey Denver | Clark et al. (1993) | 498 | Minerals, vegetation |
| USDA Beltsville | Price (1995) | 3257 | Natural, artificial |

Table 3.1: Spectral collections contained in SPECCHIO.

### 3.4.1 Spectral Library Data

The need for comprehensive and widely accessible spectral data collections has been addressed previously by several institutions and researchers, as listed in Table 3.1.

All these spectral collections have been entered into SPECCHIO, along with full documentation on sensors, measurement set-ups, operators, locations, and measurement targets. An example of data from the USGS Digital Spectral Library is shown in Fig. 3.5. Important attributes of the spectra in terms of variability are the target type and further description of the measured object, e.g., its chemical composition. Example code that has been used to enter these data into SPECCHIO reads:

```
new target type2 = Acmite | Adularia | ...
spectrum comments = Formula: NaFeSi2O6 | Formula: KAlSi3O8 | ...
```

### 3.4.2 Field Campaign Data

Spectral measurements carried out during field campaigns provide substantial information on the physical state of the Earth's surface that is required as ground truth in airborne or spaceborne imaging spectroscopy, as well as for the vicarious calibration of nadir-looking sensors. Two examples of campaign datasets are given in the next sections, from applications in limnology and vegetation analysis.

#### Limnology

In-situ spectral data were measured during a limnological study to investigate the water quality of inland lakes (Keller, 2001) using ground-based and airborne data. Measurements were carried out with a GER1500 spectroradiometer at several locations on different Swiss lakes. At each location, depth profiles of upwelling and downwelling radiance were measured in water, giving a handle on scattering and absorption properties of the water and dissolved constituents. From this set-up, it is obvious that defining descriptive attributes to these spectra are lake, measurement location, depth, and viewing direction of the sensor. Fig. 3.6 shows a sketch of the measurement set-up and part of the associated text file that was used to enter the spectra into the database. The limnological dataset is expected to be representative for the water optical properties of alpine lakes and rivers and can be used as a reference for other applications in that area.

#### Vegetation Analysis

Studying the spectral reflectance behaviour of vegetation constitutes an important part of agricultural and forestry analysis. Measuring the bi-directional angular reflectance of plants during a growing season gives information on growth status, vitality, and phenological stage. Spectral data were measured across a hemisphere with a goniometer set-up over an alfalfa canopy during a large-scale measurement campaign in Barrax (Spain). In this case, attributes that make a distinction between individual spectra are the four angles specifying the sensor-sun geometry, as depicted in Fig. 3.7, and the local time of measurement. SPECCHIO can store all these attributes and allows detailed queries on individual spectra as well as parts of measured hemispheres.

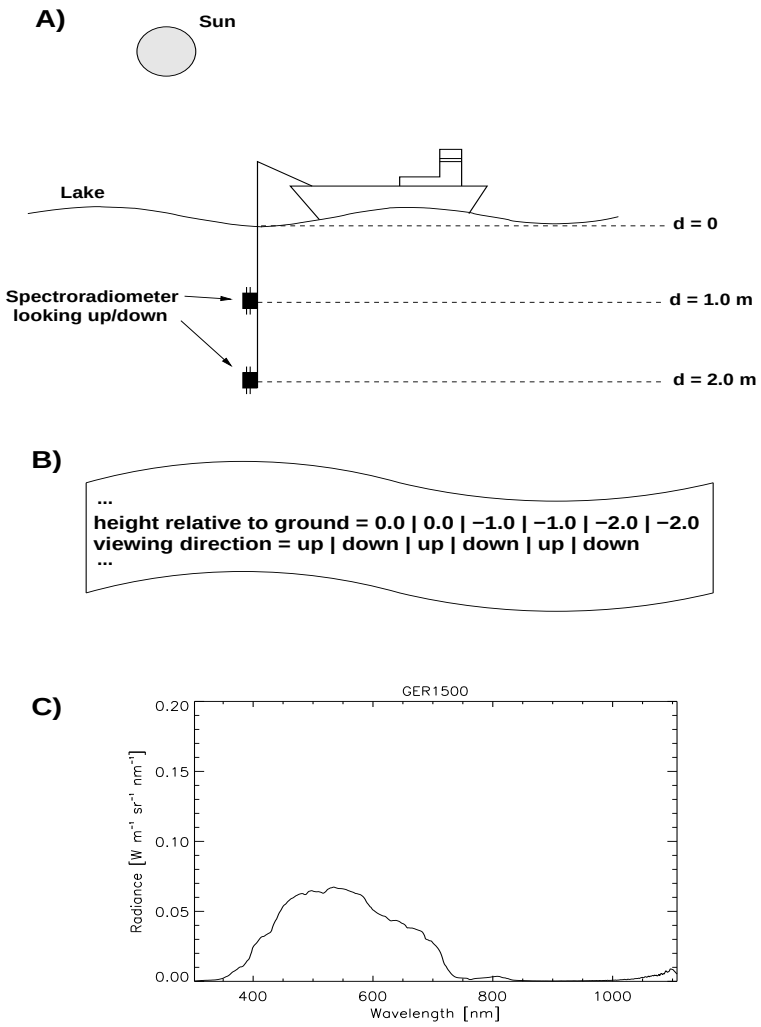


Figure 3.6: Typical measurement set-up for spectral measurement in lakes in the course of a limnology campaign (A) and part of the corresponding feed text file (B). (C) shows an example plot of downwelling radiance at lake water depth 1.0 m.

### 3.4.3 Modelled Data

The use of modelled reference spectra is widely accepted in imaging spectroscopy, since complete field or laboratory spectral series are seldom available for parameters under investigation. Thus, series of reflectance spectra using established models were generated and stored in the database. One major series was created for generic vegetation canopies using the PROSPECT (Jacquemoud and Baret, 1990) and SAIL models (Verhoef, 1984). They include parameter variations for leaf area index, leaf chlorophyll and leaf water contents. A second reference series of reflectance data was modelled for snow analysis where the snow optical thickness and its grain size have been varied systematically (Painter et al., 1998).

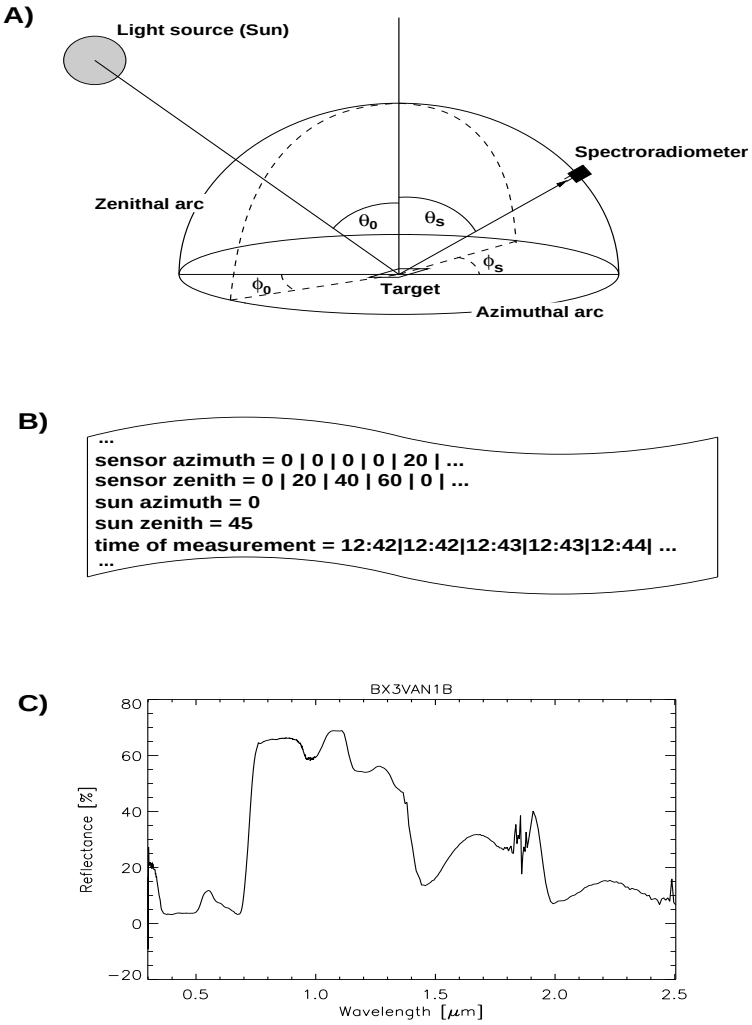


Figure 3.7: (A) Geometry of typical measurement for the study of bi-directional spectral reflectance of natural surfaces. $\phi_O, \phi_s$ are solar and sensor azimuth angles, $\theta_0, \theta_s$ are solar and sensor zenith angles, respectively. (B) Part of the feed script that describes this measurement set-up. (C) shows an example plot of green vegetation (alfalfa) reflectance for sensor zenith and azimuth angles 60 and 180 degrees, and solar zenith and azimuth angles 48 and 94 degrees, respectively.

## 3.5 Application in Imaging Spectroscopy

A typical application of the SPECCHIO reference spectrum database arises from the need for surface reflectance approximations, when airborne or spaceborne downward looking spectral measurements are analysed (Fig. 3.8). The nadir-looking spectrometer mounted on a carrier platform continuously scans the Earth perpendicular to the flight direction, yielding an image cube in three dimensions. Contiguous pixels span in two spatial directions, the third spectral dimension is reduced to one image layer for the purpose of illustration.

Generally speaking, there are four driving factors to the shape of individual pixel spectra in the image: Optical properties of (1) the surface cover, (2) the atmosphere,

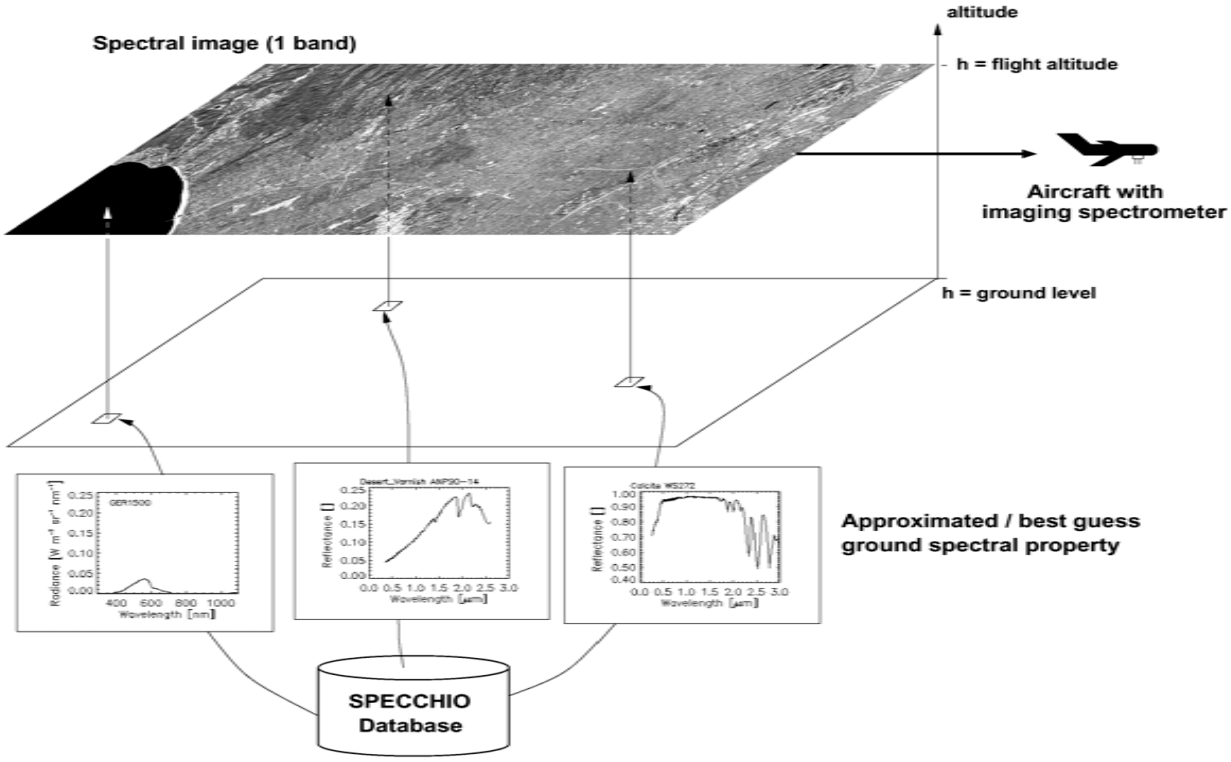


Figure 3.8: SPECCHIO providing surface spectral information to airborne or spaceborne imaging spectroscopy measurements, aiding in endmember selection for spectral unmixing of the image data.

(3) the sensor response, and (4) the extraterrestrial solar irradiance. SPECCHIO helps to better characterize both of these physical characteristics, as indicated in Fig. 3.8. Selected ensembles of spectra from the database represent a good first guess on spectral endmembers in an unmixing analysis. In case of missing in-situ ground spectral measurements especially, as is often the case in imaging spectroscopy, the use of region-specific or cover-specific spectral database information significantly improves endmember specification. For example, this results in more accurate geological mapping of minerals as well as better spatial characterization of soils.

If one is either interested in the removal of atmospheric optical influence, as necessary for case (1), or in atmospheric properties themselves (2), an approximation of the surface reflectance for certain spectral windows is required. This is particularly true over land surfaces (Kaufman et al., 1997). The atmospheric effect can then be isolated from surface radiative contributions and inverted to atmospheric parameters, such as optical thickness.

## 3.6 Conclusions

Concept, design, implementation, and parts of the content of the newly developed reference spectrum database SPECCHIO are presented in this paper. A comprehensive collection of spectral measurements from a variety of natural and artificial surfaces with intuitive user interfaces has been created. SPECCHIO contains field and laboratory campaign data, spectra from existing spectral collections, and modelled spectra. Due to the separation of database and spectrum data files, heterogeneous spectral data from a variety of sources can be stored. Web-based and command line-based interfaces allow user access to the database. Single and multiple spectral sets can be input and queried using these interfaces, including descriptive meta data.

The inversion of airborne and spaceborne imaging spectrometry data with respect to physical properties of the Earth-atmosphere system can be improved by spectral reference data from SPECCHIO. Missing in-situ surface spectral data can be replaced on an approximative basis. The database can also help to better classify spectral images by providing endmembers for spectral unmixing. Secondly, the database organizes and manages spectral data that depend on a high number of independent parameters, such as bi-directional reflectance field campaign data.

ASCII columnar and ENVI spectral library data formats are supported in the current version 1.0, and the flexibility to add other data formats is given. Input of spectral data is work in progress.

## Acknowledgements

The project is supported by the Swiss National Science Foundation (SNF), project 2000-061431.00. We kindly acknowledge the contributions of Rudolf Richter (DLR) and RSL staff. We also thank three anonymous reviewers for their valuable comments that helped improve the manuscript.

## References

Barnard, A., Zaneveld, J., and Pegau, W. (1999). In-situ determination of the remotely sensed reflectance and the absorption coefficient: closure and inversion. *Applied Optics*, 38(24):5108–5117.

Clark, R. (1990). High spectral resolution reflectance spectroscopy of minerals. *Journal of Geophysical Research*, 95(B8):12653–12680.

Clark, R. (1993). SPECtrum Processing Routines User's Manual (program SPECPR): version 3. Open File Report 93-595, United States Geological Survey, Denver, Colorado, USA. 210 pp.

Clark, R., Swayze, G., Gallagher, A., King, T., and Calvin, W. (1993). The U.S. Geological Survey Digital Spectral Library: version 1: 0.2 to 3.0 $\mu$m. Open File Report 93-592, United States Geological Survey, Denver, Colorado, USA. 1340 pp.

Date, C. (1995). *Introduction to Database Systems*. Addison-Wesley, Reading, Massachusetts, USA. 839 pp.

European Commission DG XI (1993). CORINE land cover. Technical guide EUR 12585 EN, European Commission Directorate-General Environment, Nuclear Safety and Civil Protection, Office for Official Publications of the European Communities, Luxembourg, Luxembourg. 136 pp.

Grove, C., Hook, S., and Paylor, E. (1992). Laboratory reflectance spectra for 160 minerals $0.4 - 2.5$ micrometers. Publication 92-2, Jet Propulsion Laboratory, Pasadena, California, USA. 405 pp.

Gundavaram, S. (1996). *CGI Programming on the World Wide Web*. O'Reilly & Associates, Inc., Sebastopol, California, USA. 433 pp.

Hunt, G. (1977). Spectral signatures of particulate minerals in the visible and near infrared. *Geophysics*, 42(3):501–513.

Jacquemoud, S. and Baret, F. (1990). PROSPECT: A model of leaf optical properties spectra. *Remote Sensing of Environment*, 34:75–91.

Kaufman, Y., Wald, A., Remer, L., Gao, B., Li, R., and Flynn, L. (1997). The MODIS 2.1-$\mu$m channel-correlation with visible reflectance for use in remote sensing of aerosol. *IEEE Transactions on Geoscience and Remote Sensing*, 35(5):1286–1297.

Keller, P. (2001). Comparison of two inversion techniques of a semi-analytical model for the determination of lake water constituents using imaging spectrometry data. *Science of the Total Environment*, 268:189–196.

Leach, R. (2000). *Introduction to software engineering*. CRC Press, Boca Raton, Florida, USA. 428 pp.

Li, X., Gao, F., Wang, J., and Strahler, A. (2001). A priori knowledge accumulation and its application to linear BRDF model inversion. *Journal of Geophysical Research*, 106(11):11925–11935.

McDonald, R. and Wilks, P. (1988). JCAMP-DX: a standard form for exchange of infrared spectra in computer readable form. *Applied Spectroscopy*, 42(1):151–162.

ORATCL (2002). *Oratcl Project & Documentation*. [http://oratcl.sourceforge.net].

OSI (2002). *Open Source Initiative*. [http://www.opensource.org].

Ousterhout, J. (1994). *Tcl and the Tk Toolkit*. Addison-Wesley, Reading, Massachusetts, USA. 458 pp.

Painter, T., Roberts, D., Green, R., and Dozier, J. (1998). Improving mixture analysis estimates of snow-covered-area from AVIRIS data. *Remote Sensing of Environment*, 65(3):320–332.

Price, J. (1995). Examples of high resolution visible to near-infrared reflectance spectra and a standardized collection for remote sensing studies. *International Journal of Remote Sensing*, 16(6):993–1000.

Research Systems Inc. (2000a). *ENVI User's Guide, Version 3.4*. Boulder, Colorado, USA. 930 pp.

Research Systems Inc. (2000b). *IDL User's Guide, Version 5.4*. Boulder, Colorado, USA. 320 pp.

Roberts, D., Gardner, M., Church, R., Ustin, S., Scheer, S., and Green, R. (1998). Mapping chaparral in the Santa Monica Mountains using multiple endmember spectral mixture models. *Remote Sensing of Environment*, 65(3):267–279.

Salisbury, J., Walter, L., Vergo, N., and D'Aria, D. (1991). *Infrared (2.1-25 micrometers) Spectra of Minerals*. Johns Hopkins University Press, Baltimore, Maryland, USA. 294 pp.

Ullman, R. (1999). HDF-EOS, NASA's standard data product distribution format for the Earth Observing System data information system. In *Proceedings of the IEEE 1999 International Geoscience and Remote Sensing Symposium, Hamburg*, volume 1, pages 276–278. IEEE.

Verhoef, W. (1984). Light scattering by leaf layers with application to canopy reflectance modeling: The SAIL model. *Remote Sensing of Environment*, 16:125–141.

WEBSH (2002). *Webshell Documentation*. [http://tcl.apache.org/websh].

# 4

# Aerosol Mapping over Land with Imaging Spectroscopy using Spectral Autocorrelation

*This chapter has been submitted in October 2002 for publication in Remote Sensing of Environment: S. Bojinski, D. Schläpfer, M. Schaepman, J. Keller, and K. Itten, 2002. Aerosol mapping over land with imaging spectroscopy using spectral autocorrelation.*

## Abstract

In this paper, a new method for aerosol retrieval over land is proposed that makes explicit use of the contiguous and high-resolution spectral coverage of imaging spectrometers. Spatial remote sensing of aerosols has in recent years become an invaluable means to assess the distribution of aerosol types and concentrations in the Earth's atmosphere, which affect global and regional climate as well as the atmospheric signal in spectral imagery. The proposed method is labelled Aerosol Retrieval by Interrelated Abundances (ARIA) and is based on unmixing of the short-wave infrared sensor signal by appropriate endmembers, assuming low aerosol radiative influence in this spectral region. Derived endmember abundances are transferred to the visible part of the spectrum in order to approximate surface reflectance where aerosol influence is generally strongest. Spectral autocorrelation of surface spectra is a precondition for ARIA and demonstrated for natural surfaces using a spectrum database. The remixed surface reflectance is used as input quantity for numerical inversion of aerosol parameters, such as aerosol optical depth $\tau_a(0.55\mu\text{m})$. Terrain-sensitive interpolation and smoothing of the inversion leads to mapping of regional distributions of $\tau_a(0.55\mu\text{m})$. Except for the choice of endmembers, no a priori assumptions on the atmospheric state or the image scene are required.

The potential of the presented method for aerosol retrieval is demonstrated for two scenes collected in the year 2000 by the Airborne Visible/Infrared Imaging Spectrometer (AVIRIS), over rugged heterogeneous coastal terrain and an urban area in California, using generalized soil and vegetation endmembers. Comparisons to existing single or double-band aerosol retrieval methods are made and the results discussed

for different aerosol regimes assumed in the area. It could be shown that the ARIA method leads to a more realistic representation of the spatial aerosol distribution compared to existing methods. The level of uncertainty of the derived $\tau_a(0.55\mu\text{m})$ is in the same order of magnitude. Validation of the results is performed with the Moderate Resolution Imaging Spectrometer (MODIS) aerosol product, showing the best agreement for the ARIA method.

## 4.1 Introduction

In the Earth's atmosphere, natural and anthropogenic sources give rise to highly variable geographical and seasonal aerosol distributions, which are largely confined to the troposphere. Aerosols affect the atmospheric radiative transfer of sunlight twofold: directly due to scattering and absorption of radiation at particles, and indirectly by influencing the formation of clouds, which themselves cause radiative forcing (Liou, 1992). Owing to the high spatial variability of aerosols, continuous in-situ monitoring from ground-based instrument networks (e.g., ground-based sun photometry) is insufficiently representative for both regional and global applications, and calls for imaging remote sensing techniques. In recent years, spaceborne imaging spectroscopy has become an important means to characterize aerosols on both global and regional scales (King et al., 1992; Tanré et al., 1997; Kaufman et al., 2002).

Imaging spectroscopy of the Earth's surface, in turn, often requires accurate atmospheric correction of spectral images, and therefore knowledge of the aerosol radiative effect (Gordon, 1978; Chomko and Gordon, 1998; Gao et al., 2000). Several methods have been developed to isolate radiation scattered by aerosols in the direction of the sensor from other contributions, such as reflection at the Earth's surface and Rayleigh scattering at gaseous atmospheric components (King et al., 1992; Kaufman et al., 1997a). Radiative transfer models as well as physical aerosol models have been employed for the inversion of aerosol properties from the aerosol radiative signal (Berk et al., 1989; d'Almeida et al., 1991).

In this paper, a new method for aerosol retrieval over land is proposed that makes explicit use of the contiguous and high-resolution spectral coverage of imaging spectrometers. It is based on unmixing of the short-wave infrared sensor signal by appropriate endmembers, assuming low aerosol radiative influence in this spectral region. Endmember abundances, that are obtained from the unmixing process, are then applied to the visible part of the endmembers in order to approximate surface reflectance in this spectral region where aerosol influence is generally strongest. The re-mixed surface reflectance is used as input quantity for numerical inversion of aerosol parameters. The final goal of the method consists of mapping regional distributions of aerosol parameters, leading to a characterization of the spatial distribution of aerosol properties.

Results of the aerosol parameter inversion are then presented and compared to existing methods for aerosol retrieval. Imagery from the Airborne Visible Infrared Imaging Spectrometer (AVIRIS) described by Green et al. (1998) is used as testbed data. The aerosol maps are validated with the operational aerosol product from the MODIS sensor.

The following terminology is used for spectral wavelength ranges throughout this paper: visible (VIS) range denotes wavelengths $\lambda$ between 0.4 and 0.7 $\mu$m, near

infrared (NIR) means $\lambda = 0.7 - 1.0$ $\mu$m, and short-wave infrared (SWIR) refers to wavelengths between 1.0 and 2.5 $\mu$m. From the SWIR range, the two wavelength regions between 1.4 and 1.8 $\mu$m and $1.8 - 2.5$ $\mu$m are referred to as SWIR1 and SWIR2, respectively.

## 4.2 Methods for Remote Sensing of Aerosols

The earliest studies on aerosol remote sensing from satellites used Landsat-1 data in single VIS bands for mapping dust over the ocean (Fraser, 1976). Gordon (1978) made first steps in the correction of ocean color measurements for aerosol influence using two spectral bands over the oceans, and refined the algorithm for combined ocean colour and aerosol retrieval from SeaWiFS imagery (Gordon and Wang, 1994). Tanré et al. (1997) used bands in a spectral range between 0.55 and 2.13 $\mu$m of the MODIS airborne simulator and a look-up table approach to derive aerosol properties over the ocean. Unless models or in-situ measurements exist that account for the effects of wind speed and suspended matter (Gordon and Wang, 1994), water bodies are approximated to reflect $0 - 1$ % of the downwelling irradiance above its surface in the NIR.

First studies on the retrieval of aerosol properties from satellite data over land, which is generally more complex, were aimed at atmospheric correction (Tanré et al., 1983), but soon focused equally on aerosol mapping (Kaufman and Sendra, 1988), making use of dark vegetation targets in the VIS. Dark vegetation is mostly approximated by $2 - 3$ % reflectance in the red VIS (Richter, 1996). In imagery uncorrected for the atmospheric signal, dark vegetation can be identified by thresholding of the atmospherically resistant vegetation index (ARVI) (Kaufman and Tanré, 1992).

For both dark water and dark vegetation areas, the presence of aerosols generally brightens these pixels at the sensor level, which is described by the aerosol effect $\rho_a$,

$$\rho_a = \rho_{app} - \rho_{app}(\text{no aerosols}) \tag{4.1}$$

and apparent reflectance $\rho_{app}$ at the sensor. The latter is defined by total radiance normalized by downwelling irradiance at the sensor level, and reads as (Liou, 1980)

$$\rho_{app} = \rho_o + \frac{\rho_s t E_d}{E_o \cos\theta_o (1 - s\rho_s)} \ , \tag{4.2}$$

where $\rho_o$ is path radiance, $\rho_s$ surface reflectance, $t$ total upward transmittance along the sensor's line of sight, and $E_d$ the downwelling irradiance at the surface level. $E_o \cos\theta_o$ denotes downwelling irradiance at the sensor level where the sun zenith angle $\theta_o$ is considered, and $s$ is the reflectance of the atmosphere from below, a measure for multiple scattering between atmosphere and surface. With the advent of spaceborne sensors that have the specific capability for aerosol retrieval (e.g. MODIS), the dark target approach has been refined over land. The band ratio method proposed by Kaufman et al. (1997b) is based on an empirical relationship between SWIR reflectance at $\lambda = 2.1$ $\mu$m and visible reflectances at $\lambda = 0.49$ $\mu$m and $\lambda = 0.66$ $\mu$m for a large variety of natural surfaces. It assumes a weak aerosol effect in the infrared, which holds except for very large dustlike or sea-salt particles. Airborne spectral

imagers, such as AVIRIS (Green et al., 1998), with continuous spectral coverage between 0.4 and 2.5 $\mu$m in hundreds of bands, and ground sampling distances of the order 10 m have also been used for the retrieval of aerosol parameters: Isakov et al. (1996) infer aerosol optical depth from contrast reduction of uniform artificial land surface targets with high reflectance difference, due to atmospheric blurring. Over oceans, the assumption of zero water-leaving radiance at wavelengths greater than 1.0 $\mu$m has been combined with the forward calculation of at-sensor radiance look-up tables for a selection of aerosol models and aerosol optical depths (Gao et al., 2000). Due to high spectral resolution, the wavelength dependence of $\rho_o(\lambda)$ could be aptly approximated, best fitting aerosol models and aerosol optical depth $\tau_a$ found and pixel-wise atmospheric correction applied.

## 4.3 New Method for Aerosol Retrieval over Land using Imaging Spectroscopy

### 4.3.1 Basic Principle

A new method for the retrieval of aerosol parameters from imaging spectrometer data over land is proposed. Unlike the dark target and band ratio methods, which use a small number of spectral bands for the approximation of land surface reflectance $\rho_s$ in an image pixel, the Aerosol Retrieval by Interrelated Abundances (ARIA) method is based on unmixing of the spectrally continuous sensor signal in the SWIR range, using the derived abundances to re-mix the VIS surface reflectance, and subsequent inversion of aerosol parameters with look-up tables.

As illustrated in Fig. 4.1, continuous spectral coverage of $\rho_s$(VIS) is thus achieved. Unmixing of the sensor spectrum $\rho_{app}$ in the SWIR (light grey, upper panel) uses a priori defined land surface reflectance endmembers $e_i$ (lower panel), assuming a low aerosol effect in the SWIR range. $\rho_{app}$ then reads for a linear combination of endmembers $e_i$

$$\rho_{app}(\text{SWIR}) = \sum_i a_i e_i(\text{SWIR}) \ . \tag{4.3}$$

Thus obtained abundances $a_i$ are interrelated between VIS and SWIR spectral ranges, if spectral autocorrelation of surface reflectances is given. In this case, re-mixing of the surface reflectance spectrum $\rho_s$(VIS) can be carried out by applying the abundances $a_i$ to the same set of endmembers as employed for unmixing, such that

$$\rho_s(\text{VIS}) = \sum_i a_i e_i(\text{VIS}) \ . \tag{4.4}$$

Once $\rho_s$(VIS) is obtained, radiative transfer forward modelling with look-up tables calculated for a variation of aerosol parameters and terrain heights is performed, and the best assimilation of $\rho_{app}^{sim}$ to the measured image spectrum $\rho_{app}$(VIS) is sought. Fig. 4.2 illustrates this procedure for different modelled columnar aerosol optical depths $\tau_a(0.55\mu\text{m})$ for a maritime aerosol model as defined by Shettle and Fenn (1979). $\tau_a(\lambda)$ is always evaluated for $\lambda = 0.55$ $\mu$m in the following, and henceforth denoted as $\tau_a$. The best fit curve is determined by minimizing the cost function $\epsilon_{\tau_a}$

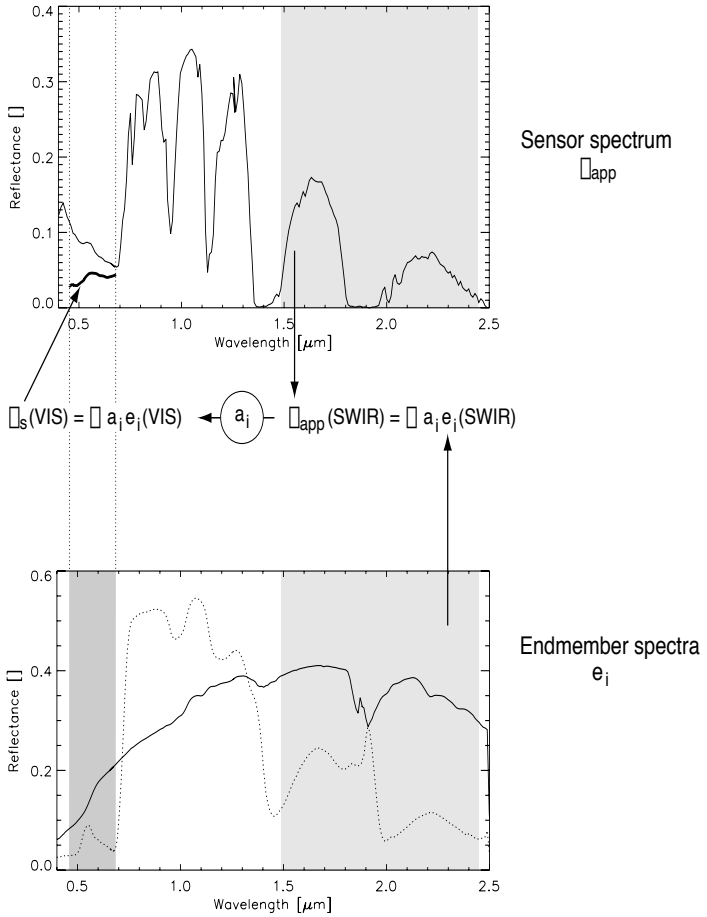


Figure 4.1: Principle of $\rho_s$(VIS) approximation by the ARIA method. It is based on spectral unmixing of the sensor spectrum $\rho_{app}$ with appropriate endmembers $e_i$ in the SWIR (light grey), obtaining abundances $a_i$, and subsequent re-mixing of endmembers (dark grey) in the VIS range. The lower panel depicts mean soil (solid line) and vegetation spectra (dashed line).

$$\epsilon_{\tau_a} = \frac{1}{n} \sum_{j=1}^{n} |\rho_{app}^{sim}(\lambda_j) - \rho_{app}(\lambda_j)| \tag{4.5}$$

with $n$ denoting the number of spectral bands. With a minimum $\epsilon_{\tau_a}$, $\tau_a^{best}$ is found, which represents the retrieved aerosol parameter. It depends on approximated surface reflectance $\rho_s$(VIS), measured $\rho_{app}$ at the sensor, and the atmospheric model that is used in the look-up table forward calculations.

### 4.3.2 Error Calculation

The uncertainty $\Delta\tau_a$ is determined from estimates of the uncertainties $\Delta\rho_s$ and $\Delta\rho_{app}$. From a correlation analysis of natural reflectance spectra in the VIS and SWIR ranges, $\Delta\rho_s(\lambda)$ has been determined for each VIS band. The uncertainty $\Delta\rho_{app}$ in the sensor

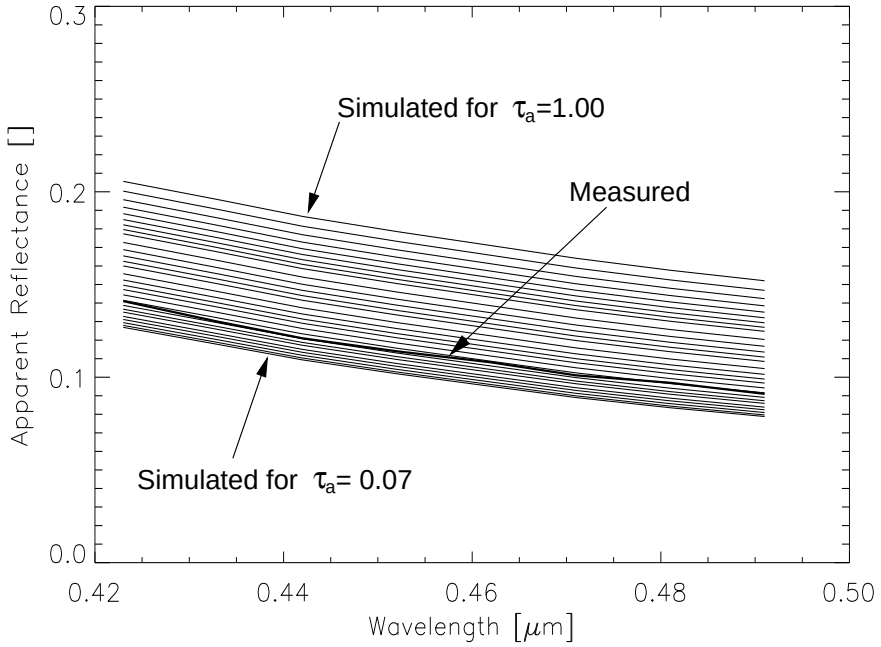


Figure 4.2: Simulated at-sensor spectra $\rho_{app}^{sim}$ for variation of $\tau_a$ between 0.07 and 1.00 for maritime aerosol type, based on re-mixed $\rho_s(\lambda)$, compared to measured $\rho_{app}$ at sensor. The VIS range $0.42 - 0.49$ $\mu$m is used for parameter inversion.

signal is given by the calibration accuracy of the sensor. The total error $\Delta\tau_a$ is then calculated as follows: maximum and minimum retrieved aerosol optical depths $\tau_a^{max}$ and $\tau_a^{min}$ are obtained as

$$\tau_a^{max} = f(\rho_s(\lambda) - \Delta\rho_s(\lambda), p(\lambda) + \Delta p(\lambda)) \text{ , and} \tag{4.6}$$

$$\tau_a^{min} = f(\rho_s(\lambda) + \Delta\rho_s(\lambda), p(\lambda) - \Delta p(\lambda)) \text{ ,} \tag{4.7}$$

following the described inversion procedure. The uncertainty $\Delta\tau_a^{'}$ is then calculated by the discrepancy between $\tau_a^{max}$, $\tau_a^{min}$, and $\tau_a^{best}$:

$$\Delta\tau_a^{'} = \frac{1}{2}(|\tau_a^{max} - \tau_a^{best}| + |\tau_a^{min} - \tau_a^{best}|) \tag{4.8}$$

The total error $\Delta\tau_a$ then reads as

$$\Delta\tau_a = \Delta\tau_a^{'} + \epsilon_{\tau_a}^{min} + \frac{1}{2}(\epsilon_{\tau_a^{min}} + \epsilon_{\tau_a^{max}}) \text{ .} \tag{4.9}$$

$\tau_a \pm \Delta\tau_a$ can be determined for each image pixel that is considered as candidate for the ARIA method. A candidate pixel mask is obtained by applying a spectral angle classifier to the raw image, using above mentioned surface reflectance endmembers.

What is the advantage of more accurate $\rho_s(\lambda)$ spectral sampling, compared to the band ratio method which uses only two bands in the VIS to retrieve aerosol parameters? The dependence of (back-)scattered radiation on wavelength by the Ångström law implies that, in the idealized case of a Junge size distribution and single scattering, two spectral estimates of $\tau_a(\lambda)$ suffice for the spectral description of $\tau_a$ and

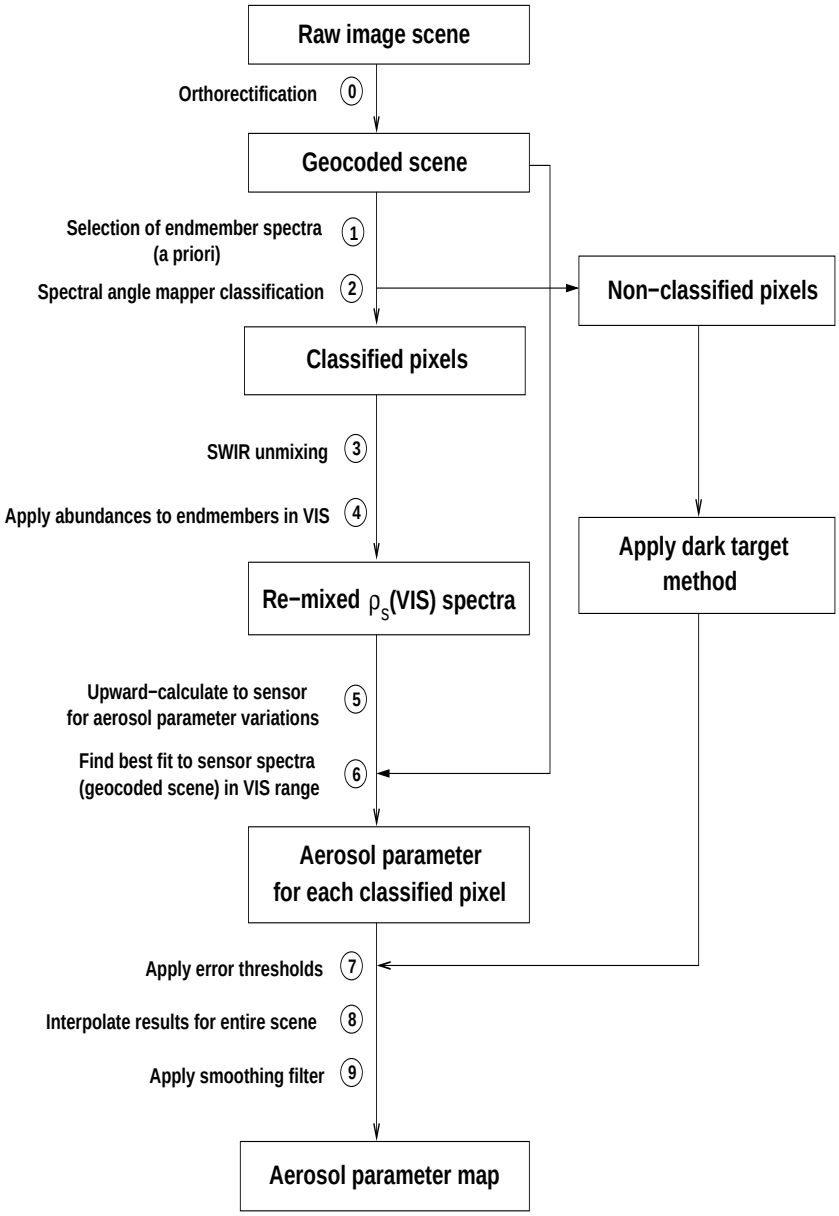


Figure 4.3: Implementation schema of the ARIA method.

therefore $\rho_a$ (Liou, 1980). First, the accuracy of approximated $\rho_s(\lambda_o)$ can be improved by simultaneous knowledge of $\rho_s(\lambda_o \pm \Delta\lambda)$ with small $\Delta\lambda$, given high autocorrelation of the surface spectrum. This can be relevant if band $\lambda_o$ is noisy or badly calibrated. Second, the Ångström law is only an approximation to reality, and higher order $\lambda$-dependence of $\rho_a$ can be of interest.

### 4.3.3 Implementation of Method

Based on the described basic principle, the implementation of the ARIA method is depicted in Fig. 4.3.

*Step (0):* As the spectral image scene over land generally contains variable topography, orthorectification is performed. A digital terrain model at approximately the same spatial resolution as the image data is needed for that purpose.

*Step (1):* Spectral endmembers can be conceived as the eigenvectors that describe each pixel spectrum in an image scene. Unfortunately, this concept is approximative, as real scenes are not really composed of small number of distinct pure materials, nor are pixels exact linear combinations of these materials. In this context, no image-based automated endmember selection algorithm that is insensitive to atmospheric perturbations could be identified in the literature. In many studies of land cover analyses using spectral unmixing (Roberts et al., 1998; Asner and Lobell, 2000), specific spectrum databases are used, that are adapted to regional conditions. To maintain generality of ARIA, such an approach is not feasible either, and availability of such data is limited. We alternatively select as endmembers averaged spectra from a reference spectrum database (Bojinski et al., 2002) for very general land cover types (e.g., vegetation, soil), assuming a priori that these land cover types be abundant in the image scene.

*Step (2):* With the spectral angle mapper (SAM) algorithm (Richards and Jia, 1999), image pixels are identified that bear sufficient similarity to one of the used endmember spectra $e_i$, in the sense that a pixel belongs to class $c$ by the condition

$$c = \begin{cases} i & : \quad \min\left(\arccos\left(\frac{\rho_{app,j} e_{i,j}}{|\rho_{app,j}||e_{i,j}|}\right)\right) \leq 0.15 \\ 0 & : \quad \text{else,} \end{cases} \tag{4.10}$$

using the spectral bands $j$, which were chosen at 0.66, 0.87, 1.04, 1.66, and 2.10 $\mu$m. This band selection is small enough to enable fast image classification, and at the same time roughly covers the spectral range of interest. "0" in equation (4.10) denotes "unclassified", i.e. not belonging to any of the classes defined by the given endmembers. In order to obtain better spatial coverage of aerosol parameters in the image, e.g. over water surfaces, the dark target method is applied. The SAM is considered fairly robust towards atmospheric perturbation of the sensor signal, and therefore the algorithm of choice. As the selection of endmembers is a very general one in terms of land covers, it is not expected that classified pixels are purely covered by the respective surface cover. This is important to note for the following processing step.

*Step (3) and (4):* In all classified pixels, the SWIR range of the sensor signal is used for the unmixing procedure, employing the singular value decomposition technique (Press et al., 1992), and all endmembers used in the classification process. The derived abundances $a_i$ do not necessarily represent actual land cover abundances in the pixel area. They are rather a measure for the composition of the SWIR sensor spectrum, as expressed by the selected endmembers. Autocorrelation analysis of natural surface spectra (see section 4.4.1) shows that the $a_i$ are interrelated between SWIR and VIS for certain spectral bands and accuracy limits. Interrelation means that the $a_i$ as derived from the SWIR can equally be used in the VIS part of the spectrum for remixing, because the spectral values have shown significant correlation. For unmixing, the use of all spectral bands in the range between 1.4 and 2.5 $\mu$m is suggested, provided the atmospheric transmission is larger than 0.85 (for a simulated maritime aerosol model and $\tau_a = 0.22$). This prevents absorption features from atmospheric gases (water vapour, carbon dioxide) affecting the SWIR spectrum. The assumption

of low aerosol effect ($\rho_a \leq 0.004$) in the SWIR is considered true for $\tau_a \leq 0.25$ in the sense that $\rho_{app}$(SWIR) is taken as is for unmixing, provided that $\overline{\rho_{app}(\text{SWIR})} < 0.15$ (Kaufman et al., 1997b). For $\tau_a > 0.25$, the aerosol effect on $\rho_{app}$(SWIR) can no longer be considered weak in general. In this case, a posteriori correction of the aerosol effect in the SWIR is needed and a second iteration of the procedure based on the result from step (9) (described below) is required. Therefore, the cases where $\tau_a > 0.25$ are not considered further in this paper.

Re-mixing of $\rho_s$(VIS), as described in equation (4.4), is performed in the spectral range between 0.42 and 0.49 $\mu$m (step (4)).

*Step (5):* Upward-calculating the approximated ground spectrum in VIS bands for aerosol parameter variations is carried out numerically by means of pre-calculated look-up tables. The MODTRAN 4.0 radiative transfer code (Berk et al., 1989) was used for that purpose, which assumes a uniformly layered atmosphere, approximately plane-parallel on a regional scale, with the following set of parameters (values in parentheses denote incremental steps of the respective parameters):

- Nadir sensor viewing direction
- Sun zenith, azimuth, day of year, sensor altitude: adapted to test dataset
- Columnar water vapour 1.41 g/cm$^2$ and ozone 7.36 g/cm$^2$
- 15 cm$^{-1}$ resolution absorption band model
- Variation in terrain height $h$: adapted to test area terrain variation in 1.0 km increments
- Variation in spectrally uniform $\rho_s$: 0.0(0.02)0.2, 0.23, 0.26, 0.3(0.05)0.5
- Variation in $V$ [km]: 6.0(0.5)10.0, 11.0(1.0)15.0, 17.0, 19.0, 21.0, 23.0 26.0, 30.0, 35.0, 40.0, 45.0, 55.0, 65.0, 80.0, 100.0, 120.0
  Corresponding $\tau_a$ for $h$=0.0 km: $1.004 - 0.076$
  Corresponding $\tau_a$ for $h$=1.0 km: $0.840 - 0.067$
- Aerosol models: maritime, rural, urban (separate look-up tables)
- Wavelength range: $0.37 - 0.80$ $\mu$m

For the numerical inversion of the aerosol effect in terms of aerosol parameters, look-up table dimensions span in $\rho_s$ and $\tau_a$ directions, for the urban, rural, and maritime aerosol models. This choice of parameters has been made according to a study by Tanré et al. (1997) for look-up table-based aerosol retrieval with the MODIS instrument. Each combination of $\rho_s$, $\tau_a$, and an aerosol model results in a simulated $\rho_{app}^{sim}$ at the sensor level (see Fig. 4.2).

*Step (6):* The procedure to find the best fitting simulated at-sensor spectrum is based on minimizing the cost function in equation (4.5). If $\rho_{app}$ exceeds the set of simulated curves in more than one used band, the inversion is cancelled for this particular pixel. In any other case, for maritime, urban, and rural aerosol models, the aerosol optical depth $\tau_a$ for each candidate pixel is obtained.

*Step (7):* Uncertainty in the retrieved aerosol parameter $\Delta\tau_a$ is expressed by equation (4.9). Pixels are excluded from further processing if the normalized uncertainty

$\Delta\tau_a/\tau_a$ exceeds a threshold value, which is chosen at 0.75. This value represents a reasonable trade-off between the number of useable pixels and the accuracy of the ARIA method. For pixels not used in the ARIA method (e.g., water), the dark target method is employed and the same thresholding applies.

*Step (8):* Interpolation of the raw aerosol map information across non-candidate (gap) pixels is performed using triangulation and considering the terrain height. If for a particular gap pixel, interpolated and real terrain height differ by $\delta h$, the interpolated $\tau_a$ value for that pixel is scaled by $\delta\tau_a = \partial\tau_a/\partial h \cdot \delta h$. The gradient $\partial\tau_a/\partial h$ is equivalent to an extinction coefficient $\sigma_{e,a}$ and obtained from linear regression of $\tau_a(h)$ within the image. The underlying assumption to the interpolation procedure is an approximately homogeneous vertical layering and smooth horizontal variation of the atmosphere in the gap pixel regions.

*Step (9):* The assumption of horizontal smoothness of the atmosphere from step (8) also paves the way for final smoothing of the aerosol optical depth map. What is considered a characteristic scale length of aerosol variation depends on pixel size and the type of application pursued. For imaging spectrometer data with pixel sizes in the order of tenths of metres, we propose smoothing with a 200 m filter size.

## 4.4 Analysis of Natural Surface Spectra

The ARIA method is based on significant autocorrelation of natural surface spectra in the VIS and SWIR spectral regions. First, the degree of this autocorrelation is investigated based on data from a spectrum database. Secondly, the ARIA principle of SWIR unmixing and VIS re-mixing is applied to those spectral regions that show significant autocorrelation, and the accuracy of re-mixing is ascertained.

### 4.4.1 Autocorrelation

Using low-altitude airborne spectral image data, a significant correlation between reflectances at 2.1 $\mu$m and reflectances at 0.49 and 0.66 $\mu$m, respectively, could be proven empirically (Kaufman et al., 1997b) for several natural surface types (vegetation, soils, sand). Karnieli et al. (2001) showed a significant correlation between bands at 0.645 and 1.6 $\mu$m for vegetation targets.

In this analysis, correlation is investigated for spectral bands between 0.4 and 0.7 $\mu$m in the VIS, and the SWIR1 and SWIR2 regions, respectively. Reflectance spectra from soil (895 spectra), vegetation (1239), and rocks/minerals (917) surfaces have been analysed. Averaged band correlations were calculated. Beyond semantic definition of vegetation spectra in the database, these particular spectra were subject to a minimum NDVI of 0.3, evaluated at 0.67 $\mu$m (red band) and 0.76 $\mu$m (near-infrared band).

The results in Fig. 4.4 show panels with Pearson's correlation coefficient $r_{xy}$, pair-wise determined for bands $x$ and $y$. It represents a measure for the degree of association between the reflectance values in the respective bands. Considering the size of spectral ensembles and assuming normally distributed reflectance values, $r_{xy} > 0.5$ indicates statistically significant correlation (cf. Press et al. (1992, p. 636)). Panels (a) in Fig. 4.4 display the correlation matrices between VIS and SWIR1, panels (b) the same for VIS and SWIR2. For the spectral ensemble of soils, $r_{xy}$ above 0.95 is ubiquitous

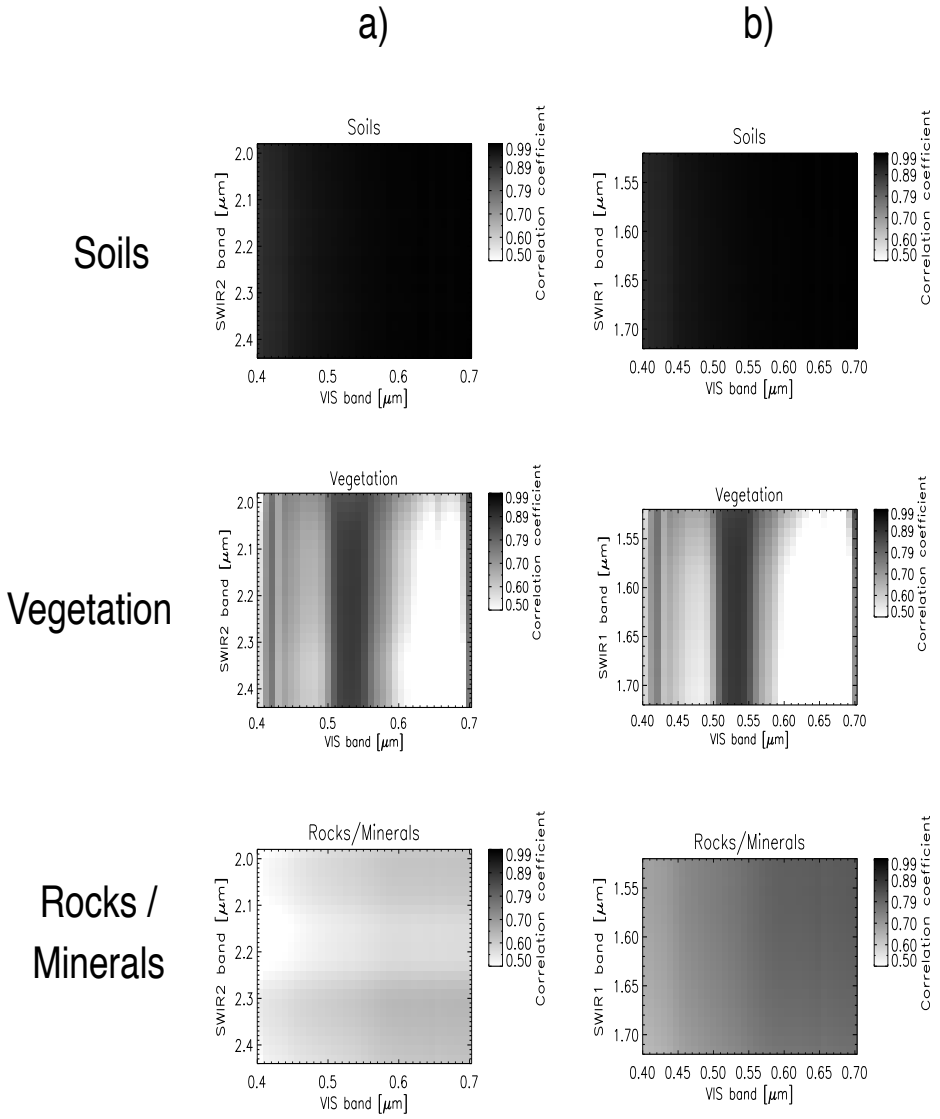


Figure 4.4: Correlation of natural reflectance from selected surface types, taken from a spectrum database.

in both matrices. For vegetation spectra, a marked peak of correlation (above 0.8) can be observed for the green peak region between 0.50 and 0.55 $\mu$m in both panels. Less correlation occurs in the short wave VIS part with values between 0.70 and 0.75; isolated higher correlation can again be seen in the shortest wavelengths $0.40 - 0.42$ $\mu$m. Correlation is clearly lowest above 0.6 $\mu$m. For the rocks/minerals spectra, the correlation matrices are smooth at a moderate level (around 0.6) in panel (a), and higher values (around 0.7) in panel (b).

The overall structure of correlation matrices shows similar behaviour in panels (a) and (b) for the soil and vegetation cases, indicating that the SWIR1 and SWIR2 spectral ranges are uniformly correlated to the VIS part. Interestingly enough, this is not true for the rocks/minerals case, which displays different levels and slightly different structure of correlations.

To conclude, for both soil and vegetation spectral ensembles, spectral regions in the VIS and SWIR ranges could be identified with significant correlation to be considered in the ARIA method. The wavelength region between 0.41 and 0.56 $\mu$m in the VIS, and the entire SWIR range appear appropriate for that purpose. Rocks/minerals spectra are excluded from further analysis due to the relatively poor degree of autocorrelation between the VIS and SWIR2 regions. The VIS/SWIR1 correlation of rock and mineral spectra may be potentially useful for future analyses.

Prior to the correlation analysis, all reflectance spectra were convolved to the AVIRIS 2000 imaging spectrometer band response. This is not expected to have considerable effect on correlation results, since inherent correlations exist between nearby wavelengths for natural surface spectra (Price, 1994).

### 4.4.2 Choice of Spectral Bands for ARIA

The best choice of bands to be used in the ARIA method takes into account the results from the foregoing correlation analysis. In this part, the accuracy of re-mixing the VIS part of the reflectance spectrum using interrelated abundances from SWIR unmixing is investigated. For that purpose, the above mentioned spectral ensemble of soil and vegetation spectra is employed. As endmembers in the unmixing/re-mixing procedure as sketched in Fig. 4.1, mean soil and vegetation spectra are calculated from the spectral ensembles and depicted in the lower panel of this figure (dashed line: mean vegetation; solid line: mean soil). Each vegetation or soil spectrum from the database is unmixed in the SWIR using both endmembers, according to step (3) in the ARIA method. The relative error in the re-mixed VIS spectrum compared to the original spectrum is calculated analogous to the cost function in equation (4.5).

Two questions are now addressed: (1) which choice of SWIR bands used in the unmixing causes least deviation between re-mixed and original spectrum averaged over all VIS bands used? (2) Once a SWIR band selection has been made, what are average relative deviations for each band in the VIS?

As for (1), the SWIR band range was varied between a minimum value shown on the ordinate of panels (a) in Fig. 4.5, and a fixed maximum value of 2.31 $\mu$m. Three different VIS ranges were evaluated: the short wavelength VIS range ($0.42 - 0.49$ $\mu$m), where aerosol effect is strongest, soil correlation high, and vegetation correlation moderate; the second VIS range ($0.42 - 0.56$ $\mu$m) additionally includes the green peak range and represents the recommended band range from the autocorrelation analysis; the third VIS range encompasses almost the entire VIS range ($0.42 - 0.68$ $\mu$m) for comparison. Average relative errors between re-mixed and original spectra in Fig. 4.5a are largely flat, which is partly due to the relatively uniform correlation of the SWIR bands to the VIS. Only for very limited SWIR unmixing ranges ($2.20 - 2.31$ $\mu$m approximately), abundances $a_i$ are significantly less representative for the VIS part, which shows up in higher average deviations there. Least average relative deviation in the VIS occurs if both SWIR1 and SWIR2 band ranges are used for unmixing, and re-mixing is done in VIS bands between 0.42 and 0.56 $\mu$m (17.9 %). This confirms the results from the autocorrelation analysis. Slightly larger relative deviation (19.7 %) is observed for the VIS range $0.42 - 0.49$ $\mu$m. As expected, average deviation increases if the entire VIS range is re-mixed (22.0 %).

To address question (2), SWIR unmixing was done in the entire range in question

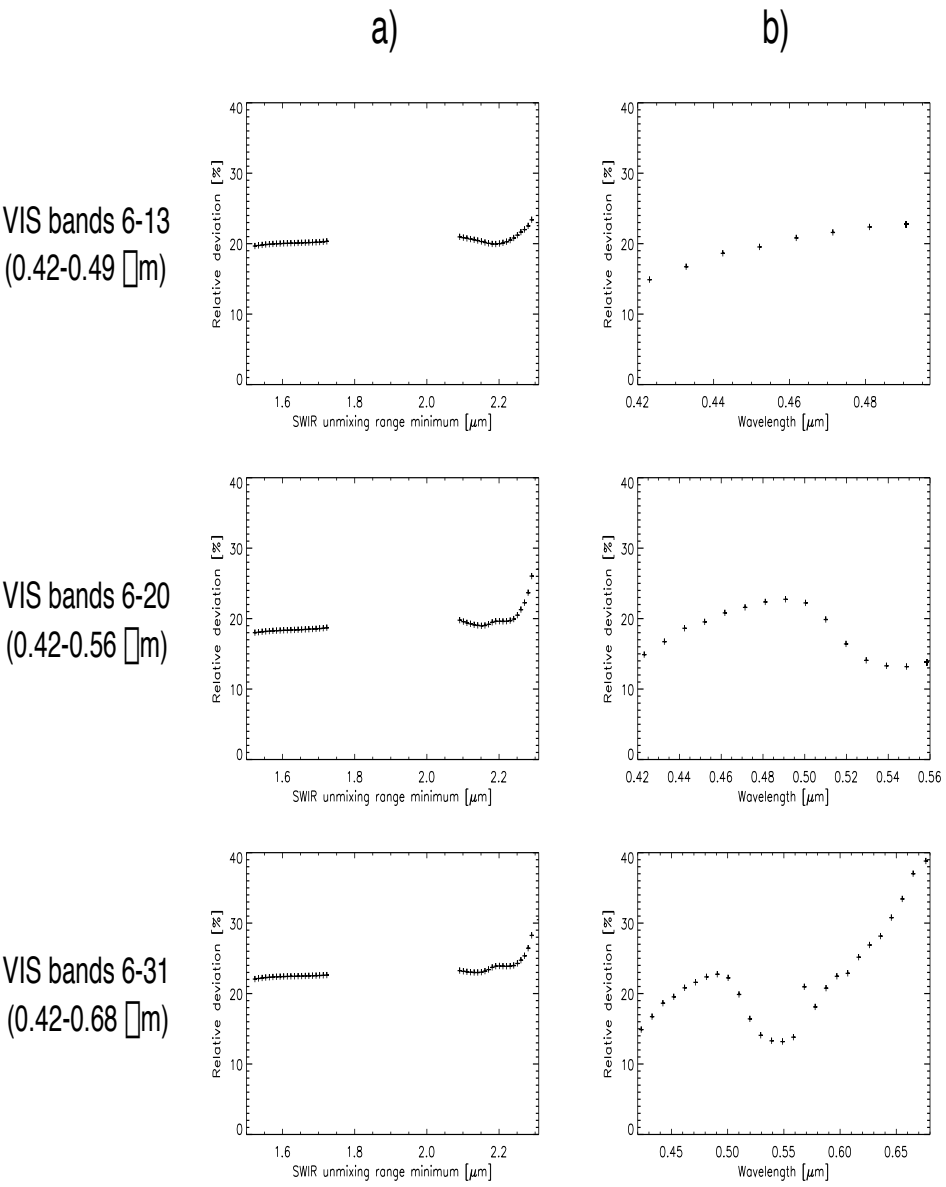


Figure 4.5: Accuracy of SWIR unmixing and VIS re-mixing, for soil and vegetation reflectance spectra convolved to AVIRIS 2000 spectral response. Spectral regions with low atmospheric transmission are not considered. a) Relative deviation averaged over different VIS band ranges between re-mixed and true $\rho_s$, depending on SWIR unmixing range, which extends from a minimum band position, shown on the horizontal axis, to 2.31 $\mu$m. b) For SWIR unmixing range $1.52 - 2.31$ $\mu$m, which gives least deviation in panels (a), average relative deviation in each used VIS band between re-mixed and true $\rho_s$ is shown.

(SWIR1 and SWIR2), and average relative deviations were calculated for each VIS band (Fig. 4.5b). The errors are roughly inversely proportional to the correlation coefficients in the vegetation case (cf. Fig. 4.4). For each VIS band, the uncertainty in the re-mixed (approximated) surface reflectance $\Delta\rho_s$(VIS) is now known.

## 4.5 Imaging Spectrometer Data

Airborne image data from the AVIRIS onboard a modified U-2 aircraft are used in this study to test the ARIA method and compare it to existing methods. An east-west flight line was acquired on 16 September 2000 at 11.00 am local time, stretching from downtown Los Angeles westward to Point Mugu near Oxnard, across a distance of 94.5 km. The north-south extension is 12.3 km, including the shoreline and the Santa Monica Mountains range (see Fig. 4.6). AVIRIS scans the surface in 224 spectral bands between 0.37 and 2.51 $\mu$m at a spectral resolution of 10 nm, maximum scan angle 15.6° at 20 km altitude above sea level, and a ground sampling distance of 20 m.

Green and Pavri (2001) state the calibration uncertainty in the AVIRIS 2000 sensor signal as $\Delta\rho_{app}(\lambda) = 0.038\rho_{app}(\lambda)$ for all bands, evaluated over a bright target ($\rho_s = 0.5$). Bands with centre wavelengths below 0.415 $\mu$m are not recommended for use due to low calibration confidence and high noise level (Green, pers. comm.). In this study, AVIRIS bands $6 - 224$ with centre wavelengths $0.42 - 2.51$ $\mu$m are considered.

The Los Angeles/Point Mugu AVIRIS flightline has been chosen as a useful testing ground for the ARIA method, because

- it has been acquired with the AVIRIS sensor in the year 2000 calibration state, with significantly lower noise in the VIS bands than in previous years (Green and Pavri, 2001),
- it is cloud-free,
- it includes different land cover types, where aerosol retrieval method performances over land can be compared,
- it includes different land use types (city, mountainous area, ocean) and strong topography, where columnar aerosol properties are expected to vary and can be indirectly validated with a terrain model.

The sun geometry for this almost perfect east-west flightline (heading 271°) was 41° sun zenith angle, and 135° sun azimuth angle. Hence, the scene is sun-illuminated from the south-east.

As exemplary test areas, two scenes have been used throughout the analysis, as depicted as (a) and (b) in Fig. 4.6: they are henceforth referred to as "Topanga" (a) and "City" (b) scenes. A look at the terrain model (lower panel in column (a)) reveals that the "Topanga" scene mainly contains mountainous areas of the Santa Monica Mountains to the north and west, mostly covered by chaparral and dry bushlands. Some patches of dark green vegetation could be identified at the valley bottoms. Bright bare soil can be identified mostly along cross-country roads and at creek mouths into the sea. Centre, east and south-east of the scene show urban areas, where brightness is roughly proportional to building density. The urban sprawl partly extends into hilly areas above the centre of the scene. A very bright beach before Santa Monica is visible, shoring the Pacific Ocean. The injection of suspended sediments at creek mouths can be distinguished below the centre of the "Topanga" scene, brightening the mostly uniform ocean water.

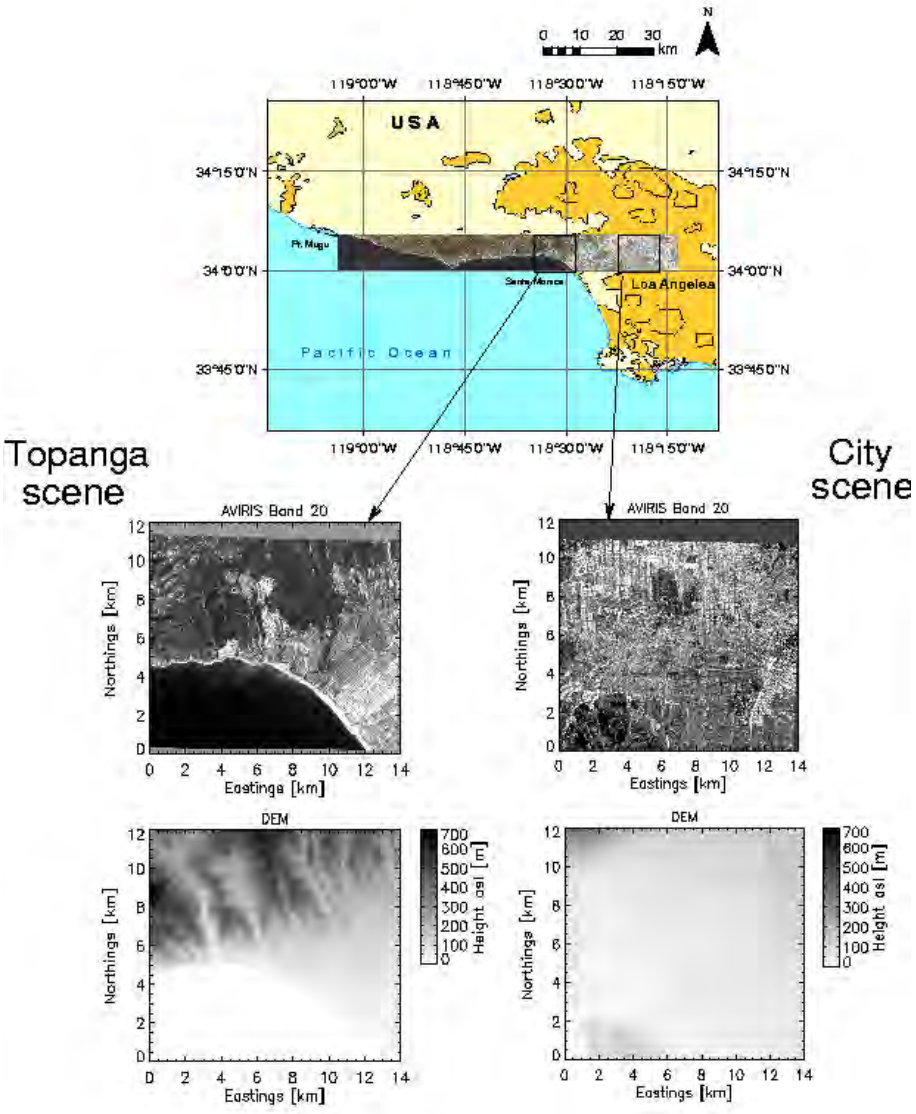


Figure 4.6: Location of AVIRIS scenes. The zoom-ins show "Topanga" and "City" scenes for AVIRIS band 20 (0.56 $\mu$m), and corresponding terrain height maps.

The "City" scene (b) neighbours to the east of the "Topanga" scene. It contains almost exclusively flat urban area, except for the north-western corner, where foothills of the Santa Monica Mountains show up. Scattered dark patches in the "City" scene mostly consist of open green areas (city parks). Downtown Los Angeles can be identified as the brightest part in the south-east corner. The south-west corner exhibits an extended area of bare soil with low average reflectance in the VIS, for which geographical map information states the Inglewood oil field.

As for the terrain model, a USGS digital elevation model with a spatial resolution of 10 m was necessary for orthorectification of the scenes, carried out with a parametric approach by Schläpfer and Richter (2002). Terrain heights vary in the "Topanga" scene between 0 and 703 m, in the "City" scene between 0 and 434 m, although relatively flat areas dominate the latter picture ($0 - 200$ m variation).

For spectral angle mapping (step (2) of ARIA), band numbers 33, 55, 73, 138, and 183 are used. The SWIR1 and SWIR2 spectral regions correspond to AVIRIS bands $124-144$ and $182-204$, respectively. The effect of varying zenith angle of the sensor viewing direction ($\pm$ 15.6°) on the sensor signal (due to increased optical path length) is considered negligible. Smoothing of the final aerosol parameter map (step (9)) was done across 10x10 AVIRIS pixels.

## 4.6 Application of Methods

### 4.6.1 ARIA

Application of the ARIA method after Fig. 4.3 is now demonstrated with the "Topanga" and "City" AVIRIS scenes. Over land, ARIA results are compared to the results as provided by alternative methods for aerosol parameter retrieval. They have been outlined before: dark vegetation and Kaufman's band ratio methods. Over water, where ARIA is not defined, the dark water method after Gao et al. (2000) is applied, to obtain a spatially contiguous aerosol parameter map in the final result.

In the re-mixing process of $\rho_s$(VIS), the SWIR-VIS correlation of surface reflectance analysis suggested the use of the spectral region between 0.42 and 0.56 $\mu$m. Here, average relative deviations compared to spectra from a spectrum database showed a minimum. However, at step (6) of ARIA processing for both "Topanga" and "City" scenes, where upward-calculated surface reflectance $\rho_{app}^{sim}$(VIS) is compared to the sensor spectrum $\rho_{app}$, large discrepancies were observed between the two for all look-up tables, particularly in the region of the green peak.

Illustrated in Fig. 4.7, this observation could be made both for pixels initially classified by the vegetation and by the soil endmembers. As a consequence, the inversion process was cancelled off, and the bands between 0.49 and 0.56 no longer used.

Two explanations are possible:

- The choice of endmembers, particularly the mean vegetation spectrum, is not representative for the actual land cover in the image.
- The correlation between the SWIR and the green peak spectral region is far lower than observed.

The second-best VIS range ($0.42-0.49$ $\mu$m) in terms of unmixing/re-mixing accuracy was subsequently selected for application in the ARIA method, omitting the critical green peak range and taking the region with maximum aerosol influence.

### 4.6.2 Dark Targets

Over land, aerosol parameter inversion was carried out over dark vegetation (DV) targets, for comparison with the ARIA method. Over water, which is essentially dark in the near-infrared, aerosol inversion results are required to complement the results over land for a spatially contiguous final product. The classification of dark water pixels was done as follows. Performing an atmospheric correction of the image with the ATCOR4 program (Richter and Schläpfer, 2002) and using uniform $\tau_a = 0.088$

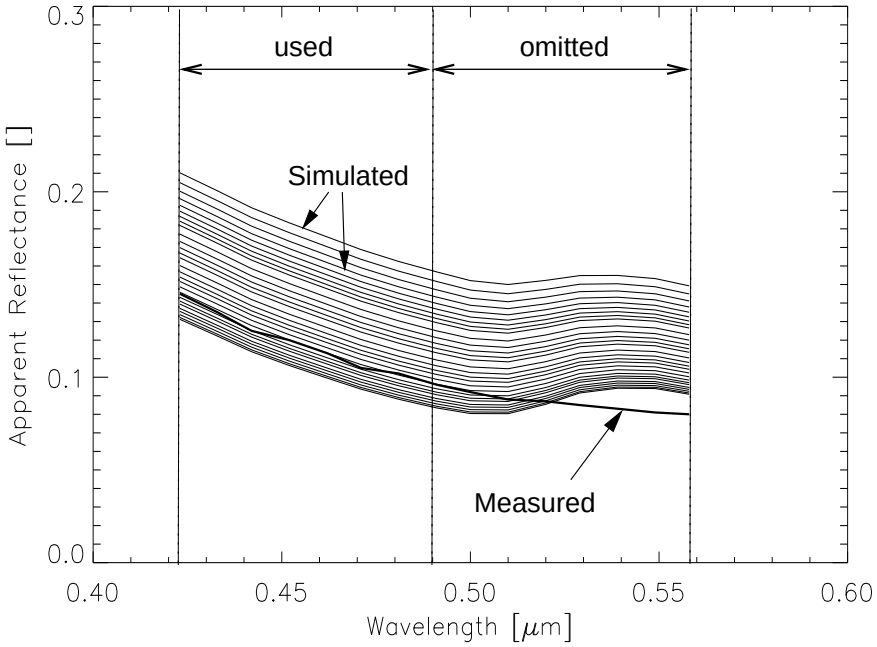


Figure 4.7: At-sensor and upward-calculated spectra using VIS bands between $0.42-0.56\mu$m (AVIRIS bands $6-20$) for inversion. Note the over-estimation of vegetation reflectance in the re-mixed $\rho_s$(VIS) spectrum that exhibits in a discrepancy to the measured spectrum in the green peak region.

above sea level ($V = 100$ km) removes the molecular scattering part of $\rho_{app}$, and $\rho^*$ is obtained. With a threshold $\rho^* \leq 0.01$ at $\lambda = 1.00$ $\mu$m (AVIRIS band 69) applied to the corrected scene (Gao et al., 2000), a water mask is obtained.

Use of the NIR band at the specified position is recommended because of high probability for suspended matter in the coastal zone in the "Topanga" scene (Gordon and Wang, 1994). No water pixels could be identified in the "City" scene. Once the water mask is obtained, water reflectance $\rho_s(1.00\,\mu\text{m})$ is assumed to be between 0.00 and 0.01.

For the identification of dark vegetation (DV), a combination of band thresholds and a vegetation index was used. Since the normalized difference vegetation index NDVI is not generally applicable to atmospherically distorted image data, as it is itself affected by aerosols, the Atmospherically Resistant Vegetation Index (ARVI) as defined by Kaufman and Tanré (1992) was employed. It is on average four times less sensitive to atmospheric effects than the NDVI, and defined by

$$\text{ARVI} = (\rho^*(\text{NIR}) - \rho^*_{rb})/(\rho^*(\text{NIR}) + \rho^*_{rb}) \tag{4.11}$$

where

$$\rho^*_{rb} = \rho^*_r - \gamma(\rho^*_b - \rho^*_r) \tag{4.12}$$

with a suggested $\gamma$ of 1.0. The subscripts $r$ and $b$ denote the red and blue bands, which are positioned at 0.47 $\mu$m (AVIRIS band 11) and 0.66 $\mu$m (33), respectively.

The NIR band is chosen at 0.87 $\mu$m (55). Quantities $\rho_r^*$, $\rho_b^*$, and $\rho^*$(NIR) are already corrected for molecular scattering and absorption analogous to the dark water case.

According to the referenced paper, the ARVI threshold is flexibly set such that 5 % of image pixels are covered. From this pixel fraction, the semi-fraction with lower reflectance in the NIR band is finally selected as candidate pixels for the dark vegetation method. In the "Topanga" scene, an ARVI threshold of 0.72 was imposed. The "City" scene required a lower threshold of 0.47, indicating less abundance of dark vegetation. Once a DV pixel map is obtained, $\rho_s(0.66\mu\text{m})$ is assumed to be 0.01, 0.02, or 0.03.

For both dark target approaches, the uncertainty in the finally retrieved aerosol parameter $\tau_a$ is calculated analogously to the ARIA method, for a single band. The different assumptions for $\rho_s$ cause an uncertainty $\Delta\tau_a^*$ in retrieved aerosol optical depth, as stated in equation (4.8). In the dark target case, $\tau_a^{max}$ and $\tau_a^{min}$ are defined as follows:

$$\tau_a^{max} = f(\rho_s^{min}, \rho_{app}(\lambda_0) + \Delta\rho_{app}(\lambda_0)) \quad \text{and} \tag{4.13}$$

$$\tau_a^{min} = f(\rho_s^{max}, \rho_{app}(\lambda_0) - \Delta\rho_{app}(\lambda_0)) \ , \tag{4.14}$$

where $\rho_s^{min}$ equals 0.00 for dark water, and 0.01 for DV, and $\rho_s^{max}$ corresponds to 0.01 for dark water, and to 0.03 for DV. In the calculation of final aerosol maps, the 0.75 error threshold was used analogously to the ARIA method.

### 4.6.3 Band Ratio

The band ratio (BR) method was applied according to Kaufman et al. (1997b) and the MODIS Algorithm Theoretical Basis Document (Kaufman and Tanré, 1998). For the 2.10 $\mu$m band (AVIRIS band 183), a maximum $\rho_{app}$ threshold of 0.05, and a minimum threshold of 0.005 is imposed, provided that at least 5 % of the pixels in the image are covered that way. Otherwise, the $\rho_{app}$ threshold is increased to 0.1. The minimum threshold guarantees the exclusion of water pixels.

In the "Topanga" scene, the 0.05 threshold in the SWIR could be successfully applied. The overall brighter "City" scene required the 0.1 threshold. The SWIR/VIS band ratios are applied to approximate the band values at 0.49 $\mu$m (AVIRIS band 13) and 0.66 $\mu$m (33) by the factors of 0.25 and 0.5, respectively. Uncertainties in the retrieved $\tau_a$ were calculated analogously to the ARIA method for two bands in the VIS. Kaufman et al. (1997b) gives an absolute uncertainty in the reconstructed band reflectance of 0.006, so total uncertainty in $\rho_s(\lambda)$ is here given by

$$\Delta\rho_s(\lambda) = 0.006 + 0.038\rho_s(\lambda)\,. \tag{4.15}$$

In the calculation of final aerosol maps, the 0.75 error threshold was used analogously to the ARIA method.

| Method | Aerosol | $\overline{\tau_a}$ | $\sigma(\tau_a)$ | $\overline{\Delta\tau_a}$ |
|---|---|---|---|---|
| ARIA | m | 0.21 | 0.04 | 0.13 |
| ARIA | r | 0.18 | 0.03 | 0.11 |
| ARIA | u | 0.44 | 0.12 | 0.40 |
| BR | m | 0.24 | 0.06 | 0.10 |
| BR | r | 0.23 | 0.06 | 0.10 |
| BR | u | 0.56 | 0.22 | 0.32 |
| DV | m | 0.30 | 0.04 | 0.18 |
| DV | r | 0.31 | 0.04 | 0.18 |
| DV | u | - | - | - |

Table 4.1: "Topanga" scene aerosol mapping results obtained with ARIA, band ratio (BR), and dark target methods (DV), using maritime (m), rural (r), and urban (u) aerosol models, evaluated on an intersection mask.

## 4.7 Results and Discussion

Aerosol optical depth $\tau_a$ is determined for maritime, rural, and urban aerosol models, for the DV, BR, and ARIA methods. For comparison of the raw inversion results, candidate pixel sets as used by the respective method were intersected and mean values $\overline{\tau_a}$, $\overline{\Delta\tau_a}$ and the spatial standard deviation $\sigma(\tau_a)$ calculated for both "Topanga" and "City" scenes. In the "Topanga" case (Table 4.1), small differences between maritime and rural models can be observed in all categories. Use of the urban model yields values for all categories that stand considerably apart. In the DV method, no average results could be determined as the fit of simulated to real data was inappropriate for the urban aerosol model. Maritime and rural results for $\overline{\tau_a}$ in the BR and DV methods are significantly higher than for the ARIA method. In-scene variations are approximately equally high for the ARIA and DV methods, although at a higher overall $\tau_a$ level for the latter, and slightly higher for the BR.

In the "City" scene (see Table 4.2), this assessment could be confirmed. $\overline{\tau_a}$ is markedly higher in this scene than in the "Topanga" case, as indicated by all three methods. ARIA in scene variation is lowest, which is an encouraging result, as $\tau_a$ is expected to vary smoothly in the horizontal direction. Again, results for the urban model inversion appear unrealistic. An aerosol optical depth of 0.82 as obtained by the BR method would mean an very hazy atmosphere with horizontal visibility around 7.5 km, which is considered rather improbable at this stage. Considering maritime and rural aerosol models only, the averaged relative error of the ARIA method amounts to values between $54-62$ % of the averaged reference value, whereas the BR ($32-43$ %) and the DV ($36-60$ %) perform better. However, in absolute terms, the ARIA method average error is smaller than in the DV method, and slightly above the BR method.

| Method | Aerosol | $\overline{\tau_a}$ | $\sigma(\tau_a)$ | $\overline{\Delta\tau_a}$ |
|---|---|---|---|---|
| ARIA | m | 0.28 | 0.09 | 0.15 |
| ARIA | r | 0.25 | 0.08 | 0.14 |
| ARIA | u | 0.86 | 0.51 | 1.49 |
| BR | m | 0.34 | 0.10 | 0.11 |
| BR | r | 0.33 | 0.10 | 0.12 |
| BR | u | 0.82 | 0.31 | 0.51 |
| DV | m | 0.44 | 0.10 | 0.16 |
| DV | r | 0.47 | 0.10 | 0.17 |
| DV | u | - | - | - |

Table 4.2: "City" scene aerosol mapping results obtained with ARIA, band ratio (BR), and dark target methods (DV), using maritime (m), rural (r), and urban (u) aerosol models, evaluated on an intersection mask.

From these results, maritime and rural aerosol models appear equally fit to describe the actual atmospheric conditions in both "Topanga" and "City" scenes. In Fig. 4.8, "Topanga" scene raw aerosol inversion results (panels (a)) and interpolated and smoothed maps (panels (b)) are shown for $\tau_a$ and a rural aerosol model. The raw results for the ARIA method reveal a smooth behaviour of the aerosol optical depth for the most part of the scene, with values between 0.14 and 0.20 (blue regions). Higher values for $\tau_a$ can be observed mainly to the east of the scene, where urban areas prevail. Very few pixels are used in the densely built-up urban area in the south-eastern corner of the scene, and none were classified in water. This is in contrast to the BR method, which erroneously included near-shoreline pixels in its inversion procedure, probably due to high concentration of suspended matter in the water. It is apparent that in this region, artificially high $\tau_a$ values are retrieved. In the land part, the BR raw result looks by and large similar to the ARIA case, although less pixels carry aerosol information. Dark vegetation pixels could be numerously identified in the scene, but pixels appear largely green, yellow and reddish, indicating high $\tau_a$ values. Urban and water areas were duly excluded in the DV method.

In Fig. 4.8b, results from the dark water retrieval were added to the respective set of pixels identified by the three methods, and interpolation and smoothing was carried out to fill the gaps between the pixels with aerosol information. $\tau_a$ values considered unrealistically high (white areas) mainly occur where very few raw pixels could be found (note south-eastern corner of the scene), or in case of erroneously classified pixels, as is the case for the BR method along the shoreline. Aerosol optical depth over the bay of Santa Monica looks reasonably uniform ($\tau_a \approx 0.25$), and continues to be so on land particularly in the urban and semi-urban regions in the eastern part of the scene. All results along the shoreline are considered artificially high, again due to the presence of suspended matter which undermines the dark water assumption.

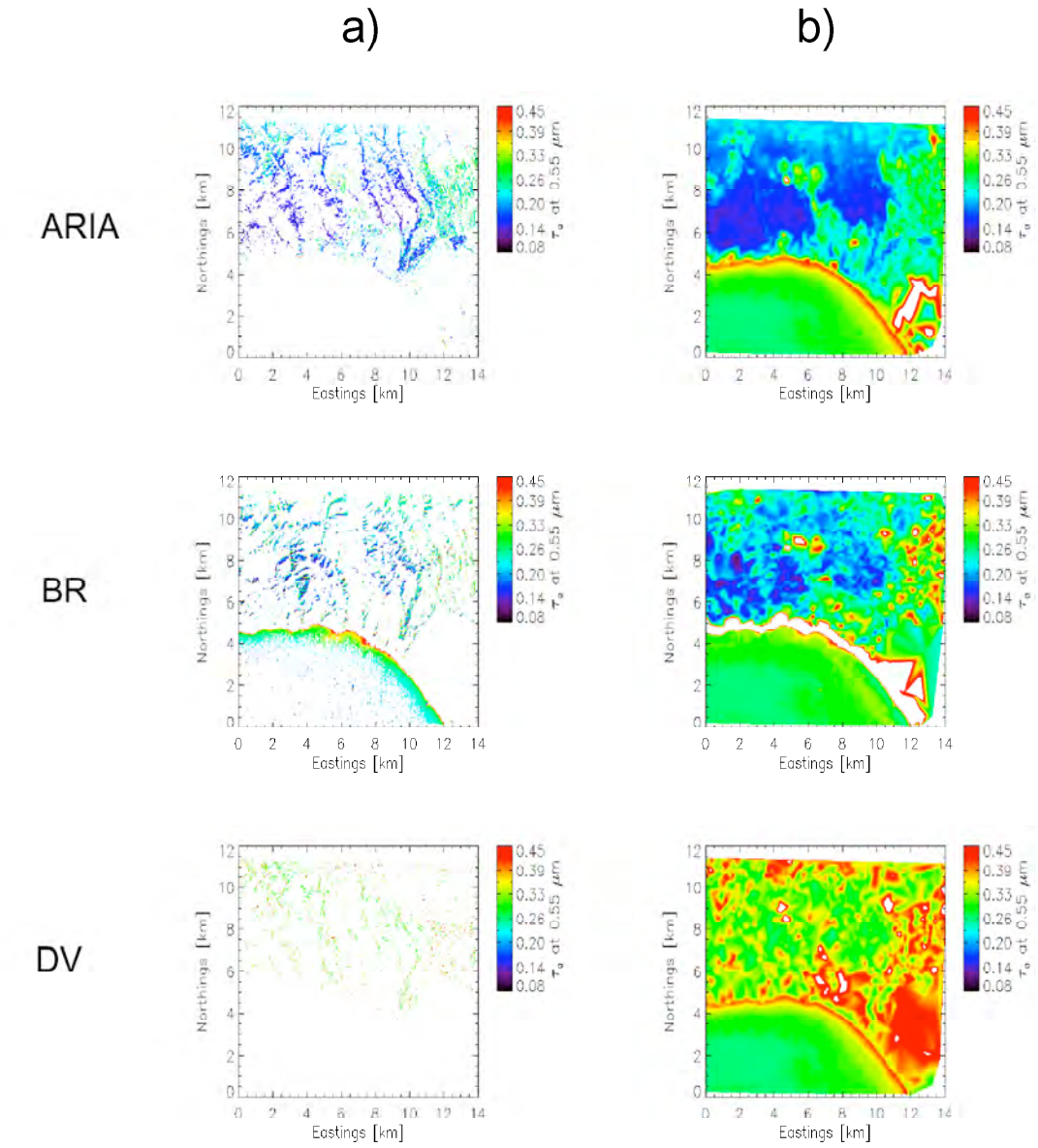


Figure 4.8: Examples for raw (a) and interpolated and smoothed (b) $\tau_a$ mapping results using rural aerosol model, for three methods ARIA, band ratio (BR), and dark vegetation (DV) in the "Topanga" scene. White areas denote non-used or out-of-area pixels (all panels), or pixels with values that are considered unrealistically high (panels (b)).

For the ARIA method, in the blue and bluish regions, markedly lower values for $\tau_a$ are observed. This is correlated to the existence of strong topography in these areas, and, for the most part, the absence of urban areas. Within the blue regions, $\tau_a$ varies between 0.1 and 0.2 approximately. Note the green patch in the centre of the scene that stretches inward to the predominantly blue region: it matches fairly well with an outskirt urban area that extends into a north-south running valley. Isolated patches

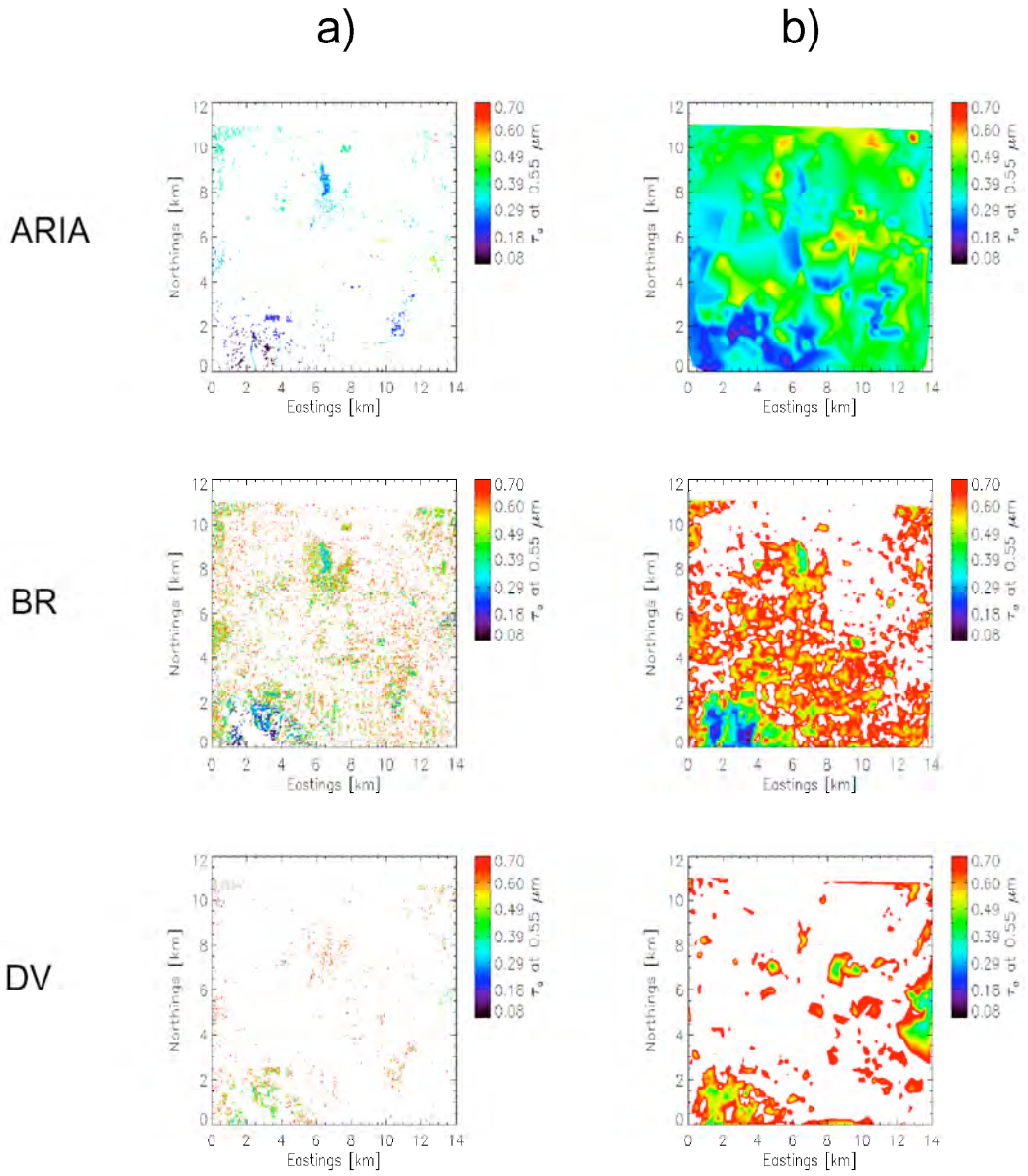


Figure 4.9: Examples for raw (a) and interpolated and smoothed (b) $\tau_a$ mapping results using rural aerosol model, for three methods ARIA, band ratio (BR), and dark vegetation (DV) in the "City" scene. White areas denote non-used or out-of-area pixels (all panels), or pixels with values that are considered unrealistically high (panels (b)).

of very high $\tau_a$ most likely correspond to spurious pixels that have been classified as vegetation or soil in the ARIA procedure, but are strongly mixed with other surface types. Panel (b) for the BR method displays a similar overall structure as the ARIA method, i.e. the distribution of blue and green regions is reproduced, but with stronger inherent variability in both blue and green areas. The overall impression is much less smooth than in the ARIA case, reflected in higher $\sigma(\tau_a)$ values. To the east

of the scene, many more artificially high patches show up in yellow and red, which are most probably not linked to actual variations in aerosol concentration. No smoke clouds have been observed in this area. The DV result appears smoother than the corresponding picture for BR, the blue regions have disappeared, but unexpectedly high $\tau_a$ values (0.45 and more) can be observed for large eastern and also central parts of the scene.

The "City" scene has been analysed analogously to the "Topanga" scene, as shown in Fig. 4.9 (note the different scale of the $\tau_a$ bar). In the raw result, many more pixels are used by the BR method than by ARIA and DV methods, but the intersected results for ARIA and BR are at comparable level (blue patches). The DV method used the fewest pixels, and inversion results show $\tau_a$ values of 0.6 and above. The interpolated results in panels (b) appear most reasonable for the ARIA method, with relatively low spatial variation of $\tau_a$ compared to BR and DV methods. Some artefacts from the interpolation procedure can be identified right to the centre of the scene, where supposedly artificially high values in red ($\tau_a \approx 0.7$) show up. A region of lower aerosol loading in the south-western edge of the scene can be identified in all three panels. In parts, this area (at around 3 km eastern and 0-1 km northern coordinate) has been identified an oil field with low average VIS reflectance compared to the rest of the image. Interpolation in the "City" scene was performed assuming flat terrain, i.e. without evaluation of terrain heights and the $\tau_a(h)$ dependence.

A significant part of the variations in the final result of the ARIA, i.e. the interpolated and smoothed image in Fig. 4.8b, is most probably not due to actual variation of the aerosol regime in the image. Considering maximum terrain height variation of 700 m and an extinction coefficient $\sigma_{e,a}$ of around $5{\cdot}10^{-2}$ km$^{-1}$, a maximum variation of columnar $\tau_a$ from terrain undulation alone would be 0.035. This is clearly exceeded in the ARIA results, but also in the results for the BR and DV methods. $\tau_a$ appears conspicuously high (green areas) over mostly urban regions that exhibit many high VIS albedo objects, such as roofs and bright concrete. A similar effect can be observed for the "City" scene (Fig. 4.9b), where areas with significantly lower reflectance in the VIS also show lower $\tau_a$ values (blue regions).

## 4.8 Validation

### 4.8.1 Indirect Validation with Terrain Height Model

In view of lacking ground truth data, an indirect means of assessing result quality is verifying the $\tau_a(h)$ dependence. The gradient $\partial\tau_a/\partial h$ is employed for terrain-dependent interpolation of the raw aerosol map. This analysis only makes sense in areas with significantly variable topography, that is, the "Topanga" scene. Table 4.3 states the results of the linear fit for raw aerosol maps obtained for each method, like panels (a) in Fig. 4.8, for the rural, maritime, and, for comparison, urban aerosol models. Negative values for $\partial\tau_a/\partial h$ can be observed throughout, which is reasonable, as the columnar quantity $\tau_a$ is expected to decrease with increasing terrain height $h$. Secondly, assuming a maximum variability for $\tau_a$ between $0.01 - 1.0$ and a vertically homogeneous atmosphere, $\sigma_{e,a}$ and hence $-\partial\tau_a/\partial h$ varies between 0.5 and $50.0{\cdot}10^{-2}\,\mathrm{km}^{-1}$. All obtained results fall within that range, except for the DV method using the urban aerosol model, where no results are available. The values

| Method | Aerosol model | | | | | |
|---|---|---|---|---|---|---|
| | m | | r | | u | |
| | $\partial_h \tau_a$ | $\sigma(\partial_h \tau_a)$ | $\partial_h \tau_a$ | $\sigma(\partial_h \tau_a)$ | $\partial_h \tau_a$ | $\sigma(\partial_h \tau_a)$ |
| ARIA | -3.07 | 0.37 | -2.83 | 0.33 | -5.91 | 1.23 |
| BR | -32.45 | 1.71 | -30.28 | 1.55 | -33.58 | 5.33 |
| DV | -3.07 | 3.13 | -3.66 | 3.24 | - | - |

Table 4.3: Average linear gradient $\partial_h \tau_a = \partial \tau_a / \partial h$ [$10^{-2}$ km$^{-1}$] and its standard error $\sigma(\partial_h \tau_a)$ for the "Topanga" scene for maritime (m), rural (r), and urban (u) aerosol models, obtained with ARIA, band ratio (BR) and dark vegetation (DV) methods.

| Scene | Aerosol model | ARIA | | BR | | DV | | MODIS | |
|---|---|---|---|---|---|---|---|---|---|
| | | $\overline{\tau_a}$ | $\overline{\Delta \tau_a}$ | $\overline{\tau_a}$ | $\overline{\Delta \tau_a}$ | $\overline{\tau_a}$ | $\overline{\Delta \tau_a}$ | $\overline{\tau_a}$ | $\overline{\Delta \tau_a}$ |
| T | m | 0.25 | 0.15 | 0.28 | 0.12 | 0.31 | 0.16 | 0.08 | 0.07 |
| T | r | 0.25 | 0.13 | 0.29 | 0.12 | 0.34 | 0.17 | 0.08 | 0.07 |
| C | m | 0.42 | 0.20 | 0.66 | 0.22 | 0.73 | 0.15 | 0.19 | 0.09 |
| C | r | 0.39 | 0.18 | 0.69 | 0.28 | 0.74 | 0.16 | 0.19 | 0.09 |

Table 4.4: Interpolated and smoothed aerosol mapping results for the "Topanga" (T) and "City" (C) scenes, obtained for maritime (m) and rural (r) aerosol models, with ARIA, band ratio (BR), and dark vegetation methods (DV), and the MODIS aerosol product.

obtained from the BR method appear less realistic compared to ARIA and DV, although the erroneously classified water pixels have been excluded from this analysis. ARIA and DV average gradients agree for the maritime model, and are in the same order of magnitude for the rural case. Standard errors $\sigma(\partial_h \tau_a)$, obtained from total uncertainties $\Delta \tau_a(h)$ and the minimizing of $\chi^2$ (Press et al., 1992, p. 660), are significantly larger in the DV method than for BR and ARIA methods. Panel (a) in Fig. 4.8 for DV reflects this fact by showing little dependence on terrain height. To conclude, the ARIA method is equally fit to produce a $\tau_a(h)$ dependence in the result data compared to the DV method. Further, ARIA results appear more realistic than for the BR method. Standard errors are in the same order of magnitude for ARIA, compared to BR and DV methods.

### 4.8.2 Validation of Aerosol Optical Depth with MODIS

Lacking direct validation data from sun photometry or other ground-based radiometric measurements, no decision can be made which model/method combination mirrors best the actual aerosol regime in the area at the time of overflight. Instead,

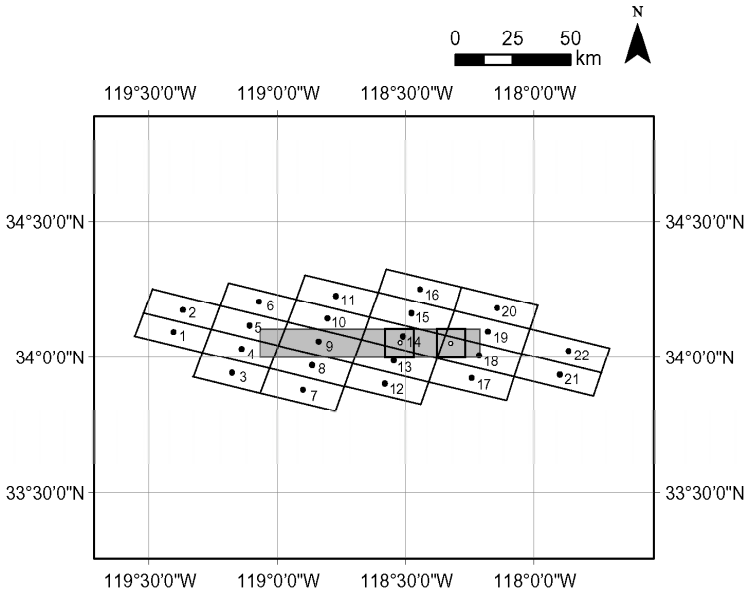


Figure 4.10: Overlay of numbered MODIS aerosol product pixels and AVIRIS scene (grey shaded area). Aerosol parameters of the "Topanga" (left hand square) and "City" (right hand square) scenes are compared at the centre points (open circles) with interpolated MODIS results.

the aerosol product MOD04_L2 of the TERRA/MODIS sensor is used here for indirect validation. The AVIRIS test area has been covered by MODIS on 16 September 2000 at 12.35 pm local time, that is, about 90 minutes after the AVIRIS flight line was flown. It can be assumed that aerosol parameters derived for both times are comparable.

The MODIS aerosol product (Kaufman and Tanré, 1998) is given at 25 km spatial resolution. Fig. 4.10 depicts the AVIRIS flight strip with the "Topanga" and "City" scenes, and pertinent MODIS pixels with the aerosol product. They are given at 25 km spatial resolution along-track (in roughly northeast-southwest direction). The values for $\tau_a$ are allocated to the centre of MODIS pixels and accurate to within their estimated uncertainties $0.05 \pm 0.2\tau_a$. Linearly interpolated values of $\tau_a$ for the centres of the "Topanga" and "City" scenes are 0.08 and 0.19, respectively. The MODIS aerosol type is given as "smoke" for all pixels, derived from geographically and seasonally defined climatology after d'Almeida et al. (1991). So it remains unclear whether the smoke aerosol type reflect actual conditions in this specific case.

Table 4.4 reveals significant differences between the results obtained in this study, and the MODIS aerosol product. For MODIS, the "Topanga" scene showed a $\tau_a$ value of 0.08, whereas the lowest value of the three methods was obtained for the ARIA procedure (0.25). The consistent discrepancy in retrieved $\tau_a$ between MODIS and the methods used in this paper may be due to the differences in scale (see Fig. 4.10). For comparison, the uncertainties in $\tau_a$ as defined by the three aerosol retrieval methods are also interpolated and smoothed across the scenes. When taking into account these uncertainties, an overlap of the error bars given for the MODIS values is achieved

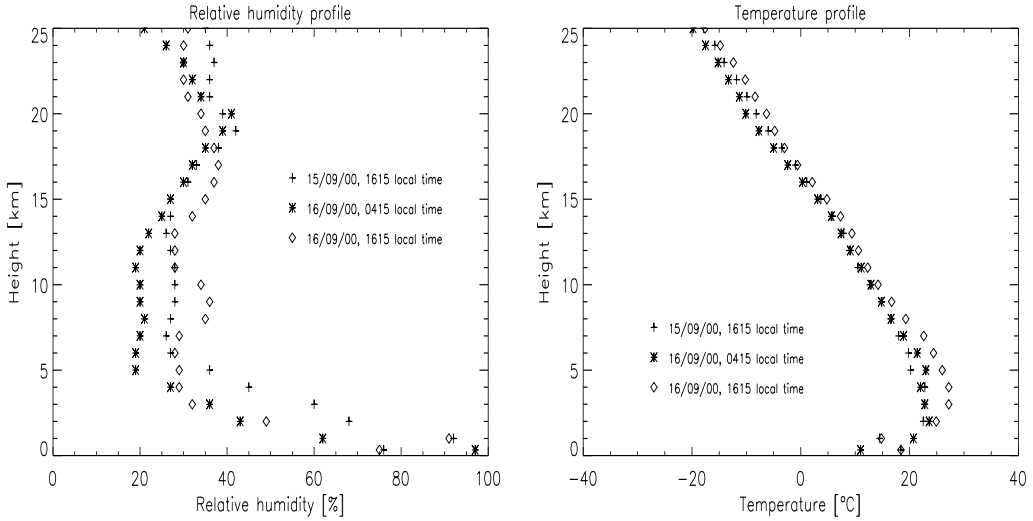


Figure 4.11: Radiosonde sounding data for Vandenberg Air Force Base, 212 km to the northwest of the Santa Monica AVIRIS scenes.

only when using the ARIA method for both scenes (e.g. 0.25-0.13 vs. 0.08+0.07 for the "Topanga" scene and rural aerosol model). This tentatively confirms the quality of the ARIA method as compared to band ratio and dark target methods, although the error bars are large (87.5 % of the reference value of the MODIS product, and 52 % for the ARIA method). Use of the rural aerosol model as the model of choice here is confirmed by the MODIS validation, as $\overline{\tau_a}$ is lowest, i.e. closest to the MODIS $\tau_a$ value.

### 4.8.3 Climatological Validation

The aerosol parameter retrieval in this study concentrated on aerosol optical depth $\tau_a$ in combination with any one of three aerosol models (rural, maritime, urban), assuming an atmosphere with stable layers, standard temperature and pressure profiles, and aerosol concentrations largely confined to the planetary boundary layer.

As for the general weather situation in the area, around the time of overflight, no precipitation was reported at least three days before and after the AVIRIS flight took place. Weak pressure variations across California gave rise to weak south-westerly winds. Temperatures at the ground showed values up to 30°C around noon, as visible in radiosonde data in Fig. 4.11. These atmospheric profiles were acquired at Vandenberg Air Force Base, about 212 km to the north-west of the Santa Monica area. Because of its location by the sea, and overall stable weather conditions, the data from the air base is considered comparable to the conditions in the area of the flight line. The weather situation corroborates the assumption that MODIS and AVIRIS aerosol data can be compared. It also confirms the lower 20 km of the atmosphere being considered homogeneously stratified.

## 4.9 Conclusions

A new method for the retrieval of aerosol parameters over land using imaging spectrometer data has been presented, representing an extension to existing methods for aerosol inversion that are based on single (dark target) or double spectral bands (Kaufman's band ratio). In comparison to band ratio and dark target methods, performance of the ARIA method is superior in terms of in-scene smoothness (due to a larger number of pixels used), and relatively successful validation with the MODIS aerosol product. Many candidate pixels, however, do not necessarily guarantee a smooth aerosol parameter picture, as can be seen in the band ratio result for the "City" scene. Indirect validation with the terrain height in the "Topanga" scene led to reasonable results for the ARIA and dark vegetation methods. Use of the urban aerosol model mostly yielded unreasonable or even no results at all in the analyses, it is most likely not adequate for the aerosol regime description in this case study, even for the "City" scene. Rural and maritime aerosol models gave similar results, the rural case was taken as the best model due to its slightly better performance in the ARIA method in terms of average uncertainty $\Delta\tau_a$.

Average uncertainties in the ARIA method for aerosol optical depth are comparable to the uncertainties for band ratio and dark target methods. Still, results are affected by the distribution of visibly bright objects, particularly in urban regions. Improbably strong variations of $\tau_a$, that cannot be attributed to terrain height undulation, and are unlikely to reflect true atmospheric conditions, are observed for all methods. The AVIRIS 2000 test imagery, collected between downtown Los Angeles and Point Mugu along the coastline, showed the desired high variation of surface cover, but most probably exhibited a rather low overall level of aerosol loading, which rendered aerosol parameter inversion independent of surface cover a difficult task.

For the validation of ARIA, the application to imaging spectrometry data is suggested where ground truth in form of in-situ ground reflectance spectra, sun photometer data (Holben et al., 1998), and/or lidar data is available. Usage of a locally-adapted spectrum database (Roberts et al., 1998) may lead to an endmember selection that is better-suited to reflect local conditions, e.g. vegetation characteristics and urban areas. In order to circumvent the need for a priori endmember choice, a number of methods for automated endmember determination has been developed (Tompkins et al., 1997; Winter, 1999). The algorithm by Plaza et al. (2001) appears particularly suited for AVIRIS data. Inclusion of automated endmember determination would represent an elegant extension for the ARIA method, completely removing the need for a priori assumptions.

## 4.10 Outlook

Our results confirm that the ARIA concept is a further step toward aerosol retrieval and atmospheric correction over land on a pixel basis using high resolution imaging spectroscopy. It performs equally well, in some aspects better than traditional single or double-band aerosol retrieval methods. Of particular value is the fact that the method does not require a priori knowledge, except for the selection of representative endmember spectra. Until SWIR and VIS high-resolution imaging spectrometer data with global coverage is commonly available, a contribution to the mapping of regional

distribution of aerosol parameters has been made. Complementary, the results from this study can be used for regional correction of atmosphere for land cover analyses.

A sensitivity study of the ARIA result with respect to the choice of unmixing endmembers may further elucidate the mechanisms behind the unmixing/re-mixing procedure proposed in the ARIA method. An analysis of this kind may also shed light on the problem encountered in the re-mixing procedure in the green peak region, which was supposed to be strongly correlated to the SWIR range for vegetation, but was only poorly reproduced under real conditions.

A next step in the inversion process would be the extension of aerosol parameter retrieval to other physical quantities, such as Ångström coefficient or single-scattering albedo. This would allow the determination of the aerosol model also, so far treated separately from the $\tau_a$ inversion. ARIA provides ideal grounds for that, as good spectral VIS coverage is available for the spectral approximation of the aerosol effect.

## Acknowledgements

The authors thank Dar Roberts and Phil Dennison (both University of California Santa Barbara) for providing AVIRIS and digital terrain data, and Donald D. Cameron (Vandenberg Air Force Base) for making the radiosonde profiles available. We are indebted to André Prévôt and Christoph Popp for their help in this project. We gratefully acknowledge financial support from the Swiss National Science Foundation, project 2000-61431.00, and the Paul Scherrer Institut, Villigen, Switzerland.

## References

Asner, G. and Lobell, D. (2000). A biogeophysical approach for automated SWIR unmixing of soils and vegetation. *Remote Sensing of Environment*, 74:99–112.

Berk, A., Bernstein, L., and Robertson, D. (1989). MODTRAN: a moderate resolution model for LOWTRAN7. Technical report, Spectral Sciences Inc., Burlington, Massachusetts, USA. 38 pp.

Bojinski, S., Schläpfer, D., Schaepman, M., and Keller, J. (2002). Aerosol mapping over rugged heterogeneous terrain with imaging spectrometer data. In *SPIE Imaging Spectrometry VIII*, volume 4816, pages 108–119, Bellingham, Washington, USA.

Chomko, R. and Gordon, H. (1998). Atmospheric correction of ocean color imagery: use of the Junge power-law aerosol size distribution with variable refractive index to handle aerosol absorption. *Applied Optics*, 37(24):5560–5572.

d'Almeida, G., Koepke, P., and Shettle, E. (1991). *Atmospheric Aerosols: Global Climatology and Radiative Characteristics*. Deepak, Hampton, Virginia, USA. 561 pp.

Fraser, R. (1976). Satellite measurements of mass of Saharan dust in the atmosphere. *Applied Optics*, 15:2471–2479.

Gao, B., Montes, M., Ahmad, Z., and Davis, C. (2000). Atmospheric correction algorithm for hyperspectral remote sensing of ocean color from space. *Applied Optics*, 39(6):887–896.

Gordon, H. (1978). Removal of atmospheric effects from satellite imagery of the oceans. *Applied Optics*, 17(10):1631–1636.

Gordon, H. and Wang, M. (1994). Retrieval of water-leaving radiance and aerosol optical thickness over the oceans with SeaWiFS: a preliminary algorithm. *Applied Optics*, 33(3):443–452.

Green, R., Eastwood, M., Sarture, C., Chrien, T., Aronsson, M., Chippendale, B., Faust, J., Pavri, B., Chovit, C., Solis, M., Olah, M., and Williams, O. (1998). Imaging spectroscopy and the airborne visible/infrared imaging spectrometer (AVIRIS). *Remote Sensing of Environment*, 65:227–248.

Green, R. and Pavri, B. (2001). AVIRIS inflight calibration experiment measurements, analyses, and results in 2000. In *Summaries of the Tenth Annual JPL Airborne Geoscience Workshop*, volume 1, pages 205–218, Pasadena, California, USA.

Holben, B., Eck, T., Slutsker, I., Tanré, D., Buis, J., Setzer, A., Vermote, E., Reagan, J., Kaufman, Y., Nakajima, T., Lavenu, F., Jankowiak, I., and Smirnov, A. (1998). AERONET - a federated instrument network and data archive for aerosol characterization. *Remote Sensing of Environment*, 66:1–16.

Isakov, V., Feind, R., Vasilyev, O., and Welch, R. (1996). Retrieval of aerosol spectral optical thickness from AVIRIS data. *International Journal of Remote Sensing*, 17(11):2165–2184.

Karnieli, A., Kaufman, Y., Remer, L., and Wald, A. (2001). AFRI - aerosol free vegetation index. *Remote Sensing of Environment*, 77:10–21.

Kaufman, Y. and Sendra, C. (1988). Algorithm for automatic atmospheric corrections to visible and near-IR satellite imagery. *International Journal of Remote Sensing*, 9(8):1357–1381.

Kaufman, Y. and Tanré, D. (1992). Atmospherically resistant vegetation index (ARVI) for EOS-MODIS. *IEEE Transactions on Geoscience and Remote Sensing*, 30(2):261–270.

Kaufman, Y. and Tanré, D. (1998). *Algorithm for remote sensing of tropospheric aerosols from MODIS*. NASA Goddard Space Flight Center, Greenbelt, Maryland, USA. 85 pp.

Kaufman, Y., Tanré, D., and Boucher, O. (2002). A satellite view of aerosols in the climate system. *Nature*, 419:215–223.

Kaufman, Y., Tanré, D., Gordon, H., Nakajima, T., Lenoble, J., Frouin, R., Grassl, H., Herman, B., King, M., and Teillet, P. (1997a). Passive remote sensing of tropospheric aerosol and atmospheric correction for the aerosol effect. *Journal of Geophysical Research*, 102(D14):16815–16830.

Kaufman, Y., Wald, A., Remer, L., Gao, B., Li, R., and Flynn, L. (1997b). The MODIS 2.1-$\mu$m channel-correlation with visible reflectance for use in remote sensing of aerosol. *IEEE Transactions on Geoscience and Remote Sensing*, 35(5):1286–1297.

King, M., Kaufman, Y., Menzel, W., and Tanré, D. (1992). Remote sensing of cloud, aerosol, and water vapor properties from the moderate resolution imaging

spectrometer (MODIS). *IEEE Transactions on Geoscience and Remote Sensing*, 30(1):2–27.

Liou, K.-N. (1980). *An Introduction to Atmospheric Radiation*. Academic Press, New York, New York, USA. 392 pp.

Liou, K.-N. (1992). *Radiation and Cloud Processes in the Atmosphere*. Oxford University Press, New York, New York, USA. 485 pp.

Plaza, A., Martinez, P., Gualtieri, J., and Perez, R. (2001). Spatial/spectral identification of endmembers from AVIRIS data using mathematical morphology. In *Summaries of the Tenth Annual JPL Airborne Geoscience Workshop*, volume 1, pages 309–319, Pasadena, California, USA.

Press, W., Teukolsky, S., Vetterling, W., and Flannery, B. (1992). *Numerical Recipes in C*. Cambridge University Press, Cambridge, UK, 2nd edition. 994 pp.

Price, J. (1994). Band selection procedure for multispectral scanners. *Applied Optics*, 33(15):3281–3288.

Richards, J. and Jia, X. (1999). *Remote Sensing Digital Image Analysis*. Springer-Verlag, Berlin, Germany, 3rd edition. 363 pp.

Richter, R. (1996). A spatially adaptive fast atmospheric correction algorithm. *International Journal of Remote Sensing*, 17(6):1201–1214.

Richter, R. and Schläpfer, D. (2002). Geo-atmospheric processing of airborne imaging spectrometry data. Part 2: atmospheric/topographic correction. *International Journal of Remote Sensing*, 23(13):2631–2649.

Roberts, D., Gardner, M., Church, R., Ustin, S., Scheer, S., and Green, R. (1998). Mapping chaparral in the Santa Monica Mountains using multiple endmember spectral mixture models. *Remote Sensing of Environment*, 65(3):267–279.

Schläpfer, D. and Richter, R. (2002). Geo-atmospheric processing of airborne imaging spectrometry data. Part 1: parametric orthorectification. *International Journal of Remote Sensing*, 23(13):2609–2630.

Shettle, E. and Fenn, R. (1979). Models for the aerosols of the lower atmosphere and the effects of humidity variations on their optical properties. Technical Report AFGL-TR-79-0214, Air Force Geophysics Laboratory, Hanscom AFB, Massachusetts, USA. 94 pp.

Tanré, D., Herman, M., and Deschamps, P. (1983). Influence of the atmosphere on space measurements of directional properties. *Applied Optics*, 22(5):733–741.

Tanré, D., Herman, M., and Mattoo, S. (1997). Remote sensing of aerosol properties over oceans using the MODIS/EOS spectral radiances. *Journal of Geophysical Research*, 102(D14):16971–16988.

Tompkins, S., Mustard, J., Pieters, C., and Forsyth, D. (1997). Optimization of endmembers for spectral mixture analysis. *Remote Sensing of Environment*, 59:472–489.

Winter, M. (1999). N-FINDR: an algorithm for fast autonomous spectral endmember determination in hyperspectral data. In *SPIE Imaging Spectrometry V*, volume 3753, pages 266–275, Bellingham, Washington, USA.

# Conclusions

The reference spectrum database SPECCHIO for input, output, display, and administration of field-based, laboratory, and modelled spectral data has been conceptually designed, implemented, and used for the remote sensing of aerosols with imaging spectroscopy. To the author's knowledge, SPECCHIO is a new reference spectrum database approach in the remote sensing field. The availability of spectrum data sources with a reference character, such as SPECCHIO, is expected to become increasingly important in future applications of imaging spectroscopy, as these data need to be available on a routine basis. For example, automated classification of spectral image data, possibly robust towards the atmosphere, can be enhanced by the provision of reference spectra from a database. In cases where an adaptation to local area conditions is possible in the database, SPECCHIO is expected to (partly) substitute the need for field campaigns.

The potential of SPECCHIO to aid imaging spectroscopy has been demonstrated in the novel ARIA method for the retrieval of aerosol parameters over land. In comparison to existing methods for aerosol inversion from aircraft or satellites that are based on single (dark target) or double spectral bands (Kaufman's band ratio), performance of the ARIA method is superior in terms of in-scene smoothness of aerosol optical depth variation, and relatively successful cross-validation with the aerosol product from the operational satellite sensor MODIS. Average uncertainties in aerosol optical depth as obtained with ARIA are slightly higher than respective band ratio values, but lower than with the dark target method. Observed dependencies of retrieved aerosol optical depth on surface reflectance over land in parts of the final results of ARIA, especially in urban areas, are most likely attributed to the abundance of surface types that are not reflected in the endmember choice for unmixing/re-mixing within ARIA.

To this end, the sensitivity of aerosol retrieval over land with regard to the choice of endmembers has to be explored in the future. This could be achieved using a spectral subset out of SPECCHIO adapted to local area conditions, e.g., by comparison of spectral samples measured in-situ to spectral ensembles in the database, constrained by a relative deviation threshold. Mathematical search criteria on single spectra, such as the application of spectral indices, are helpful for that purpose and will be available in the next software version of SPECCHIO.

Analysis of the autocorrelation of surface reflectance spectra, as carried out with SPECCHIO data as a precondition for ARIA, requires further investigation. Results in this dissertation for the best spectral ranges in the SWIR and VIS used in the ARIA unmixing/re-mixing procedure, and the related re-mixing accuracy, strongly depend on the current spectral ensembles for soil, vegetation, and rocks/minerals as provided

by SPECCHIO. Inclusion of additional spectral data from a wide variety of sources (soil and vegetation reflectance spectra from different climate zones, vegetation in different phenological states) would allow a reassessment of the present results on a more generalized basis.

The overall results for ARIA are encouraging and warrant the application of ARIA to spectral imagery from imaging spectrometers other than AVIRIS. For example, data from the operational spaceborne HYPERION sensor could be used for aerosol parameter retrieval on a global scale. Repeated analysis of aerosol distributions around major aerosol sources, e.g., industrialized areas in China, would be facilitated with satellite-borne imagery. At the same time, calibration accuracy of the sensor in use must be better than 3.8 % in both visible and short-wave infrared spectral ranges in order to guarantee the error limits found for ARIA. Spectral resolution of the imaging spectrometer in the order of the AVIRIS sensor (10 nm) and $10^2 - 10^3$ m ground sampling distances are appropriate. Constraining aerosol retrieval to the aerosol optical depth parameter with a given aerosol model is recommended as long as the ARIA approach has not been firmly established in complementary studies.

Validation of aerosol retrieval results with ground-based sun photometry has to be a primary goal in future work with ARIA. Comparison of the MODIS aerosol product given at 25 km spatial resolution with averaged results for the airborne AVIRIS scenes, as done in this study by interpolation, is considered less reliable than the use of ground truth data.

As for SPECCHIO, the upcoming technology of the wireless internet allows, during field campaigns, quick and on-site storage and comparison of measured spectral data to the reference database. Therefore, the next version of SPECCHIO is expected to include improved, standardized interfaces to common data sources (e.g., field spectroradiometers), and extended visualization options on the web, e.g. for the display of three-dimensional BRDFs.

# Acknowledgements

This work was carried out in the framework of the Swiss National Science Foundation projects 20-50727.97 and 2000-061431.0, and a research grant from Paul Scherrer Institute (PSI), Villigen, Switzerland. Many persons gave me valuable support for realizing the two quite different parts of this thesis, that were both new to me at the beginning of the work. I wish to thank for their generous help: My chief supervisor Klaus Itten for giving me the opportunity to carry out this research in the Remote Sensing Laboratories (RSL), Department of Geography, University of Zurich; My RSL supervisors Michael Schaepman and Daniel Schläpfer for their enduring assistance, back-up, and time for discussions; My supervisors Johannes Keller and André Prévôt at PSI for their willingness to discuss problems and ideas, their moral support, and my smooth integration into the PSI Laboratory for Atmospheric Chemistry (LAC); Dar Roberts and Phil Dennison from the University of California Santa Barbara for making the AVIRIS test imagery and accompanying digital terrain model available; Donald D. Cameron (Vandenberg AFB) for the radiosonde profile data; Felix Bucher (Netcetera AG), who introduced me to thinking in data models and gave me a programming jump start; Rolf Richter from DLR Oberpfaffenhofen for thorough discussions on aerosol retrieval methods; Silvia Henning and Urs Baltensperger (LAC) for their enthusiasm that was incentive enough for me to get into the remote sensing of clouds; My office mates Peter Keller and Stefan Dangel for their company, criticism, and passion for blackboards; Gabi Schaepman-Strub and Mathias Kneubühler from the Spectroscopy Lab at RSL for accompanying me throughout the thesis, and helping me out with the calibration of spectroradiometers; the APEX team for allowing me to glimpse into an ESA project; the paper reviewers for their valuable comments. I am also indebted to the following persons for the odd hand they gave me: Othmar Wigger (UNIX system administration), Daniel Wirz (Oracle database software), Tobias Kellenberger (PCI), Martin Galanda (ArcView), Andi Bachmann and Uli Beisl (LaTeX), Markus Furger and Stephan Henne (interpretation of weather maps, thanks for pointing me at the Innsbruck IAMAS conference!), Nicolas Bukowiecki (aerosol in-situ measurements), Christoph Popp (aerosol retrieval methods), Dave Bailey (proofreading the manuscript). I wish to express my gratitude to the University of Zurich MNF Faculty for providing travel grants to conferences. I thank Martin Steinmann for musical inspiration, and Daniel Nüesch for his effort to acquaint me with the delicious Foiferweggli (got it in the end!). Finally, I deeply acknowledge the continuous support and love by my family and friends, who after all enabled me to complete this thesis.

# Curriculum Vitae

| | |
|---|---|
| Name | Bojinski |
| First Name | Stephan |
| Date of Birth | 16 November 1972 |
| Place of Birth | Neustadt (Weinstrasse), Germany |
| Nationality | German |

Education

| | |
|---|---|
| 1979 – 1983 | Primary school in Neustadt, Germany |
| 1983 – 1992 | Grammar school (German gymnasium) in Neustadt, Germany |
| 1992 – 1994 | Geophysics first degree (Vordiplom) at University of Karlsruhe, Germany |
| 1994 – 1995 | Equivalent of First Class Hons Geophysics at University of Edinburgh, UK |
| 1995 – 1998 | MSc Geophysics at University of Karlsruhe, Germany<br>Topic of thesis: Seismic characterization of fractured composite media by statistical wavefield analysis |
| 1999 – 2003 | PhD thesis at University of Zurich (Switzerland) and Paul Scherrer Institut, Villigen (Switzerland) |

Dissertation title

Imaging Spectroscopy of Aerosols using a Reference Spectrum Database

Dissertation supervisor

Prof. Dr. Klaus Itten (Remote Sensing Laboratories,
Department of Geography, University of Zurich)

Present affiliation

PhD student at University of Zurich and Paul Scherrer Institut, Villigen